Leakage Detection in Hydraulic Actuators based on Wavelet Transform

by

Amin Yazdanpanah Goharrizi

A thesis

presented to the University of Manitoba

in partial fulfillment of the

thesis requirement for the degree of

Doctor of Philosophy

Department of Mechanical and Manufacturing Engineering

University of Manitoba

Winnipeg, Manitoba, Canada

Abstract

Hydraulic systems are complex dynamical systems whose performance can be degraded by certain faults, specifically internal or external leakage. The objective of this research is to develop an appropriate signal processing approach for detection and isolation of these faults. By analyzing the dynamics of the hydraulic actuator, an internal leakage is shown to increase the damping characteristic of the system and change the transient response of the pressure signals. An external leakage, on the other hand, drops the pressure signals without having a significant effect on transient responses.

Offline detection of internal leakage in hydraulic actuators is first examined by using fast Fourier, wavelet and Hilbert-Huang transforms. The original pressure signal is decomposed using these transform methods and the frequency component which is sensitive to the internal leakage is identified. The root mean square of the processed pressure signal is used and a comparison of the three transforms is made to assess their ability to detect internal leakage fault, through extensive validation tests. The wavelet transform method is shown to be more suitable for internal leakage detection compared to the other two methods. The wavelet based approach is then extended to an online detection method of internal leakage fault. The online approach considers the more realistic case of an actuator that is driven in a closed-loop mode to track pseudorandom position reference inputs against a load emulated by a spring. Furthermore, the method is shown to remain effective even with control systems which are tolerant to leakage faults.

Next, the application of wavelet transform to detect external leakage fault using both offline and online applications in hydraulic actuators is described. The method also examines the isolation of this fault from actuator internal leakage in a multiple-fault environment. The results show that wavelet transform is a fast and easily-implementable method for leakage detection in hydraulic actuators without any need to explicitly incorporate the model of actuator or leakage. Internal leakages as low as 0.124 lit/min, are shown to be detectable, for 80% of the times using structured input signal. For online application, internal leakages in the range of 0.2-0.25 lit/min can be identified. External leakages as low as 0.3 lit/min can be detected in all offline and online applications. Other methods such as observer based and Kalman filter methods, which require the model of

the actuator or leakage fault, cannot report leakage detection of magnitudes as low as that reported in this work. The low leak rate detection and not requiring a model of the actuator or leakage make this method very attractive for industrial implementation.

Acknowledgments

My appreciation first goes to my supervisor, Dr. Nariman Sepehri for his fabulous supervision which brought about a unique academic life at University of Manitoba for me. I appreciated his guidance, encouragement and helpful discussions. The work presented here would certainly not have been accomplished without his influence and support. From my supervisor, I have learned a great deal about problem solving and presentation of the results of my research work. I would also like to thank the other members of my dissertation committee: Dr. Subramaniam Balakrishnan, Dr. Shaahin Filizadeh, and Dr. Guy Dumont from University of British Columbia.

My gratitude extends to the members of the research group of my professor, especially Mr. Kurosh Zareinia, who provided me with an appropriate atmosphere to perform this research.

I ultimately would like to pay my gratitude to my parents. Without the inspiration that they provided this work would not have been possible. This dissertation belongs more to them than to me.

Contents

List of Tables

List of Figures

Nomenclature

x_v	Position of the valve spool (m)
$\dot{x}_v$	Velocity of the valve spool (m/s)
w_v	Natural frequency (rad/s)
ξ	Servovalve damping ratio
K_v	Servovalve flow gain ($m^{3/2}/kg^{1/2}$)
k_v	Servovalve spool position gain (m/V)
w	Servovalve area gradient (m)
u	Input signal (V)
x_p	Actuator position (m)
$\dot{x}_p$	Actuator velocity (m/s)
V	Volumes of fluid contained in each chamber of the actuator (m^3)
V_t	Total volumes of fluid contained in both chambers of the actuator (m^3)
P_s, P_r	Supply and return pressures respectively (Pa)
P_1, P_2	Actuator chamber pressures (Pa)
P_L	Load pressure (Pa)
m	Combined mass of the position, actuator rod and load (kg)
d	Equivalent viscous damping coefficient, which describes the combined effect of the viscous friction between the piston and the cylinder walls (Ns /m)
A	Piston annulus area (m^2)
β	Fluid bulk modulus (Pa)
K_{e1}, K_{e2}, K_i	Leakage coefficients ($m^3/s/Pa^{1/2}$)
K_{1f}, K_{2f}, K_f	Linearized servovalve flow coefficients (m^2/s)
K_{1p}, K_{2p}, K_p	Linearized flow-pressure coefficients ($m^3/s/Pa$)
ρ	Density of hydraulic fluid (kg/m^3)
q_1, q_2	Servovalve control flows (m^3/s)
q_{el1}, q_{el2}	Actuator external leakage flows (m^3/s)
q_{il}	Actuator internal leakage flow (m^3/s)

Chapter 1

1. Introduction[1]

Valve-controlled hydraulic systems are widely used in industry due to their ability to produce high forces or torques with low inertia, reduced vibration and shock. They are popular in applications such as robotics, airplane flight control, and off-highway machines. Reliability and safety are important issues in above applications. A perfect diagnostic system is crucial to prevent the system from further deteriorating. As a consequence, fault detection and isolation (FDI) techniques for hydraulic systems have been growing for the past decade. In this thesis, the detection and isolation of faults associated with hydraulic actuators are studied.

With respect to hydraulic systems, faults cover a wide range, from component failure and fluid contamination, to pipe leakage and material wear (Skormin and Apone, 1995; Zhou et al., 2002; Zavarehi et al., 1999; Khan et al., 2002; Zhang and Jiang, 2002). Supply pressure fluctuation is a common type of fault that occurs in hydraulic systems. When the pump does not work properly, it causes the supply pressure to fluctuate and affect the performance of the actuator. In most commercial power supplies, the pressure is regulated by adjusting the pressure relief valve. Merritt (1967) indicated that for the valve controlled hydraulic systems the efficiency is high when the maximum load pressure is approximately 68% of nominal supply pressure. Therefore, when the pressure drops in supply pressure, the efficiency decreases as well and may cause the actuator to stall, in the worst case scenario. On the other hand, excessive supply pressure expedites the wear of hydraulic components and may lead to unexpected damages.

[1]The main portion of this Section has been taken from Ph.D. theses by An (2007) and Karpenko (2008).

There are different reasons for fluctuation of supply pressure. In some cases, the problem is caused by malfunctioning components of the pumps and valves. This leads to a change in pump's characteristics, such as the motor efficiency and total inertia (Yu et al., 1997). A nonlinear observer to detect a 10% drop in pump pressure was designed by Preston et al. (1996). Any damage in the pump or rest of the system may cause a drop in the pressure. In some cases, the supply pressure may be reduced to 40% (Crowther et al., 1998) and 60% (Niksefat and Sepehri, 2002) of the nominal value.

Contamination of fluids also causes problems by changing the effective bulk modulus (EBM) of the hydraulic fluid. EBM is associated with the hydraulic stiffness of the actuator. EMB can be sensitive to the air and water contamination which is a common problem with hydraulic fluid. Small amount of solid particles such as sand, dirt or metal does not affect the EBM much; however, water and/or air contaminants can change the EBM significantly. The bulk modulus of air is smaller than that of the hydraulic fluid and this can result in a reduction of the EBM of the hydraulic circuit. This reduces the stiffness of the hydraulic actuator and results in a slower response of the system when a load is applied. Skormin and Apone (1995) reported a drop of 20% in EBM where air contamination is present. Accumulation of water increases the EBM in hydraulic fluid since the density of water is much higher than that of the hydraulic fluid. This leads to an increase in the stiffness of the system. An increase of 10% in EBM can be caused by water contamination as reported by Skormin and Apone (1995). A change of 10% in EBM in a hydraulic drive system has been detected by Yu (1997).

The mechanical failures of servovalve which sends the control command to run the actuator, can also impact the performance of a fluid power system. These failures can be due to the wear or scoring of the valve spool and bushing. The increased friction can also change the spool position response time and affect the overall accuracy of the servovalve as reported by Zavarehi et al. (1999). They can diagnose the servovalve faults caused by component wear, which is the main cause for the change of the effective orifice area.

Wear of the actuator cylinder and the seals also cause changes in the friction characteristic which can significantly affect the dynamic performance of an actuator.

Lischinsky et al. (1999) showed that the friction can increase up to the 30% of the total driving force. Crowther et al. (1997) analyzed dynamic friction of the load using a bleed valve across the load and examined the change of friction coefficient with a trained neural network. The pilot spool friction in a two-stage servovalve was monitored by Zavarehi at al. (1999).

Research on mechanical and electrical failure is relatively sparse. Loss of magnetism of pump motor was studied by Skormin and Apone (1994). Zhou et al. (2002) presented loss of compressed air that was supplied to the reservoir in aircraft applications.

One of the greatest concerns regarding fluid power systems is the leakage of hydraulic fluid. Depending on its location, leakage can be classified into two types: (i) internal (cross-port) leakage where the fluid leaks to another part of the circulation within the system and (ii), external leakage where the fluid leaks out of the hydraulic circulation. Internal leakage fault is caused by the wear of piston seal that closes the gap between the moveable piston and the cylinder wall. Wear of the seals separating the actuator rod and the cylinder results in external leakage. External leakage can also be caused by failure of hydraulic supply line or connection between the valve and the actuator's chambers. Leakages, in general, influence the system's response and efficiency. While external leakage can, to an extent, be inspected visually, internal leakage cannot be detected until the actuator seal is completely damaged and the actuator fails to respond to a control signal. Internal leakage also produces heat which can change some of the system parameters such as EBM. Both external and internal leakages, affect the dynamic performance of the system since the entire flow is not available to move the piston against a load.

Although a great deal of work has been carried out on development of fault detection and isolation (FDI) systems (Isermann,1997), research on actuator leakage fault identification, in spite of its importance, is still limited. To name a few, Skormin et al. (1994,1995) constructed a linear model for a flight actuation system in which leakage in the hydraulic pump, was studied via simulations. Alternatively, Tan and Sepehri (2002) applied the Volterra nonlinear modeling concept to detect actuator leakage faults. The method reported by them required a model of leakage. Leakage is a type of nonideality

that cannot be modeled exactly (Garimella and Yao, 2005); therefore, the uncertainty associated with modeling a leak can become an issue within the framework of model-based fault detection. An and Sepehri (2005) studied the feasibility of using extended Kalman filter to detect actuator internal and external leakage faults. In their work, external and internal leakages were assumed to occur singly. They further extended this work to include both friction and loading as unknown external disturbances (2008). Although the requirement of using a model for leakage was removed in their work, the need for knowing the model of hydraulic actuator still remained a challenge. In order to overcome the difficulties associated with modeling nonlinear hydraulic systems, a linearized model with an adaptive threshold, to compensate for the error due to linearization, was used by Shi et al. (2005) to detect internal and external leakage faults. Le et al. (1998) proposed a neural network approach to detect both internal and external leakages in a hydraulic actuator, even when they occur at the same time; however, leakages could only be detected effectively over 1 lit/min. This rate is considered to be high. Small leakages are most useful for early detection of faults. Crowther et al. (1998) emulated the cross-port leakage of an actuator by opening a cross-line bleed valve between the annulus and the piston side. Werlefors and Medvedev (2008) utilized nonlinear observers with static feedback for external leakage detection in hydraulic servo systems by the use of simulation results.

1.1. Fault detection and isolation (FDI) in hydraulic systems[2]

There are many methods developed by researchers, for general fault detection and isolation (FDI) in hydraulic actuators since the safety of these systems is very important. FDI in Hydraulic system is relatively difficult due to the strong nonlinearity of hydraulic components. In spite of this, researchers have developed many approaches. Some of the most important methods are reviewed here.

1.1.1. Parametric model-based FDI schemes

One of the approaches for detection of a fault is to estimate the parameters of a system. In most cases, when a malfunction or a fault happens, the parameters of the system

[2] Some parts of this Section are taken from Ph.D. thesis by An (2007).

change. One of the most well-known parameter estimation techniques is the least squares (LS) algorithm or, in a more efficient form, the recursive least squares (RLS) algorithm. This algorithm is based on fitting a model, also known as auto regressive with exogenous input (ARX) model, to the real system. The task of parameter identification is to determine the estimation values of the parameters in the model according to the input-output data measured from the actual system input-output vectors. The accuracy of the model can be measured by the squares sum of the difference between the estimation outputs of model and the actual outputs of the system. By minimizing the squares sum of the difference, it is believed that the parameter identification of model is completed.

Since the implementation of a model is not unique, appropriate selection of the model is crucial for correct parameter estimates (Isermann, 1992). Yu (1997) used an ARX model for parameter estimation of a hydraulic torque rig. If the basic structure of the model is known, the order of the LS model or the dimension of parameter vector can be readily obtained. Otherwise, theoretical determination of the ARX model is impossible, which is common in actual applications. Obtaining a best-fit parameter vector without losing too much system information is the only feasible strategy. Hahn at al. (2001) applied an empirical model for parameters identification of a hydraulic actuator in a vehicle power transmission control system. The order of the ARX model was estimated by trial and error and starting from second order and ending with the tenth order.

One of the problems using the ARX model is that, if the order of the system is not known exactly, over or under fitting may occur, i.e., the parameters of the model are higher or lower than the actual system. In order to solve this problem, Tan and Sepehri (2002), constructed a Volterra nonlinear model with recursive estimation to estimate the parameters of that model.

A problem associated with the RLS algorithm is that, because of its linear nature, it is impossible to apply a system which is not linear with respect to its parameters. This algorithm can be modified by using a forgetting factor. The forgetting factor discards the old data when new data is available. The convergence of this algorithm is a concern

especially when there is not sufficient data from the nonlinear system. Son and Sepehri (2002), used the RLS algorithm with forgetting factor for pump pressure fluctuation fault when a sinusoidal signal was applied to the control valve.

1.1.2. Observer-based FDI schemes

To estimate the states of a linear system the concept of an observer has been developed. This concept has been extended for nonlinear systems as well. Different kinds of nonlinear observers have been proposed for state estimation and abnormal monitoring of nonlinear system. According to Garcia and Frank (1997), observers can be categorized as nonlinear identity observer (NIO), nonlinear unknown input observer (NUIO), disturbance-decoupling nonlinear observer (DDNO), adaptive nonlinear observer (ANO) and bilinear systems state observer (BSO).

NIO is asymptotically stable when a feedback gain matrix fulfils certain conditions (Adjallah et al. 1994). Gaddouna and Ouladsine (1997) reported the application of a linear state observer with unknown input for health monitoring of a hydraulic system. A similar approach was used by Hahn (2001) and the state model was identified using RLS algorithm.

NUIO puts the system model in an observable canonical form and a constant state transformation is constructed. Since transforming a general system into the required form is difficult, its application is limited. Khan et al. (2002) applied a nonlinear observer to detect incorrect supply pressure in hydraulic systems. DDNO has an improvement over NUIO since it uses a nonlinear state transformation rather than a linear one. DDNO linearizes the system around its operating point and approximates the system by omitting the second and higher order terms in the linear expansion of the system. Yu et al. (1994) used a bilinear fault detection observer for hydraulic motor loading system to detect the pump shaft speed sensor fault or changes effective viscous coefficient. Similar work has been conducted by Prestone et al. (1996).

ANO was developed to solve the problem of the weakness in detecting slowly developing faults. The application of a nonlinear model based adaptive robust observer to the fault detection and diagnosis of some common faults that occur in hydraulic

systems has been presented by Garimella and Yao (2005). The methodology was designed by explicitly taking into account the nonlinear system dynamics. Typical faults in hydraulic cylinders like sensor failure, fluid contamination, and lack of sufficient supply pressure were considered. They employed the estimate of the bulk modulus to detect fluid contaminants using the simulation results.

1.1.3. Kalman Filtering FDI schemes

The Kalman filter (KF) theory is another useful technique in nonlinear and stochastic system modeling such as navigation problems (Sridhar et al., 1993). KF can estimate the states of a system recursively. KF theory obtains a posteriori estimate of the current states by correcting a priori estimate using the current measurements of the outputs. If the system is fully observable, all the states of the system can be estimated using KF. For application of KF theory toward state estimation in nonlinear systems, an extension of it has been developed which is called extended Kalman filter (EKF). The basic idea of EKF is to linearize the system based on the latest estimation of system states. If the sampling interval is small enough, the output of EKF converges to the system output with satisfactory precision.

The successful application of EKF toward fluid power fault diagnosis has also been reported in many research articles. Zavarehi et al. (1999) showed the feasibility of applying an EKF algorithm on modeling a two-stage proportional servovalve. They showed that using EKF, it is possible to monitor key parameters of a servovalve. Zhang and Jiang (2002) developed an active fault tolerant control scheme for which an adaptive Kalman filter was employed to detect parameter changes due to faulty conditions. Chinniah et al. (2003) developed an EKF-based method to estimate actuator viscous friction as well as the EBM. Similarly, An and Sepehri (2003) studied the feasibility of using EKF to detect incorrect supply pressure. The scheme was then employed to detect actuator internal and external leakage faults (An and Sepehri, 2005). They further extended this work to include both friction and loading as unknown external disturbances (An and Sepehri, 2008). Wang and Syrmos (2008) developed an EKF-based estimation scheme to detect changes in torque motor equivalent and EBM.

The method used multiple models to estimate key parameters and assess against baseline values.

1.1.4. Signal processing based methods

Signal processing is an area that deals with the analysis of signals, in either discrete or continuous time. One of the most common signal processing methods is the Fourier transform which breaks down a signal into constituent sinusoids of different frequencies and amplitudes. With this decomposition, the most prevalent frequency components of a signal can be identified. Fourier analysis is limited as it has no time resolution. The short-time Fourier transform (STFT) covers some of the Fourier disadvantages. However, it has the disadvantage of fixed time-frequency resolution which is not desirable in many situations. Fast Fourier transform (FFT) has been used in some applications for fault detection. Al-Ammar et al. (2008) used FFT for fault detection in transformer impulse test. Lim et al. (2006) used FFT residuals of the vibration signals for the purpose of fault detection in induction motors.

Another well known signal processing method is wavelet transform (WT) which decomposes a signal into components of mother wavelets (Daubechies, 1992). Fourier transform decomposes a signal into scaled versions of a sine wave, whereas wavelet transform decomposes a signal into both scaled and shifted versions of a mother wavelet while maintaining the time information of the signal. The wavelet transform is so far the most popular technique for fault detection as it possesses both time and frequency localization properties. Despite the satisfactory results using the wavelet analysis in many applications, there are still some issues making this approach unsuitable in some applications. The first shortcoming of the wavelet method is the fact that the analysis depends on the choice of the mother wavelet function. This leads to a subjective, a priori, assumption on the characteristics of the investigated phenomenon (Loutridis, 2004). As a consequence, only signal features that correlate well with the shape of the wavelet function have a chance to lead to high value coefficients. All other features will be masked or completely ignored (Loutridis, 2004). The second shortcoming lies in the overlap between frequency bands associated with the wavelet signals. However, a high

order mother wavelet can reduce this overlapping. The application of discrete wavelet transform is simple and the patterns that arise from the application of this transform are clear and reliable, making it a robust tool for the diagnosis of the fault (Antonino-Davin et al., 2009). Moreover, the method is very easy to implement and the computational requirement are negligible (Antonino-Davin et al., 2009). A wavelet-based method for detection of sensor faults was developed by Zhang and Yan (2001). Wavelet transform for online hydraulic pump health diagnosis was employed by Gao et al. (2003). The pulsation pressure signal was used and faults contributing to pump malfunctioning were isolated based on the detail wavelet coefficients. Cusido et al. (2008) applied two different methods, based on short-time Fourier transform (STFT) and wavelet decomposition to investigate fault detection in induction machines. They concluded that the wavelet analysis achieves better results than STFT to detect faults associated with induction machines. Additionally, WT was shown to be more sensitive and robust than the FFT approach, in detecting faults associated with hydraulic pumps (Gao et al., 2005). However, to the best of the author's knowledge, there is no published report on comparing the capability of applying FFT and WT approaches for internal (cross-port) leakage detection in valve-controlled hydraulic actuators.

A recent signal processing technique for analyzing nonlinear and nonstationary time series data is Hilbert-Huang transform (HHT) developed by Huang et al. (1998). HHT starts by using empirical mode decomposition (EMD) to decompose a signal into a collection of intrinsic mode functions (IMFs) based on the local characteristic time scale of the signal. The IMFs represent the natural oscillatory mode embedded in the signal. Once the IMFs are obtained, the Hilbert transform (HT) can be applied to each individual IMF to obtain the instantaneous frequency and amplitude. The IMFs originates from the signal itself making the basis functions. The strength of this technique lies in its use of a posteriori-defined basis. Unlike traditional signal decomposition techniques such as wavelets and STFT that decompose the original signal into a series of constituents of fixed predetermined frequencies, the generated IMFs do not necessarily have constant frequency or amplitude, and it is for this reason that it is often difficult to assign any physical meaning to them. This can create problems for selecting the most suitable numbers of IMFs to be considered for detection

of the fault (Antonino-Davin et al., 2009). EMD is a relatively new method and applications of it have been reported in various fields, such as biomedical diagnostics (Balocchi et al., 2004), structural testing (Quek et al., 2003) and rotating machine fault diagnosis (Gao et al., 2008).

1.2. Objective of this research

Given the background mentioned earlier, it can be stated that hydraulic FDI is still attracting much attention. One of the greatest concerns regarding hydraulic actuators is the leakage of hydraulic fluid. Depending upon whether the hydraulic fluid is lost to the atmosphere or is displaced to another location within the hydraulic circuit, leakage can be classified as external or internal respectively. Research on actuator leakage fault identification in valve-controlled hydraulic actuator, in spite of its importance, is still limited and all the previous developed methods are model based. In valve-controlled hydraulic actuators flows of fluid to the actuator are controlled by a servovalve as opposed to pump-controlled hydraulic actuators in which flows of fluid are controlled by the pump itself.

The primary objective of this research is to develop a leakage diagnosis method that does not rely on model of the system or fault. Therefore, this research is initiated by employing three different signal processing methods for internal leakage detection. The first method is based on Fourier transform that breaks down a signal into constituent sinusoids of different frequencies and amplitudes. The second approach is wavelet analysis that decomposes an original signal into components of mother wavelets (Daubechies, 1992). The applicability of recently developed Hilbert-Huang transform (HHT) for internal leakage detection is also investigated. These techniques have recently drawn widespread attention as promising tools to deal with fault detection. To the best of the author's knowledge, there is no published report on health diagnosis of electrohydraulic actuators by the use of the mentioned methods. The main focus of this thesis is placed on using wavelet transform for both offline and online diagnosis of internal and external leakages.

Condition monitoring of hydraulic systems can be done using offline or online approaches. In offline approach, a structured predefined input signal is normally applied to the system under ideal (no-load) condition. Information on the system response, obtained over the entire test period, is then used for diagnosis. In the online approach, data on the states of the system are obtained and analyzed while the system is operating through its routine work cycle. Within the context of hydraulic actuation, this implies that the actuator must track reference position signals of various magnitude and duration and under various loading conditions. An example would be positioning of an aircraft control surface. As opposed to the offline approach where the diagnosis can be conducted using responses from the system under open-loop control, the online approach uses data from the system operating in a closed-loop position control mode. Thus, the diagnosis method should preferably function independently from the controller type or effectiveness. Furthermore, during the online approach, information is obtained from limited-duration segments of the continuous stream of measurements collected online. Online fault detection is more interesting than the offline detection, since it provides information about the health of the system without interrupting routine operation. Online fault detection can also provide a support for active fault tolerant controllers to reconfigure their control actions in response to changing conditions due to the occurrence of faults. Isolation of external and internal leakages in a multiple-fault environment using both offline and online applications is the final objective of this thesis.

The significance of the proposed approaches, as compared to previous studies, is as follows:

1-The method does not require any information about the model of hydraulic actuator, or the mechanism by which the internal leakage happens. This is very desirable since there are many situations in practice, where an accurate model is either unavailable or too complex to use.

2-The scheme requires only the measurement of pressure signal at one of the actuator chambers which is easy to obtain.

3-The method can detect internal leakages of small values that could not be identified by any of the previously published methods. Small leakages are most interesting for early detection of fault.

4- The method remains effective even with control systems that are tolerant to leakage fault given any reference step input or loading condition with regards to online diagnosis.

These aspects make the method very attractive from the industrial implementation viewpoint.

1.3. Thesis outline

The rest of this thesis is organized as follows:

Chapter 2, describes the valve-controlled hydraulic system on which all the experiments are performed along with the model of a typical hydraulic actuator, subject to external and internal leakages. The linearized model is provided to observe the influence of leakages on the dynamics of the actuator and to justify the use of pressure signal for analysis.

In Chapter 3, a short introduction to fast Fourier transform (FFT), wavelet analysis and Hilbert-Huang transform (HHT) is given. The methods are applied for fault detection in a laboratory-based hydraulic actuator. The focus is placed on internal and external leakages of the actuator.

Chapter 4 describes the offline detection of internal leakage based on FFT, wavelet transform and HHT. The methods analyze pressure signal at one side of the actuator. The superiority of both wavelet transform and HHT over the FFT is verified for internal leakage detection. The wavelet transform is shown to be better for internal leakage identification. The effects of changes in friction properties of the actuator on the proposed diagnosis methods are also studied.

An extension of wavelet based approach towards online detection of internal leakage fault is developed in Chapter 5. The more realistic case of an actuator that is driven in a closed-loop mode to track pseudorandom position references is considered. Additionally,

the actuator is subject to loading. Furthermore, limited-duration pressure signals are obtained using a sliding window technique applied to the stream of online measurements.

In Chapter 6, the application of wavelet transform to detect external leakage fault in hydraulic actuators is described. The method also examines the isolation of this fault from actuator internal leakage in a multiple-fault environment considering both offline and online applications.

The concluding remarks are given in Chapter 7.

Chapter 2

2. Description of the system under study

2.1. Experimental test rig

The hydraulic actuator test rig upon which all tests are conducted is shown in Fig. 2.1. Powered by a motor-driven hydraulic pump, the actuation system operates with the fluid pressure of 17.2MPa (2500 psi). The movement of the actuator (with a 610 mm stroke) is controlled by a high performance Moog D765 servovalve with a flow capacity of 34 lit/min at 21 MPa supply pressure. The valve accepts analog command signals from a high-speed PC equipped with a data acquisition board. The displacement of the actuator is obtained by a rotary optical encoder via a Metrabyte M5312 quadrature incremental encoder card and the chamber pressures are measured by sensors located at each side of the cylinder (Karpenko, 2008).

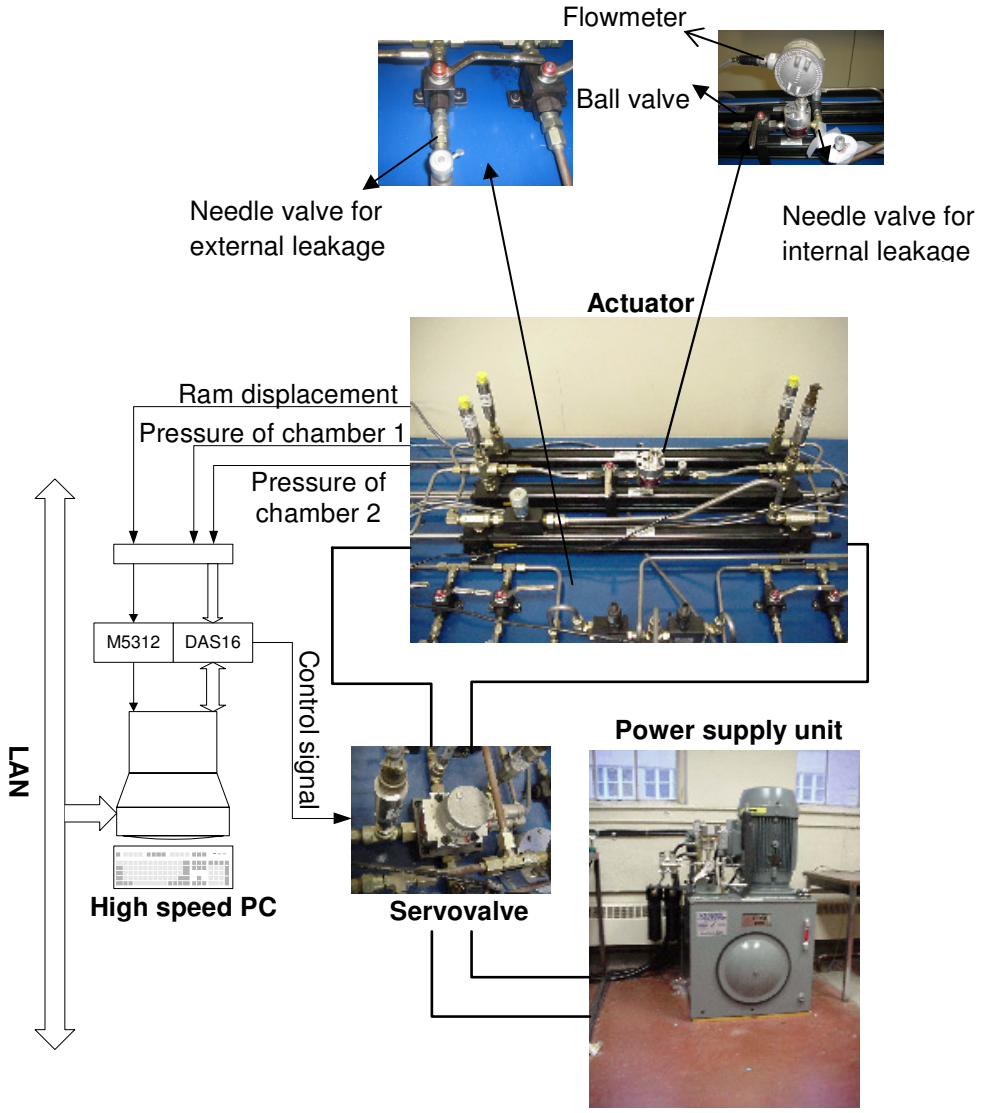

Figure 2.1: Test rig upon which all experiments are carried out (An, 2007).

Figure 2. 2 shows the schematic of the test rig as well as the manner in which a leakage fault is produced. Fig. 2.2 illustrates that to create an external leakage, a portion of the fluid flow from either side of the actuator, is bypassed to the reservoir by opening the corresponding needle valves (see the inset in Fig. 2.1). External leakage flows, q_{el1} and q_{el2}, are measured using positive-displacement flowmeters. An internal leakage is produced by bypassing fluid across the piston. This is achieved by connecting the two chambers of the actuator and controlling the flow by an adjustable needle valve (see

Fig. 2.1). The internal leakage flow rate q_{il} is also measured by a positive displacement flowmeter (JVA-KL series by AW Company) with a (0-7.6) lit/min range and accuracy of ±0.5% (An and Sepehri, 2008).

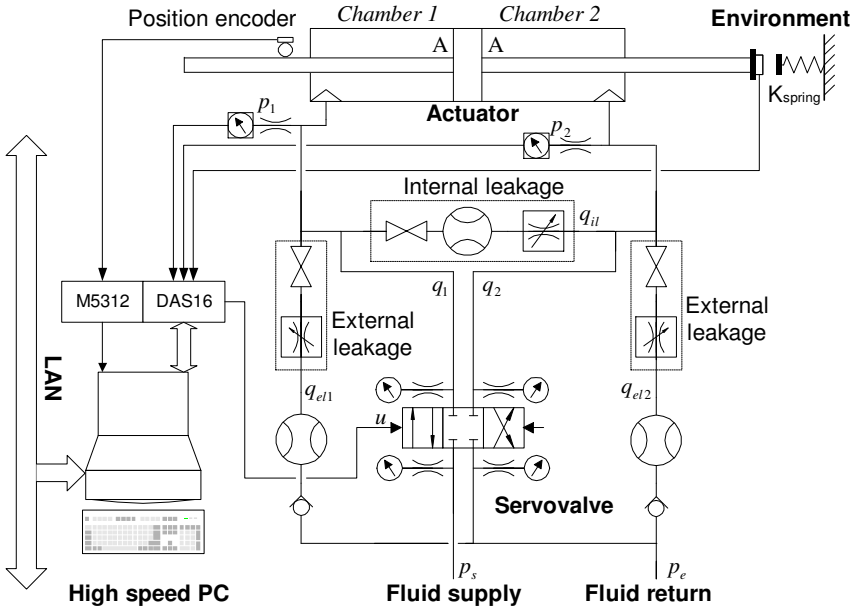

Figure 2.2: Schematic of test station. Internal and external leakage fault producing components are enclosed in dotted lines (An, 2007).

The schematic of a servovalve-controlled hydraulic actuator is shown in Fig. 2. 3

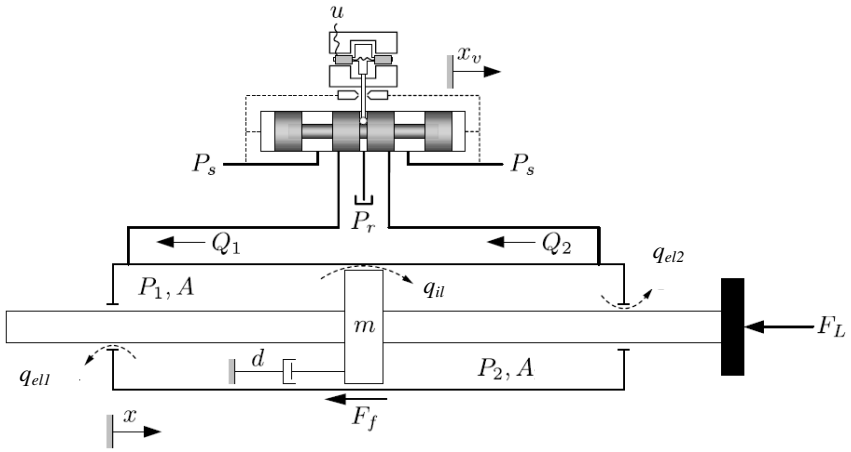

Figure 2.3: Schematic of a typical valve-controlled hydraulic actuator (Karpenko, 2008).

The equations that describe the actuator dynamics between control valve input u and the piston position x_p can be formed as (Karpenko, 2008):

$$\begin{aligned}
\dot{x}_p &= v_p \\
\dot{v}_p &= \frac{1}{m}(AP_1 - AP_2 - dv_p) \\
\dot{P}_1 &= \frac{\beta}{V + Ax_p}(q_1 - q_{il} - q_{el1} - Av_p) \\
\dot{P}_2 &= \frac{\beta}{V - Ax_p}(-q_2 + q_{il} - q_{el2} + Av_p) \\
\dot{x}_v &= v_v \\
\dot{v}_v &= -w_v^2 x_v - 2\xi w_v v_v + k_v w_v^2 u
\end{aligned} \tag{2.1}$$

Referring to (2.1), the system states are actuator position x_p, actuator velocity v_p and line pressures (P_1, P_2). Parameters m and d are the mass of the load and the effective viscous damping of the actuator, respectively. Parameter A refers to the annulus area of the piston and β is the effective bulk modulus of the hydraulic fluid. Parameter V is the volume of fluid contained on either side of the actuator when it is centered. The valve spool dynamics are expressed as a second-order lag where k_v is the valve spool position gain and parameters w_v and ξ represent the servovalve natural frequency and damping ratio, respectively.

For a valve with a critically-lapped spool and having matched and symmetrical orifices, the flows q_1 and q_2, through the valve follow the turbulent orifice equation. The nonlinear governing equations can be written in the following form (Karpenko, 2008):

$$\begin{aligned}
q_1 &= K_v w x_v \sqrt{\frac{P_s - P_r}{2} + \operatorname{sgn}(x_v)\left(\frac{P_s + P_r}{2} - P_1\right)} \\
q_2 &= K_v w x_v \sqrt{\frac{P_s - P_r}{2} + \operatorname{sgn}(x_v)\left(P_2 - \frac{P_s + P_r}{2}\right)}
\end{aligned} \tag{2.2}$$

where K_v is the valve flow gain, and w is the area gradient. The supply and tank pressures are denoted by P_s and P_r, respectively. The function sgn(x) is the sign function and defined as:

$$\text{sgn}(x)=\begin{cases}+1 & x>0\\ 0 & x=0\\ -1 & x<0\end{cases} \tag{2.3}$$

Leakage is a kind of nonideality that cannot be modeled exactly (Garimella and Yao, 2005). The actuator leakage is assumed to be turbulent or linear, and thus follows the following relationships (Karpenko, 2008):

$$\begin{aligned} q_{el1} &= K_{e1}\sqrt{P_1}\\ q_{el2} &= K_{e2}\sqrt{P_2}\\ q_{il} &= K_i\sqrt{|P_1-P_2|}\,\text{sgn}(P_1-P_2)\end{aligned} \tag{2.4}$$

or as (Meritt, 1967):

$$\begin{aligned} q_{el1} &= K_{e1}P_1\\ q_{el2} &= K_{e2}P_2\\ q_{il} &= K_i(P_1-P_2)\end{aligned} \tag{2.5}$$

where K_{e1}, K_{e2} and K_i are the leakage coefficients whose values depend on the severity of leakage fault.

Note that q_{il}, q_{el1} and q_{el2} are zero for an actuator under normal operating condition. However, when the piston seals begin to wear, leakage of hydraulic fluid across the sealing surfaces occurs. When a leakage occurs the dynamic performance of the system is affected; this is because the entire flow is no longer available to move the piston against the load.

Referring to (2.1), the first four equations collectively describe the nonlinear dynamics of the actuator, while the last two equations describe the valve spool dynamics. Considering the turbulent leakage equation and putting Eqs. (2.4) and (2.2) into Eq. (2.1), the final nonlinear equation is as follows:

$$
\begin{aligned}
&\dot{x}_p = v_p \\
&\dot{v}_p = \frac{1}{m}(AP_1 - AP_2 - dv_p) \\
&\dot{P}_1 = \frac{\beta}{V + Ax_p}(K_v w x_v \sqrt{\frac{P_s - P_r}{2} + \mathrm{sgn}(x_v)(\frac{P_s + P_r}{2} - P_1)} \\
&- K_i \sqrt{|P_1 - P_2|}\,\mathrm{sgn}(P_1 - P_2) - K_{e1}\sqrt{P_1} - Av_p) \\
&\dot{P}_2 = \frac{\beta}{V - Ax_p}(-K_v w x_v \sqrt{\frac{P_s - P_r}{2} + \mathrm{sgn}(x_v)(P_2 - \frac{P_s + P_r}{2})} \\
&+ K_i \sqrt{|P_1 - P_2|}\,\mathrm{sgn}(P_1 - P_2) - K_{e2}\sqrt{P_2} + Av_p) \\
&\dot{x}_v = v_v \\
&\dot{v}_v = -w_v^2 x_v - 2\xi w_v v_v + k_v w_v^2 u
\end{aligned}
\tag{2.6}
$$

Next the linearized model of nonlinear dynamic of the actuator using the first four equations in (2.6) is obtained. In deriving the linearized model, the assumption that the variation in the actuator displacement is quite small i.e., $V >> A|x_p|$ is used (Meritt, 1967). Using this assumption and linearizing about an operating point in the centre of the actuator, *o*, the linearized equations are:

$$
\begin{aligned}
&\Delta\dot{x}_p = \Delta v_p \\
&\Delta\dot{v}_p = \frac{1}{m}(A\Delta P_1 - A\Delta P_2 - d\Delta v_p) \\
&\Delta\dot{P}_1 = \frac{\beta}{V}(K_{1f}\Delta x_v - K_{1p}\Delta P_1 - \frac{K_{e1}}{2\sqrt{P_{10}}}\Delta P_1 - \frac{K_i}{2\sqrt{|P_{L0}|}}\Delta P_L - A\Delta v_p) \\
&\Delta\dot{P}_2 = \frac{\beta}{V}(-K_{2f}\Delta x_v - K_{2p}\Delta P_2 - \frac{K_{e2}}{2\sqrt{P_{20}}}\Delta P_2 + \frac{K_i}{2\sqrt{|P_{L0}|}}\Delta P_L + A\Delta v_p)
\end{aligned}
\tag{2.7}
$$

In (2. 7), Δ, denotes a perturbation from the operating point value, e.g., $\Delta x_p = x_p - x_{po}$. where $P_L = P_1 - P_2$ is the pressure applied to the load. K_{1f} and K_{2f} are valve flow gains:

$$K_{1f} = K_v w\sqrt{\frac{P_s}{2} + \text{sgn}(x_{v0})(\frac{P_s}{2} - P_{10})} \tag{2.8}$$
$$K_{2f} = K_v w\sqrt{\frac{P_s}{2} + \text{sgn}(x_{v0})(P_{20} - \frac{P_s}{2})}$$

K_{1p} and K_{2p} are the flow-pressure coefficients:

$$K_{1p} = \frac{K_v w|x_{v0}|}{2\sqrt{\frac{P_s}{2} + \text{sgn}(x_{v0})(\frac{P_s}{2} - P_{10})}} \tag{2.9}$$
$$K_{2p} = \frac{K_v w|x_{v0}|}{2\sqrt{\frac{P_s}{2} + \text{sgn}(x_{v0})(P_{20} - \frac{P_s}{2})}}$$

Assuming only external leakages on both sides and $k_{e1} = \frac{K_{e1}}{2\sqrt{P_{10}}}$, $k_{e2} = \frac{K_{e2}}{2\sqrt{P_{20}}}$ the following can be derived:

$$\begin{aligned}
\Delta\dot{x}_p &= \Delta v_p \\
\Delta\dot{v}_p &= \frac{1}{m}(A\Delta P_1 - A\Delta P_2 - d\Delta v_p) \\
\Delta\dot{P}_1 &= \frac{\beta}{V}(K_{1f}\Delta x_v - K_{1p}\Delta P_1 - k_{e1}\Delta P_1 - A\Delta v_p) \\
\Delta\dot{P}_2 &= \frac{\beta}{V}(-K_{2f}\Delta x_v - K_{2p}\Delta P_2 - k_{e2}\Delta P_2 + A\Delta v_p)
\end{aligned} \tag{2.10}$$

Taking the Laplace transform and denoting:

$$\begin{aligned}
\Delta P_1(s) &= \Delta P_1 \\
\Delta P_2(s) &= \Delta P_2 \\
\Delta V_p(s) &= \Delta V_p \\
\Delta X_v(s) &= \Delta X_v
\end{aligned} \tag{2.11}$$

The second equation in (2.10) can be written as:

$$s\Delta V_p = \frac{1}{m}(A\Delta P_1 - A\Delta P_2 - d\Delta V_p) \Rightarrow (ms + d)\Delta V_p = A(\Delta P_1 - \Delta P_2) \tag{2.12}$$

Substituting Eq. (2.12) into the following equation:

$$\begin{aligned}
sV\Delta P_1 &= \beta(K_{1f}\Delta X_v - K_{1p}\Delta P_1 - k_{e1}\Delta P_1 - A\Delta V_p) \\
sV\Delta P_2 &= \beta(-K_{2f}\Delta X_v - K_{2p}\Delta P_2 - k_{e2}\Delta P_2 + A\Delta V_p)
\end{aligned} \tag{2.13}$$

The following can be obtained:

$$sV\Delta P_1 = \beta(K_{1f}\Delta X_v - K_{1p}\Delta P_1 - k_{e1}\Delta P_1 - A^2\frac{(\Delta P_1 - \Delta P_2)}{ms+d})$$
$$sV\Delta P_2 = \beta(-K_{2f}\Delta X_v - K_{2p}\Delta P_2 - k_{e2}\Delta P_2 + A^2\frac{(\Delta P_1 - \Delta P_2)}{ms+d}) \quad (2.14)$$

Rearranging the above equations:

$$[Vs + \beta(K_{1p} + k_{e1}) + \frac{\beta A^2}{(ms+d)}]\Delta P_1 - \frac{\beta A^2}{(ms+d)}\Delta P_2 = \beta K_{1f}\Delta X_v$$
$$-\frac{\beta A^2}{(ms+d)}\Delta P_1 + [Vs + \beta(K_{2p} + k_{e2}) + \frac{\beta A^2}{(ms+d)}]\Delta P_2 = -\beta K_{2f}\Delta X_v \quad (2.15)$$

Now, solving the Eq. (2.15), the following transfer functions are obtained:

$$\frac{\Delta P_1}{\Delta X_v} = \frac{G_1}{H}$$
$$\frac{\Delta P_2}{\Delta X_v} = \frac{G_2}{H} \quad (2.16)$$

where

$$G_1 = [mK_{1f}Vs^2 + (\beta mK_{1f}K_{2p} + \beta mK_{1f}k_{e2} + VK_{1f}d)s + \beta A^2(K_{1f} - K_{2f}) + d\beta(K_{2p} + k_{e2})K_{1f}]\beta$$
$$G_2 = -[mK_{2f}Vs^2 + (\beta mK_{2f}K_{1p} + \beta mK_{2f}k_{e1} + VK_{2f}d)s + \beta A^2(K_{2f} - K_{1f}) + d\beta(K_{1p} + k_{e1})K_{2f}]\beta$$
$$H = V^2ms^3 + [m\beta V(K_{2p} + k_{e2}) + m\beta V(K_{1p} + k_{e1}) + dV^2]s^2 +$$
$$[\beta(K_{1p} + k_{e1})dV + m\beta^2(K_{1p} + k_{e1})(K_{2p} + k_{e2}) + Vd\beta(K_{2p} + k_{e2}) + V\beta A^2 + V\beta A^2]s$$
$$+ \beta^2(K_{1p} + k_{e1})(K_{2p} + k_{e2})d + \beta^2(K_{1p} + k_{e1})A^2 + \beta^2(K_{2p} + k_{e2})A^2$$

Assuming only internal leakage and defining $k_i = \frac{K_i}{2\sqrt{P_{L0}}}$,

$$\Delta\dot{x}_p = \Delta v_p$$
$$\Delta\dot{v}_p = \frac{1}{m}(A\Delta P_1 - A\Delta P_2 - d\Delta v_p)$$
$$\Delta\dot{P}_1 = \frac{\beta}{V}(K_{1f}\Delta x_v - K_{1p}\Delta P_1 - k_i\Delta P_L - A\Delta v_p)$$
$$\Delta\dot{P}_2 = \frac{\beta}{V}(-K_{2f}\Delta x_v - K_{2p}\Delta P_2 + k_i\Delta P_L + A\Delta v_p) \quad (2.17)$$

Taking the Laplace transform of the last two equations in (2.17) the following can be written:

$$sV\Delta P_1 = \beta[K_{1f}\Delta X_v - K_{1p}\Delta P_1 - k_i(\Delta P_1 - \Delta P_2) - A^2\frac{(\Delta P_1 - \Delta P_2)}{ms+d}] \tag{2.18}$$

$$sV\Delta P_2 = \beta[-K_{2f}\Delta X_v - K_{2p}\Delta P_2 + k_i(\Delta P_1 - \Delta P_2) + A^2\frac{(\Delta P_1 - \Delta P_2)}{ms+d}]$$

Rearranging the Eq. (2.18) as follows:

$$[Vs+\beta(K_{1p}+k_i)+\frac{\beta A^2}{(ms+d)}]\Delta P_1 - [\beta k_i + \frac{\beta A^2}{(ms+d)}]\Delta P_2 = \beta K_{1f}\Delta X_v \tag{2.19}$$

$$-[\beta k_i + \frac{\beta A^2}{(ms+d)}]\Delta P_1 + [Vs+\beta(K_{2p}+k_i)+\frac{\beta A^2}{(ms+d)}]\Delta P_2 = -\beta K_{2f}\Delta X_v$$

Now, if $K_{t1} = K_{1p} + k_i$ and $K_{t2} = K_{2p} + k_i$, and solving the Eq. (2.19), the following transfer functions are obtained:

$$\frac{\Delta P_1}{\Delta X_v} = \frac{G_1}{H} \tag{2.20}$$

$$\frac{\Delta P_2}{\Delta X_v} = \frac{G_2}{H}$$

where,

$$G_1 = [mK_{1f}Vs^2 + (\beta mK_{2p}K_{1f} + \beta mk_iK_{1f} + VK_{1f}d - m\beta K_{2f}k_i)s + \beta A^2(K_{1f} - K_{2f}) + d\beta(K_{2p}+k_i)K_{1f} - \beta dK_{2f}k_i]\beta$$

$$G_2 = -[mK_{2f}Vs^2 + (\beta mK_{1p}K_{2f} + \beta mk_iK_{2f} + VK_{2f}d - m\beta K_{1f}k_i)s + \beta A^2(K_{2f} - K_{1f}) + d\beta(K_{1p}+k_i)K_{2f} - \beta dK_{1f}k_i]\beta$$

$$H = V^2ms^3 + [m\beta V(K_{2p}+k_i) + m\beta V(K_{1p}+k_i) + dV^2]s^2 +$$
$$[\beta(K_{1p}+k_i)dV + m\beta^2(K_{1p}+k_i)(K_{2p}+k_i) + Vd\beta(K_{2p}+k_i) + V\beta A^2 + V\beta A^2 - m\beta^2k_i^2]s$$
$$+\beta^2(K_{1p}+k_i)(K_{2p}+k_i)d + \beta^2(K_{1p}+k_i)A^2 + \beta^2(K_{2p}+k_i)A^2 - d\beta^2k_i^2 - 2\beta^2A^2k_i$$

The above transfer functions are hard to interpret. In order to make the analysis more manageable $\Delta P_1 + \Delta P_2 \approx 0$ (Merrit, 1967), is further considered which leads to the following approach. The above assumption is valid if the actuator is symmetric.

Having the linearized model:

$$\begin{aligned}
\Delta\dot{x}_p &= \Delta v_p \\
\Delta\dot{v}_p &= \frac{1}{m}(A\Delta P_1 - A\Delta P_2 - d\Delta v_p) \\
\Delta\dot{P}_1 &= \frac{\beta}{V}(K_{1f}\Delta x_v - K_{1p}\Delta P_1 - \frac{K_{e1}}{2\sqrt{P_{10}}}\Delta P_1 - \frac{K_i}{2\sqrt{|P_{L0}|}}\Delta P_L - A\Delta v_p) \\
\Delta\dot{P}_2 &= \frac{\beta}{V}(-K_{2f}\Delta x_v - K_{2p}\Delta P_2 - \frac{K_{e2}}{2\sqrt{P_{20}}}\Delta P_2 + \frac{K_i}{2\sqrt{|P_{L0}|}}\Delta P_L + A\Delta v_p)
\end{aligned} \tag{2.21}$$

Considering only second and third equations in (2.21):

$$\begin{aligned}
\Delta\dot{v}_p &= \frac{1}{m}(A\Delta P_1 - A\Delta P_2 - d\Delta v_p) \\
\Delta\dot{P}_1 &= \frac{\beta}{V}(K_{1f}\Delta x_v - K_{1p}\Delta P_1 - k_{e1}\Delta P_1 + k_i(\Delta P_1 - \Delta P_2) - A\Delta v_p)
\end{aligned} \tag{2.22}$$

As mentioned $\Delta P_1 + \Delta P_2 \approx 0$, then one has:

$$\begin{aligned}
\Delta\dot{v}_p &= \frac{1}{m}(A2\Delta P_1 - d\Delta v_p) \\
\Delta\dot{P}_1 &= \frac{\beta}{V}(K_{1f}\Delta x_v - K_{1p}\Delta P_1 - k_{e1}\Delta P_1 + k_i(2\Delta P_1) - A\Delta v_p)
\end{aligned} \tag{2.23}$$

By taking the Laplace transform of the Eq. (2.23), the transform functions between the chamber one and two pressures, (P_1, P_2), and the spool valve displacement, x_v, are:

$$\frac{\Delta P_1(s)}{\Delta X_v(s)} = \frac{\beta K_{1f}(ms+d)/mV}{s^2 + [\frac{d}{m} + \frac{\beta(K_{1p}+k_{e1}+2k_i)}{V}]s + \frac{\beta d(K_{1p}+k_{e1}+2k_i)+2\beta A^2}{mV}} \tag{2.24}$$

$$\frac{\Delta P_2(s)}{\Delta X_v(s)} = \frac{-\beta K_{2f}(ms+d)/mV}{s^2 + [\frac{d}{m} + \frac{\beta(K_{2p}+k_{e2}+2k_i)}{V}]s + \frac{\beta d(K_{2p}+k_{e2}+2k_i)+2\beta A^2}{mV}} \tag{2.25}$$

Also, according to (Meritt, 1967)

$$d(K_{1p}+k_{e1}+2k_i) << A^2, d(K_{2p}+k_{e2}+2k_i) << A^2 \tag{2.26}$$

Then the above transfer function can be written in the following forms:

$$\frac{\Delta P_1(s)}{\Delta X_v(s)} = \frac{0.5(ms+d)K_{1f}\omega_h^2 / A^2}{s^2 + 2\zeta_{1h}\omega_h s + \omega_h^2} \tag{2.27}$$

$$\frac{\Delta P_2(s)}{\Delta X_v(s)} = \frac{-0.5(ms+d)K_{2f}\omega_h^2 / A^2}{s^2 + 2\zeta_{2h}\omega_h s + \omega_h^2} \tag{2.28}$$

where, ω_h, is the hydraulic natural frequency:

$$\omega_h = \sqrt{\frac{2\beta A^2}{mV}} \tag{2.29}$$

and, ζ_{1h}, ζ_{2h}, are the hydraulic damping:

$$\zeta_{1h} = \frac{dV\omega_h}{4\beta A^2} + \frac{m(0.5k_{el1} + k_{il} + 0.5K_{1p})\omega_h}{2A^2} \tag{2.30}$$

$$\zeta_{2h} = \frac{dV\omega_h}{4\beta A^2} + \frac{m(0.5k_{el2} + k_{il} + 0.5K_{2p})\omega_h}{2A^2}$$

Note that, due to the relationship between P_1 and P_2, it is quite often the case that $K_{1f} \approx K_{2f} = K_f$ and $K_{1p} \approx K_{2p} = K_p$.

To obtain the state equations, the same procedure as (Merrit, 1967) can be followed. Consider the nonlinear dynamic of the actuator:

$$\begin{aligned}
\dot{x}_p &= v_p \\
\dot{v}_p &= \frac{1}{m}(AP_1 - AP_2 - dv_p) \\
\dot{P}_1 &= \frac{\beta}{V + Ax_p}(q_1 - q_{il} - q_{el1} - Av_p) \\
\dot{P}_2 &= \frac{\beta}{V - Ax_p}(-q_2 + q_{il} - q_{el2} + Av_p)
\end{aligned} \tag{2.31}$$

Employing the assumption $V >> A|x_p|$ and using the last two equations of (2.31) the following equations can be derived:

$$\frac{V\dot{P}_1}{\beta} = (q_1 - q_{il} - q_{el1} - Av_p) \tag{2.32}$$

$$\frac{V\dot{P}_2}{\beta} = (-q_2 + q_{il} - q_{el2} + Av_p)$$

Then subtracting the above two equations the following equation can be obtained:

$$\frac{V(\dot{P}_1 - \dot{P}_2)}{\beta} = (q_1 + q_2 - 2q_{il} - q_{el1} + q_{el2} - 2Av_p) \tag{2.33}$$

Dividing both sides by two and defining $Q_L = \frac{q_1 + q_2}{2}$, then the state equations describing the dynamic system of the system are:

$$\begin{aligned} \dot{x}_p &= v_p \\ \dot{v}_p &= \frac{1}{m}(AP_L - dv_p) \\ \dot{P}_L &= \frac{4\beta}{V_t}(Q_L - q_{il} + \frac{q_{el2} - q_{el1}}{2} - Av_p) \end{aligned} \tag{2.34}$$

where $V_t = 2V$.

In this case Q_L depends upon the turbulent orifice equation:

$$Q_L = K_v w x_v \sqrt{\frac{P_s - \text{sgn}(x_v)P_L}{\rho}} \tag{2.35}$$

where ρ is the density of the hydraulic fluid, and P_s is the supply pressure. Term '$\text{sgn}(x_v)$' is used to account for the directionality of the valve spool.

Here, the same flow rate for external leakage is considered, i.e. $k_{e1} = k_{e2} = k_e$. By linearizing the nonlinear dynamics of the actuator about the operating point, *o*, the linearized state equations are:

$$\begin{aligned} \Delta\dot{x}_p &= \Delta v_p \\ \Delta\dot{v}_p &= \frac{1}{m}(A\Delta P_L - d\Delta v_p) \\ \Delta\dot{P}_L &= \frac{4\beta}{V_t}(K_f \Delta x_v - K_p \Delta P_L - k_i \Delta P_L - \frac{k_e}{2}\Delta P_L - A\Delta v_p) \end{aligned} \tag{2.36}$$

where K_f is valve flow gains:

$$K_f = K_v w \sqrt{\frac{P_s - \text{sgn}(x_{vo})P_{Lo}}{\rho}} \tag{2.37}$$

And K_p is the flow-pressure coefficients:

$$K_p = \frac{K_v w |x_{v0}|}{2\sqrt{\rho(P_s - \mathrm{sgn}(x_{vo})P_{Lo})}} \tag{2.38}$$

By taking the Laplace transform of the linearized equations, the transform function between the load pressure, P_L, and the spool valve displacement, x_v, is:

$$\frac{P_L(s)}{X_v(s)} = \frac{(ms+d)K_f \omega_h^2 / A^2}{s^2 + 2\zeta_h \omega_h s + \omega_h^2} \tag{2.39}$$

In (2.39), $\omega_h = \sqrt{\frac{4\beta A^2}{mV_t}}$ is the hydraulic natural frequency, $\zeta_h = \frac{dV_t}{8\beta A^2}\omega_h + \frac{m(K_p + k_i + 0.5k_e)}{2A^2}\omega_h$ is the hydraulic damping.

As can be seen, both the external and internal leakage faults contribute to the damping the system. Given the same amount of rate for external and internal leakages, the coefficient k_i is much bigger than k_e. This implies that internal leakage contributes more to damping the pressure responses than the external leakage. Furthermore, as opposed to internal leakage, a part of fluid is lost from the circuit when an external leakage occurs. This causes the static pressure signals to drop when an external leakage happens. External leakage can therefore be considered as a bias or drift fault. To further clarify this, the system described by nonlinear equations (2.1), is simulated by applying a step input of 1.5 V to the control valve. Table 2.1 shows the values of the parameters in the nonlinear model, which closely match those of the experimental test rig (An and Sepehri, 2005; 2008). Leakage rates are assumed to be linear (see Eq. 2.5).

The pressure response in chamber one is plotted in Fig. 2. 4, for normal and faulty conditions. To have similar external and internal leakages of ≈0.25 lit/min, the values for K_i and K_{ei} (i=1,2) are set to 2.5×10^{-11} $\mathrm{m}^3/\sqrt{\mathrm{Pa}}.\mathrm{s}$ and 5×10^{-13} $\mathrm{m}^3/\sqrt{\mathrm{Pa}}.\mathrm{s}$, respectively. As seen, the pressure signal with an internal leakage fault reaches the same steady-state value as the one under normal condition but with damped oscillation. On the other hand, the pressure signal for the actuator with external leakages, shows a transient behavior similar to the normal condition, but fails to reach the same steady-state value as the one

under normal operating condition. The same observation can be obtained by plotting the pressure signal in chamber two of the actuator. It is therefore concluded that external leakage alters the steady-state response (trend), while internal leakage contributes to changing the transient response of the pressure signal at either side of the actuator, an observation which has also been cited by others (Le et al., 1998). Furthermore, the Bode plot of the transfer function (2.27) is plotted in Fig.2.5, given the parameters in Table. 2.1. Note that for the normal operating condition $K_i = 0$. Assuming the turbulent equation for internal leakage, $K_i = 5.83 \times 10^{-8}\,\mathrm{m}^3/\sqrt{\mathrm{Pa}}.\mathrm{s}$ is used. As can be seen, an internal leakage changes the Bode magnitude around the hydraulic natural frequency, ω_h, which is found to be 70 Hz for the system under investigation. The Bode plot of transfer function (2.28) displays the same results.

The next Chapter will explain the proposed approaches for pressure signal processing. One of the main areas of signal processing is feature detection. Feature detection refers to detection of some particular type of behavior in a signal. If a signal feature of interest is not strong in the original signal, it is often necessary to process the signal to enhance the feature in question. Even when a feature of interest is strong, it can be helpful to develop some types of automatic detection procedure (Anant, 1997). This is referred to as signal processing. In the next Chapter, three signal processing methods will be explained.

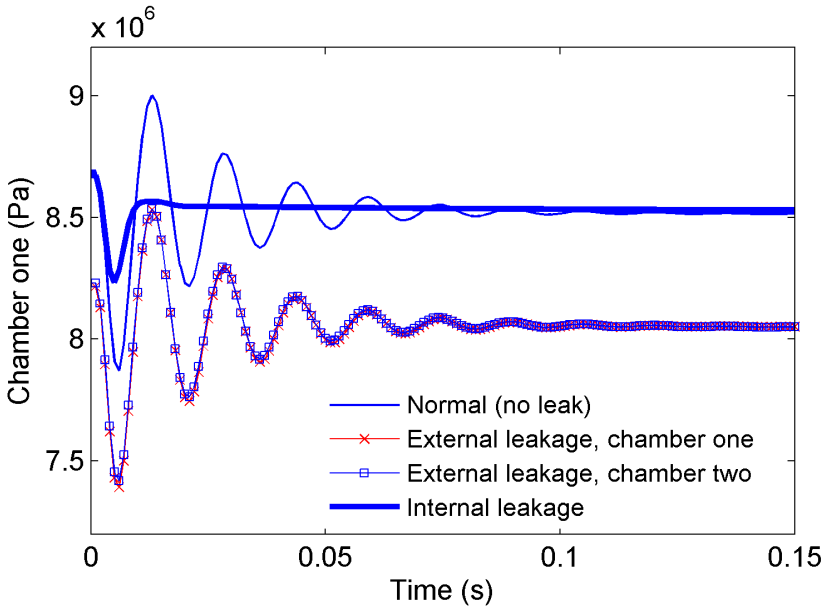

Figure 2.4: Pressure in chamber one under normal and different leakage type faults.

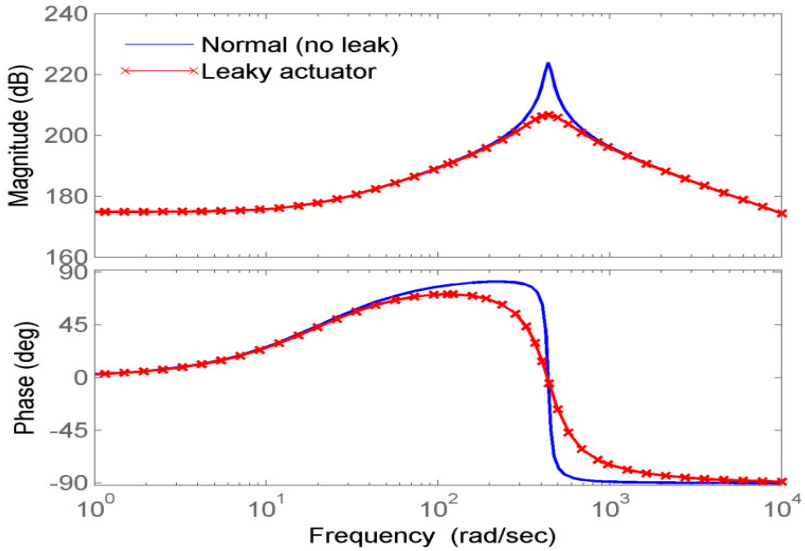

Figure 2.5: Bode plot of transfer function relating pressure to valve displacement for normal and leaky actuator.

Table 2.1: Parameters of hydraulic actuator

Parameter	**Symbol**	**Value**
Supply pressure	P_s	17.2 MPa
Combined mass of piston and rod	m	12.3 Kg
Viscous damping coefficient	d	250 N.sec/m
Actuator stroke	L	0.6 m
Piston area	A	633 mm^2
Volume of fluid in either side of actuator	V	234 cm^3
Valve orifice area gradient	w	20.75 mm^2/mm
Valve spool position gain	k_v	0.0406 mm/V
Valve flow coefficient	K_v	0.0292 $m^{3/2}/kg^{1/2}$
Valve natural frequency	w_v	150 Hz
Valve damping ratio	ξ	0.7
Fluid bulk modulus	β	689 MPa

Chapter 3

3. Methodologies of data processing

3.1. Introduction

Signal processing is a method that deals with analysis of signals, in either discrete or continuous time and to extract features from those signals. One of the most common signal processing methods is the Fourier transform. Another well known signal processing method is wavelet analysis. A novel signal processing technique for analyzing nonlinear and nonstationary time series data is Hilbert-Huang transform. In this Chapter, mentioned signal processing methods used for the analysis of pressure signals are described.

3.2. Fourier analysis

Fourier analysis breaks down a signal into constituent sinusoids of different frequencies. It can be categorized as either continuous Fourier transform (CFT) or discrete Fourier transform (DFT). The Fourier transform of a continuous time signal, $x(t)$, is defined as:

$$X(w) = \int_{-\infty}^{+\infty} e^{-jwt} x(t) dt \tag{3.1}$$

$X(w)$, is a complex decomposition of the original signal $x(t)$, into constituent exponential functions at each frequency w. The DFT, on the other hand, converts a sampled time representation of a signal into a sampled frequency representation. The

DFT shows a relationship between frequency and amplitude of a signal. The DFT is given as follows:

$$X[n] = \sum_{k=0}^{N-1} x[k]\, e^{-2\pi i n k / N} \qquad n = 0,1,..., N-1 \tag{3.2}$$

where $x[k]$ is the original signal and N is the length of the sampled original signal. For efficient calculation of the DFT, a fast Fourier transform (FFT) algorithm can be used (Proakis and Manolakis, 2007). Fourier analysis has been shown to be extremely useful for the analysis of periodic, time-invariant or stationary phenomena.

For example consider the following signal which consists of two cosine components of 100Hz and 30 Hz (Gao et al., 2008):

$$x(t) = \cos(2\pi \times 100t) + 0.5 \times \sin(2\pi \times 30t) \tag{3.3}$$

The original signal alone with its FFT is shown in Fig.3.1. This figure shows that the FFT of the original signal reveals the two dominant frequency components. By using the Fourier analysis, the most prevalent frequency components of a signal can be observed. The serious drawback of the Fourier analysis is that the time information of a signal is lost when it is transformed to the frequency domain (The Mathworks, 2005). By observing Fourier transform of a signal, it is impossible to see *when* a particular event happened. When the signal properties do not change over time — which is called a *stationary* signal — this does not cause any trouble; however, most signals in practice have many nonstationary or transitory characteristics such as: drift, trends, abrupt changes, etc (The Mathworks, 2005). If these characteristics are important, the Fourier analysis is useless. This deficiency of the Fourier analysis can be solved to some extent by analyzing a small section of the signal at a time—a technique called *windowing* the signal (The Mathworks, 2005). This leads to an analysis technique known as the short-time Fourier transform (STFT). The problem with the STFT is that the size of the time-window is the same for all frequencies. This problem can be removed using wavelet analysis, which will be explained next.

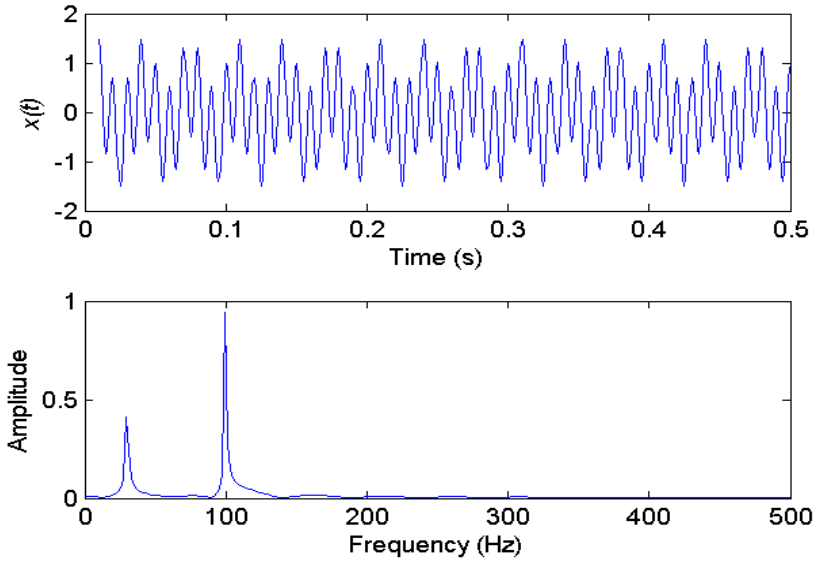

Figure 3.1: Signal, $x(t)$ as in (3.3), and its FFT.

3.3. Wavelet transform

This Section will give an overview of the wavelet transform used throughout this thesis. A wavelet is an oscillatory waveform of effectively limited duration with an average value of zero (Burrus et al., 1998). The energy of a wavelet is concentrated in time to be suitable for the analysis of transient, nonstationary or time-varying phenomena. Wavelet still has the characteristic of an oscillating wave but also has the ability to allow time and frequency analysis simultaneously with a flexible mathematical background (Burrus et al., 1998).

As mentioned in Section 3.2, Fourier analysis breaks down a signal into sine waves of different frequencies, whereas wavelet analysis breaks down a signal into shifted and scaled versions of the original (or mother) wavelet (The Mathworks, 2005). In Fig. 3.2, the basis function for wavelet transform (Daubechies-8 mother wavelet) is shown:

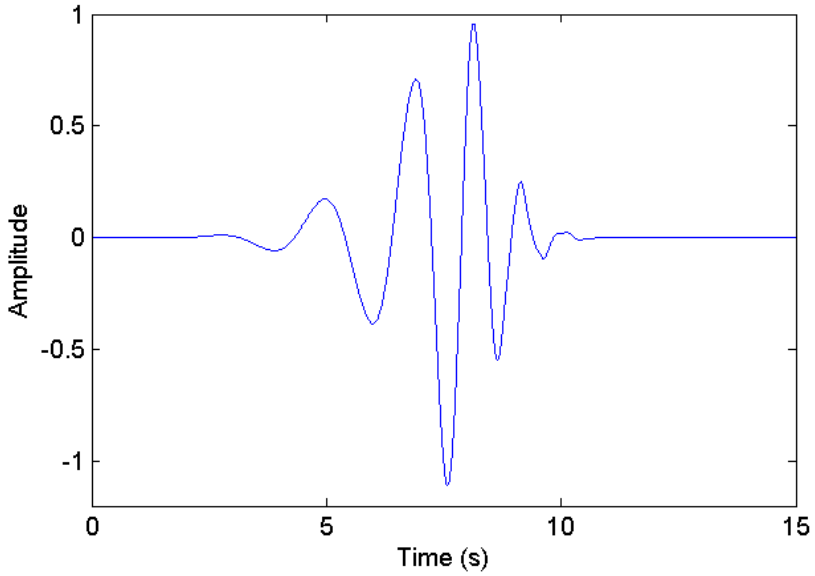

Figure 3.2: Daubechies mother wavelet.

Wavelet analysis uses a windowing technique with variable-sized regions. The wavelet analysis allows long time intervals when low-frequency information is required, and shorter regions when high-frequency information is needed (The Mathworks, 2005). In Fig.3.3, the time domain, frequency-domain, STFT and wavelet views of signal analysis are shown.

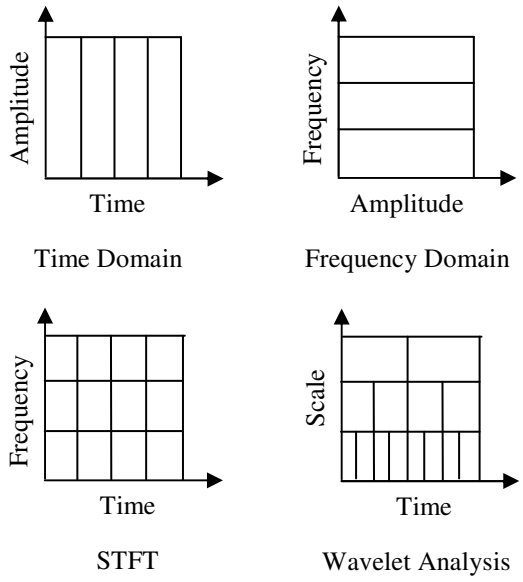

Figure 3.3: Time, Frequency, STFT and wavelet view of signal analysis.

3.3.1. Continuous wavelet transform (Burrus et al., 1998)

The continuous wavelet transform (CWT) is defined as the sum over all time of the signal multiplied by the scaled and shifted versions of the wavelet function ψ. The CWT of a signal $x(t)$ is defined as:

$$CWT(a,b) = \int_{-\infty}^{+\infty} x(t)\psi_{a,b}^{*}(t)dt \tag{3.4}$$

With an inverse transform:

$$x(t) = \int_{-\infty}^{+\infty}\int_{-\infty}^{+\infty} CWT(a,b)\psi_{a,b}^{*}(t)dadb \tag{3.5}$$

where

$$\psi_{a,b}(t) = |a|^{-1/2}\psi(\frac{t-b}{a}) \tag{3.6}$$

$\psi(t)$ is the mother wavelet, the asterisk in Eq. (3.5) denotes a complex conjugate, and $a,b \in R,\ a \neq 0$ (R is a real continuous number system) are the *scaling* and *shifting* parameters, respectively. $|a|^{-1/2}$ is the normalization value of $\psi_{a,b}(t)$ so that if $\psi(t)$ has a unit length, then its scaled version $\psi_{a,b}(t)$ also has a unit length.

The basis functions are localized in frequency for both Fourier and wavelet transforms. The most important difference between these transforms is that wavelet functions are localized in time and Fourier basis functions are active for all the time.

This localization feature, along with wavelets localization of frequency, makes wavelet to be suitable in different applications such as data compression, detecting features in signals and de-noising (Burrus et al., 1998).

3.3.2. Discrete wavelet transform (Ukil and Zivanovic, 2006)

Instead of continuous scaling and shifting, the mother wavelet can be scaled and shifted discretely by choosing $a = a_0^m, b = na_0^m b_0, t = kT$ in Eqs. (3.5) and (3.7), where T is the sampling time and $k,m,n \in Z$ (Z is the set of positive integers). Then, the discrete wavelet transform (DWT) is defined as:

$$DWT(m,n) = a_0^{-m/2}[\sum x(k)\psi^*(\frac{k - na_0^m b_0}{a_0^m})] \tag{3.7}$$

By careful selection of a_0 and b_0, the scaled and shifted mother wavelets constitutes an orthonormal basis. An orthonormal basis is a basis that consists of a set of vectors **S** such that **u**・ **v** = 0 (here '・' indicates the dot product) for each distinct pair of **u**, **v**. $a_0 = 2$ and $b_0 = 1$ can be chosen to constitute the orthonormal basis to have the WT called a *dyadic-orthonormal* WT. As will be seen, with this choice of a_0 and b_0, there exists a well-known algorithm, known as *multiresolution signal* decomposition (Mallat, 1989) technique, to decompose a signal into scales with different time and frequency resolution.

The inverse transform of DWT for any $x(t) \in L^2(R)$ is:

$$x(t) = \sum_{j=1}^{l}\sum_{k=-\infty}^{+\infty} d_j(k)\psi(2^{-j}t - k) + \sum_{k=-\infty}^{+\infty} a_l(k)\varphi(2^{-l}t - k) \tag{3.8}$$

The function $\psi(t)$ is known as the mother wavelet, while $\varphi(t)$ is known as the scaling function. The set of functions $\{\psi(2^{-j}t - k), \varphi(2^{-l}t - k) \mid j \le l, j, k, L \in Z\}$, where Z is the set of integers, is an orthonormal basis for $L^2(R)$.

The $a_l(k)$ are known as the approximation coefficients at scale l, while $d_j(k)$, are known as the detail coefficients at scale j. The approximation and detail coefficients can be expressed as:

$$a_l(k) = \frac{1}{\sqrt{2^l}}\int_{-\infty}^{+\infty} x(t)\varphi(2^{-l}t - k)dt \tag{3.9}$$

$$d_l(k) = \frac{1}{\sqrt{2^j}}\int_{-\infty}^{+\infty} x(t)\psi(2^{-j}t - k)dt$$

3.3.3. Example of wavelets

Among many wavelet functions, only three examples are presented here. Fig. 3.4 illustrates three different types of wavelet basis functions along with their scaling functions (The Haar, Daubechies of order 8 =db8, Symlets of order 6=sym6).

The Haar basis is the simplest wavelet basis. The Haar basis functions are members of many wavelet families, such as Daubechies wavelets and spline wavelets (Alle Meije Wink, 2004). The scaling function $\psi(t)$ and the wavelet $\varphi(t)$ are given by:

$$\varphi(t) = \begin{cases} 1 & 0 \le t < 1 \\ 0 & otherwise \end{cases} \qquad \psi(t) = \begin{cases} 1 & 0 \le t < 0.5 \\ -1 & 0.5 \le t < 1 \\ 0 & otherwise \end{cases} \tag{3.10}$$

Figure 3.4 shows the Haar scaling and wavelet functions. Haar basis functions have a number of favorable properties. They are symmetric and have compact support. Disadvantages of the Haar basis functions are: poor approximation, and bad localization in the frequency domain (Alle Meije Wink, 2004).

Daubechies' wavelets (Daubechies, 1988) are among the most popular wavelets in use. They are classified by their number of vanishing moments which will be introduced later. Daubechies-1 is the Haar basis. Daubechies-2 has two vanishing moments. Daubechies' filters are the shortest filters that generate an orthogonal wavelet basis, given a number of vanishing moments (Alle Meije Wink, 2004). As a result, Daubechies' wavelets can be implemented efficiently via the fast wavelet transform (FWT) which will be discussed later. Better localization in the frequency domain and better approximation is obtained by using higher vanishing numbers (at the cost of longer filters). The symlets are almost symmetrical wavelets proposed by Daubechies. The properties of the two wavelet families are similar (Alle Meije Wink, 2004).

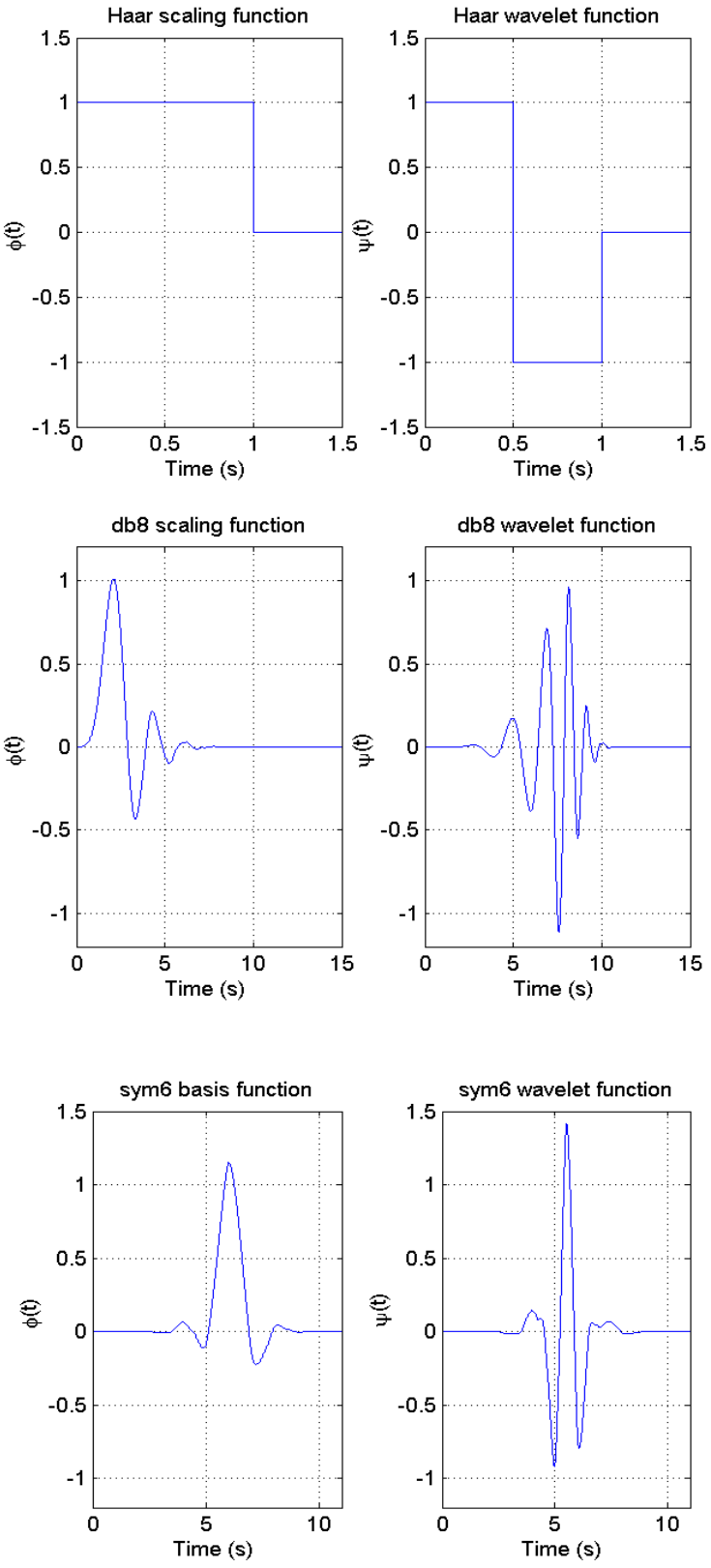

Figure 3.4: Different types of wavelet basis functions along with their scaling functions (The Haar, Daubechies of order 8 =db8, Symlets of order 6=sym6).

3.3.4. Vanishing moments

The smoothness of wavelet function and the flatness of the frequency response of wavelet filters depend on the number of vanishing moments. A wavelet with p vanishing moments, fulfills the following equation:

$$\int_{-\infty}^{+\infty} t^m \psi(t)dt = 0 \qquad for \;\; m = 1,..., p-1 \tag{3.11}$$

The length of the filters, in general, increases with the number of vanishing moments; and, the complexity of computing the DWT coefficients increases with the size of the wavelet filters (Rao, 2001).

3.3.5. Fast wavelet transform algorithm (Rao, 2001; Ukil and Zivanovic, 2006)

The discrete wavelet transform (DWT) coefficients can be computed by using Mallat's fast wavelet transform algorithm (Mallat, 1989). This algorithm is sometimes referred to as the *two-channel sub-band coder*. To explain the implementation of the fast wavelet transform algorithm consider the following equations (Burrus et al., 1998):

$$\varphi(t) = \sum_{k=-\infty}^{+\infty} h(k)\sqrt{2}\varphi(2t-k)$$

$$\psi(t) = \sum_{k=-\infty}^{+\infty} g(k)\sqrt{2}\varphi(2t-k) \tag{3.12}$$

$$\sum_{k=-\infty}^{+\infty} h(k)h(k-2m) = \delta(m) \qquad if \;\; and \;\; only \;\; if \qquad |H(w)|^2 + |H(w+\pi)|^2 = 2$$

where $H(w)$ is the discrete time Fourier transform of $h(k)$ defined as:

$$H(w) = \sum_{k=-\infty}^{k=+\infty} h(k)e^{-jwk} \tag{3.13}$$

As the wavelets should span orthogonal complement spaces, the wavelet coefficients are required to be related to the scaling function coefficients as:

$$g(k) = (-1)^k h(1-k) \tag{3.14}$$

The first equation in (3.12) is known as the *twin-scale relation* (or the dilation equation) and defines the scaling function φ. The next equation relates the wavelet ψ to the scaling function φ. The third equation expresses the condition required for the wavelet to be orthogonal to the scaling function and its translates.

The coefficients $h(k)$ in the above equations is the impulse response coefficients for a low pass filter which must fulfill the following conditions:

$$\sum_{k=-\infty}^{+\infty} \left|h(k)\right|^2 = 1 \quad and \quad \sum_{k=-\infty}^{+\infty} h(k) = \sqrt{2} \tag{3.15}$$

A signal can be decomposed into its detailed and smoothed versions using the multiresolution signal decomposition (MSD) technique (Mallat, 1989). Let $x[n]$ be a discrete-time signal; then MSD technique decomposes the signal in the form of WT coefficients at scale 1 into $a_1[n]$ and $d_1[n]$. $a_1[n]$ is the approximation version of the original signal and $d_1[n]$ is the detailed version of the original signal $x[n]$ which are defined as:

$$a_1[n] = \sum_k h[k-2n]x[k], \tag{3.16}$$

$$d_1[n] = \sum_k g[k-2n]x[k],$$

where $h[n]$ and $g[n]$ are the associated low- and high pass filter coefficients that decompose $x[n]$ into $a_1[n]$ and $d_1[n]$, respectively. Downsampling is done in the process of decomposition so that the resulting $a_1[n]$ and $d_1[n]$ are each *n*/2 point signals. The next higher scale decomposition will be based on $a_1[n]$.

The decomposition process can be continued, with successive approximations being decomposed in turn, so that the original signal is broken down into many lower resolution components. This is called the *wavelet decomposition tree* (Mallat, 1998).

MSD technique can be realized with the cascaded *quadrature mirror filter* (QMF) banks (Strang and Nguyen, 1996). Each QMF pair consists of two finite impulse response filters; the first is a low-pass filter (LPF) and the second is a high-pass filter (HPF). The QMF pair divides the input signal into low- and high-frequency components at the dividing point of halfway between 0Hz and half the data sampling frequency. The output of the low-pass filter is the approximation version of the input signal and can be used as the next QMF pair's input. The output of the high-pass filter is the detail version of the original signal. Fig. 3.5 shows the MSD technique and the QMF pairs.

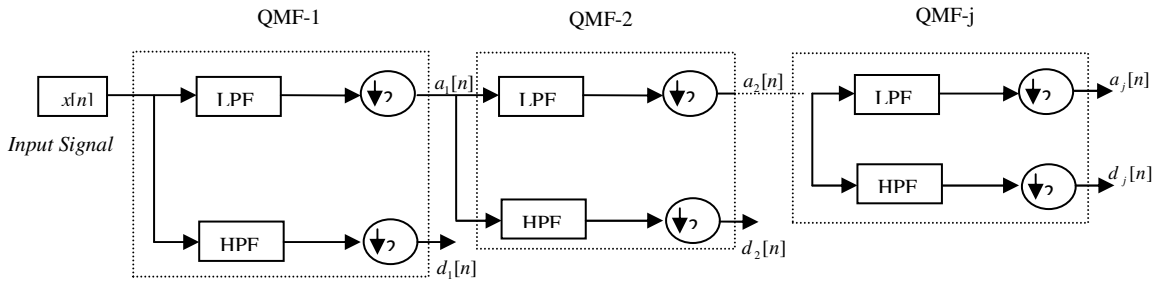

Figure 3.5: Multiresolution signal decomposition.

For example in Fig. 3.6 the frequency response of the db8 low- and high pass filters are plotted. This figure shows that the high pass filter suppresses the low frequencies and the low pass filter suppresses the high frequencies.

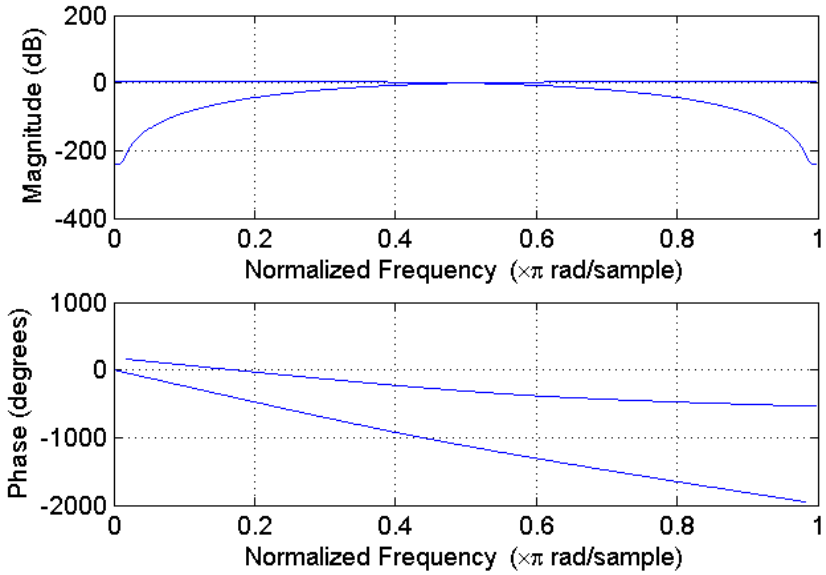

Figure 3.6: The frequency response of the db8 low- and high pass filters.

Wavelet decomposition tree can reveal valuable information about a signal. Fig. 3.7 shows the wavelet decomposition to level 2 of a sample signal S. As can be seen the original signal is decomposed into low- and high frequency components with different resolutions. Since the analysis process is iterative, it can be continued indefinitely in theory. In reality, the decomposition can only proceed until the vector has a single sample. Normally, there is no advantage obtained in decomposing a signal beyond a certain level. The selection of the optimal decomposition level depends on the nature of the signal being analyzed or another suitable criterion (The Mathworks, 2005). This is important to determine which frequency bands carry the signature signals. The

appropriate levels of decomposition should be able to effectively isolate either the low or high frequency noises and greatly improve the sensitivity of wavelet analysis (Gao et al., 2003). Wavelet analysis allows a segment of the original signal to be decomposed into 2^j different signal encoding schemes, and the frequency band width of decomposed signals in those packets is determined by dividing the sampling frequency by 2^j, where j is the decomposition level. For extracting an informative sample segment from the original signal, each packet should carry a sufficient length of data sequence (Gao et al., 2003).

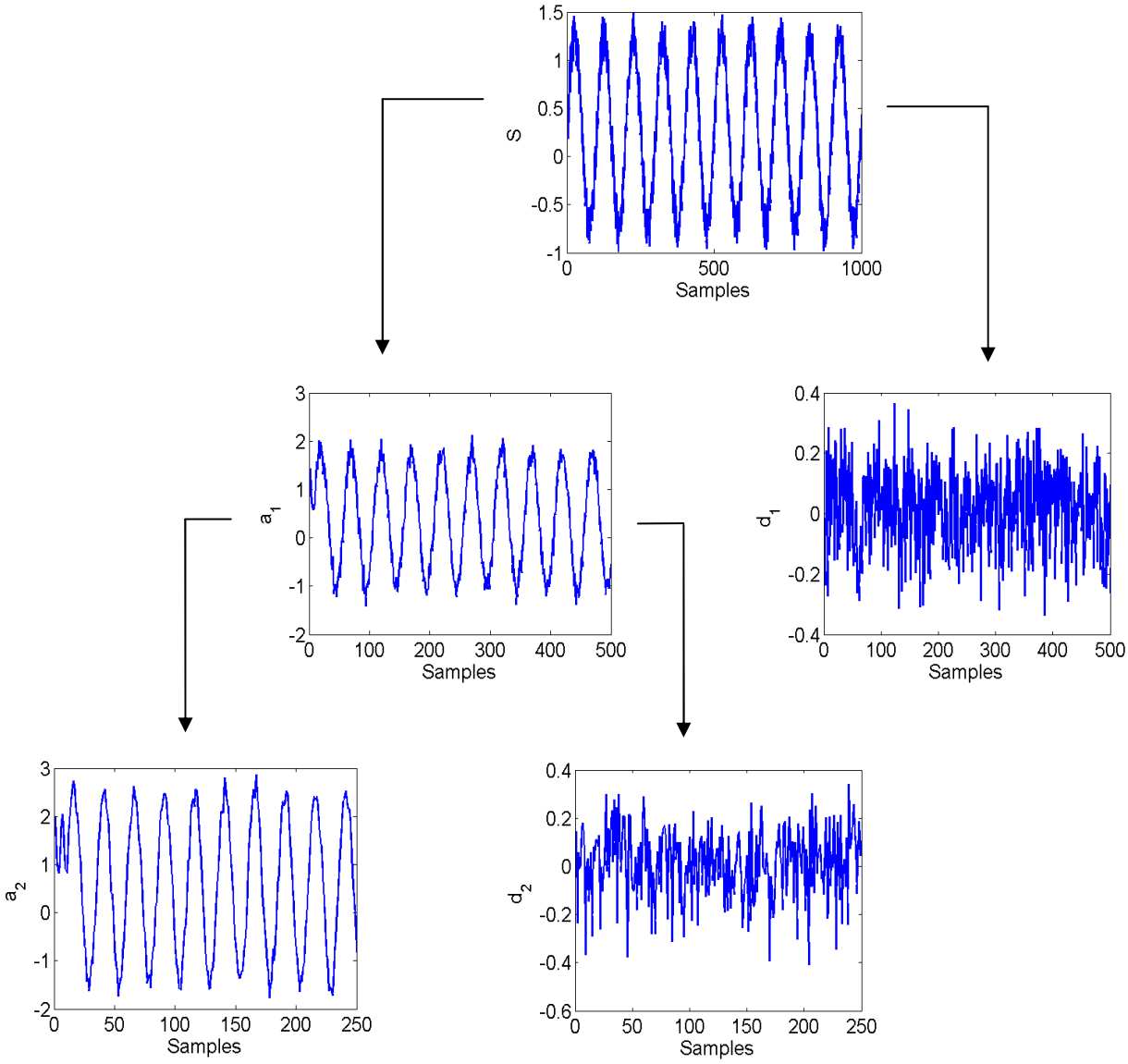

Figure 3.7: Level 2 decomposition of sample signal S.

3.3.6. Choice of mother wavelets

The choice of wavelet depends on the nature of the particular application. For smooth signals, a wavelet that is itself smooth is needed. In contrast, signals that contain discontinuities are better analyzed using wavelets with good spatial localization to accurately map rapid changes in the signal (Thomas A. Ridsdill-Smith, 2000). There are other useful properties that the wavelets can possess. In order to have a sparse representation of a signal using wavelet analysis, a function has to be selected, which best resembles the features of the signal under investigation (Daubechies, 1992). Thus, the shape of the wavelet function must be similar to that of the signal. Certain wavelets can be optimized for particular applications, such as the Perrier wavelet for potential-field data (Thomas A. Ridsdill-Smith, 2000).

3.3.7. Properties of wavelets

A number of issues are important in designing wavelet functions. This section explains these issues and their effects.

Linearity: The WT is *linear* which means that the transform of the sum of two signals equals the sum of their transforms. Furthermore, if the scaling function and wavelet form an orthonormal basis, there is a Parseval's theorem that relates the energy of the signal $x(t)$ to the energy of the wavelet coefficients as (Burrus et al., 1998):

$$\int \left|x(t)\right|^2 dt = \sum_k \left|a_l(k)\right|^2 + \sum_j \sum_k \left|d_j(k)\right|^2 \tag{3.17}$$

Smoothness: Smoothness of wavelet functions is very important. If the wavelets have discontinuities or strong singularities, then coefficient quantization errors will cause these discontinuities and singularities to appear in analyzed signals. These effects are highly objectionable, particularly in smooth regions of signals (Zafarifar, 2002).

Approximation accuracy: Accuracy of approximation is another important design criterion. Wavelet analysis allows constructing smooth, compactly supported bases that can exactly reproduce any polynomial up to a given degree. If a continuous-valued function $x(t)$ is locally equal to a polynomial, then with only a few wavelet coefficients

that portion of $x(t)$ can be exactly reproduced. The degree of a polynomial that can be exactly reproduced is determined by the number of vanishing moments of the wavelet. Compactly supported bases for $L^2(R)$ for which the wavelet has p vanishing moments can locally reproduce polynomials of degree p – 1 (Davis and Nosratinia, 1998; Zafarifar, 2002).

Compact support: Compactly supported scaling function and wavelet function lead to finite filters (FIR).

3.3.8. Advantages of using wavelets

Wavelet transform has several advantages. This part is taken from (Burrus et al., 1998 and Zafarifar, 2002):

1- The size of wavelet coefficients $a_j(k)$ or $d_j(k)$ drop off rapidly with j and k for a large class of signals. This property makes wavelets effective in signal and image compression, denoising and detection. Donoho (1993) showed that the wavelets are near optimal for a wide class of signals for compression, denoising and detection.

2- A more accurate local description and separation of signature characteristics can be obtained by wavelet. As opposed to a Fourier coefficient which cannot represent temporary events, a wavelet coefficient represents a component that is itself local and easier to interpret.

3- For each individual application, a suitable mother wavelet can be found since there is not just one wavelet.

4- Wavelets are smooth, which can be characterized by their number of vanishing moments.

5- Discrete wavelet transform and its inverse can be calculated with fast and efficient algorithms.

6- Wavelets are based on multi-resolution signal analysis. Wavelet decomposition allows analyzing a signal at different resolution levels (scales), which results in superior objective and subjective performance.

3.4. Hilbert-Huang transform (HHT)

Recently, Huang et al. (1998) proposed a new signal processing, known as Hilbert-Huang transform (HHT), which consists of two parts: the empirical mode decomposition (EMD) and the Hilbert spectral analysis (HSA). The EMD is a multi-resolution decomposition technique that decomposes a non-stationary and nonlinear signal into basis functions that are originated from the signals itself. Unlike Fourier-based method which uses sines and cosines predefined basis functions, this technique uses *posteriori*-defined basis functions (Ayenu-Prah and Attoh-Okine, 2009). The EMD basis functions are also known as intrinsic mode functions (IMFs). IMFs are locally non-overlapping time-scale components having instantaneous frequency and amplitude defined for them at each point (Ayenu-Prah and Attoh-Okine, 2009). In addition, IMFs are almost orthogonal and form a complete basis set. The IMFs reveals the natural frequency mode embedded in the signal. Unlike the classical Fourier analysis, which performs global analysis of signals, the EMD is a local decomposition method (Ayenu-Prah and Attoh-Okine, 2009).

Description of the method, which has been taken from (Huang et al., 1998 and Loutridis, 2004) is given below. The procedure to decompose a signal $x(t)$ into IMFs is as follows:

First, the local extrema of the signal $x(t)$ are identified. The local maxima are connected together by a cubic spline to form the upper envelope, $u(t)$, and the procedure is repeated for the local minima to produce the lower envelope, $l(t)$.

The mean is then defined as:

$$m_1(t) = \frac{l(t) + u(t)}{2} \tag{3.18}$$

Next, $m_1(t)$ is subtracted from the original signal $x(t)$, resulting in the first component $h_1(t)$, i.e.:

$$h_1(t) = x(t) - m_1(t) \tag{3.19}$$

The component $h_1(t)$ is now examined to ensure it satisfies the conditions of being IMF. An IMF must satisfy the following two conditions (Huang et al., 1998):

(i) The number of extrema and the number of zero crossings must either equal or differ at most by one in whole data sets.

(ii) The mean value of the envelope defined by the local maxima and the envelope defined by the local minima is zero at every point.

If these conditions are not satisfied, a process named by Huang as the sifting process should be continued until $h_1(t)$ becomes an IMF. In the sifting process $h_1(t)$ is considered as the new data. The local extrema are identified, the lower and upper envelopes are formed and the associated mean $m_{11}(t)$ is subtracted from $h_1(t)$ forming a new component $h_{11}(t)$, that should satisfy the criteria for being an IMF:

$$h_{11}(t) = h_1(t) - m_{11}(t) \tag{3.20}$$

The sifting process is to be continued as many times as required and eventually the component $h_{1k}(t)$ will be the first IMF of the data series $x(t)$ denoted by $C_1(t)$. The first IMF is subsequently subtracted from the original signal $x(t)$, the difference called the first residue $r_1(t)$:

$$r_1(t) = x(t) - C_1(t) \tag{3.21}$$

The residue $r_1(t)$ is then taken as the new signal and the sifting process is applied to it from the beginning. The signal $x(t)$ will be then decomposed into a finite number of IMFs $C_j(t)$. The EMD is stopped when the final residue, $r_N(t)$, becomes a monotonic function, or a constant, which is usually indicative of the trend of the original data. The sum of the IMFs and the residual recovers the original signal. The signal $x(t)$ is then written as:

$$x(t) = \sum_{j=1}^{N} C_j(t) + r_N(t) \tag{3.22}$$

Each IMF reveals the internal structure of the signal. The first IMF, $C_1(t)$, contains the highest frequency components of the signal, then, the frequency components contained

in the IMF $C_2(t),...,C_N(t)$, range from high to low, while the residue $r_N(t)$ represents the mean trend of low frequency.

The Hilbert transform of the IMFs subsequently forms a full energy–frequency–time distribution of the signal known as the Hilbert spectrum. The Hilbert transform of a real-valued function $C_j(t)$, is given by:

$$y_j(t) = \frac{1}{\pi} \int_{-\infty}^{+\infty} \frac{C_j(\tau)}{t-\tau} d\tau \tag{3.23}$$

The function $C_j(t)$ and its Hilbert transform $y_j(t)$ form an analytic signal $z_j(t)$ given by:

$$z_j(t) = C_j(t) + iy_j(t) = a_j(t)e^{i\theta_j(t)} \qquad j = 1,..., N \tag{3.24}$$

where $a_j(t)$ is the instantaneous amplitude, and θ_j is the phase function. By definition, the instantaneous frequency is given as:

$$\omega_j(t) = \frac{1}{2\pi} \frac{d\theta_j(t)}{dt} \tag{3.25}$$

Essentially, Eq. (3.23) defines the Hilbert transform as the convolution of $C_j(t)$ with $1/t$; therefore it gives the local properties of $C_j(t)$. To further clarify this, a numerical example will be presented next. The same signal as presented in Section 3.2., is considered as an example. By using EMD, the signal is decomposed into two IMFs and a residue, as shown in Fig.3.8. The IMF $C_1(t)$ illustrates the amplitude and frequency characteristics of the harmonic component of cosine of 100 Hz, while the IMF $C_2(t)$ reveals the harmonic component of 30 Hz. The residue $r_2(t)$ is almost a zero vector. It is shown that EMD can extract the intrinsic oscillation features of a signal correctly; also, by applying the Hilbert transform to both IMFs, the instantaneous frequency and amplitude of them are obtained (see Fig. 3.9).

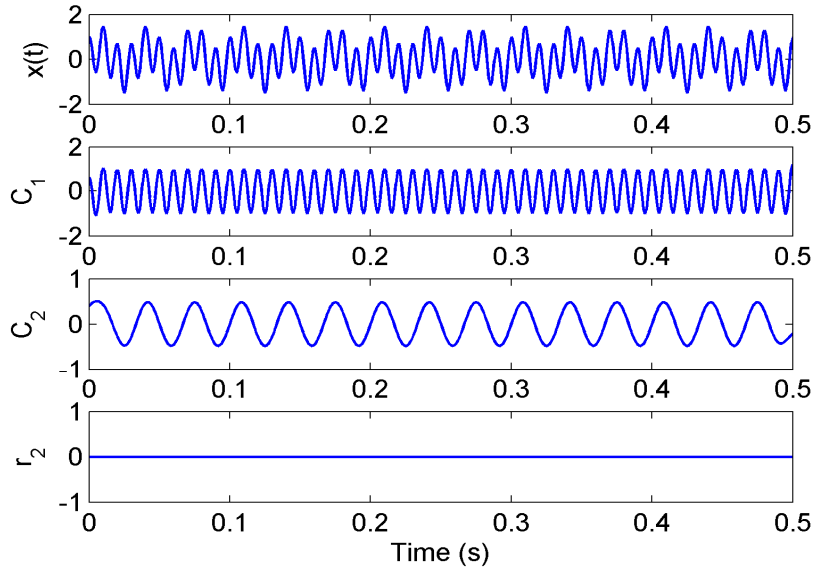

Figure 3.8: The imperial mode decomposition of $x(t)$.

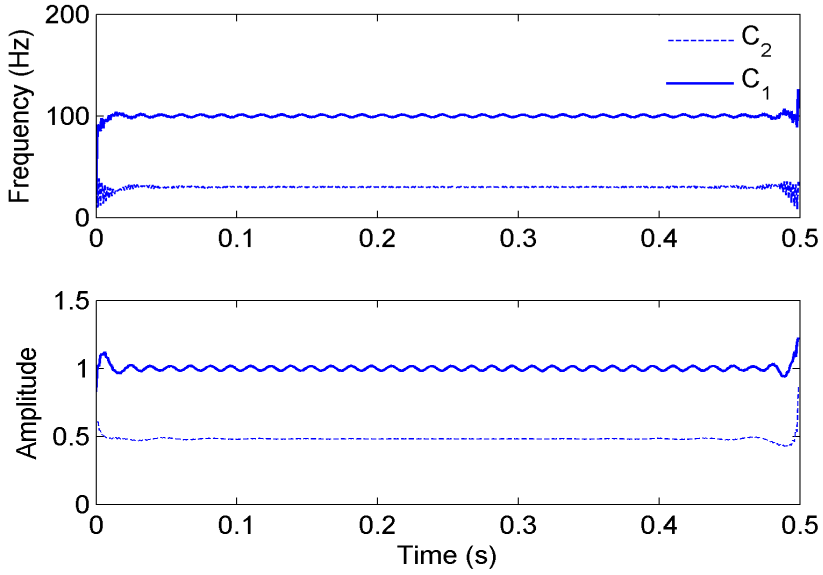

Figure 3.9: Instantaneous frequency and amplitude of two IMFs obtained from $x(t)$.

Chapter 4

4. Internal leakage detection[1]

4.1. Introduction

This Chapter focuses on the internal (cross-port) fault detection in hydraulic actuators. Internal leakage in an actuator is caused by the wear of piston seal that closes the gap between the moveable piston and the cylinder wall; as a result the hydraulic fluid is displaced between the two chambers of the actuator. Internal leakage affects the dynamic performance of the system since the entire flow is not available to move the piston against the load. Internal leakage cannot be detected until the actuator seal is completely damaged and the actuator fails to respond to a control signal (Karpenko, 2008). Here, the capability of three transform techniques, FFT, DWT and HHT, are investigated experimentally for detecting hydraulic internal leakage fault. Identification of small leakages and the ease of implementation are key features in this work. As concluded in Chapter 2, the net effect of internal leakage is to increase the damping characteristic of the hydraulic actuator. Given the purpose of this Chapter, it is important to also capture the frequency range within which the pressure signal is sensitive to the internal leakage. The internal leakage changes the Bode magnitude around the hydraulic natural frequency for system under investigation (see Fig. 2.5). Therefore, by processing pressure signal at one side of hydraulic actuator using FFT or DWT, the frequency band sensitive to effect of internal leakage can be captured.

[1] Some materials in this Chapter have been published in IEEE Transaction on Industrial Electronics, vol. 57, no. 5, pp.1755-1762, 2010.

4.2. Application of FFT using a structured input signal

First, fast Fourier transform (FFT) is used for internal leakage detection. As was mentioned earlier, internal leakage introduces damping to the dynamics of the hydraulic actuation system and alters the transient response of the chamber pressures. Here, the sub-band informative signals sensitive to the effect of internal leakage, are obtained by decomposing the original pressure signal at one side of the hydraulic actuator using FFT. For all experiments, a periodic square wave signal with 3V (peak-to-peak) amplitude is applied to the servovalve as the input. This structured input signal is suitable for offline applications as it is simple and includes low and high frequency components allowing rich excitation of the pressure signals from which, the effect of internal leakage can be observed. The input signal and the resulting actuator displacement for a healthy actuator are shown in Fig. 4.1. The pressures at the actuator chambers are shown in Fig. 4.2. The sampling rate at which the data are collected is 500Hz. Next, an internal leakage, with mean value of 1.54 lit/min, is introduced. The plot of internal leakage is shown in Fig. 4.3, given the same input signal as in Fig. 4.1. The corresponding pressure signals are plotted in Fig. 4.4.

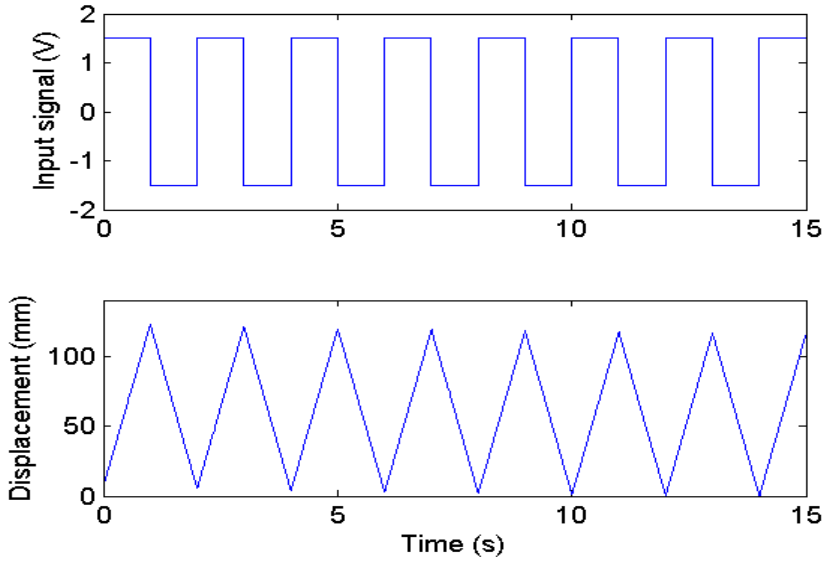

Figure 4.1: Input signal and displacement response of hydraulic actuator under normal operating condition.

Note that internal leakage alters the transient responses in the line pressures, which can be detected by carefully comparing Figs. 4.2 and 4.4.

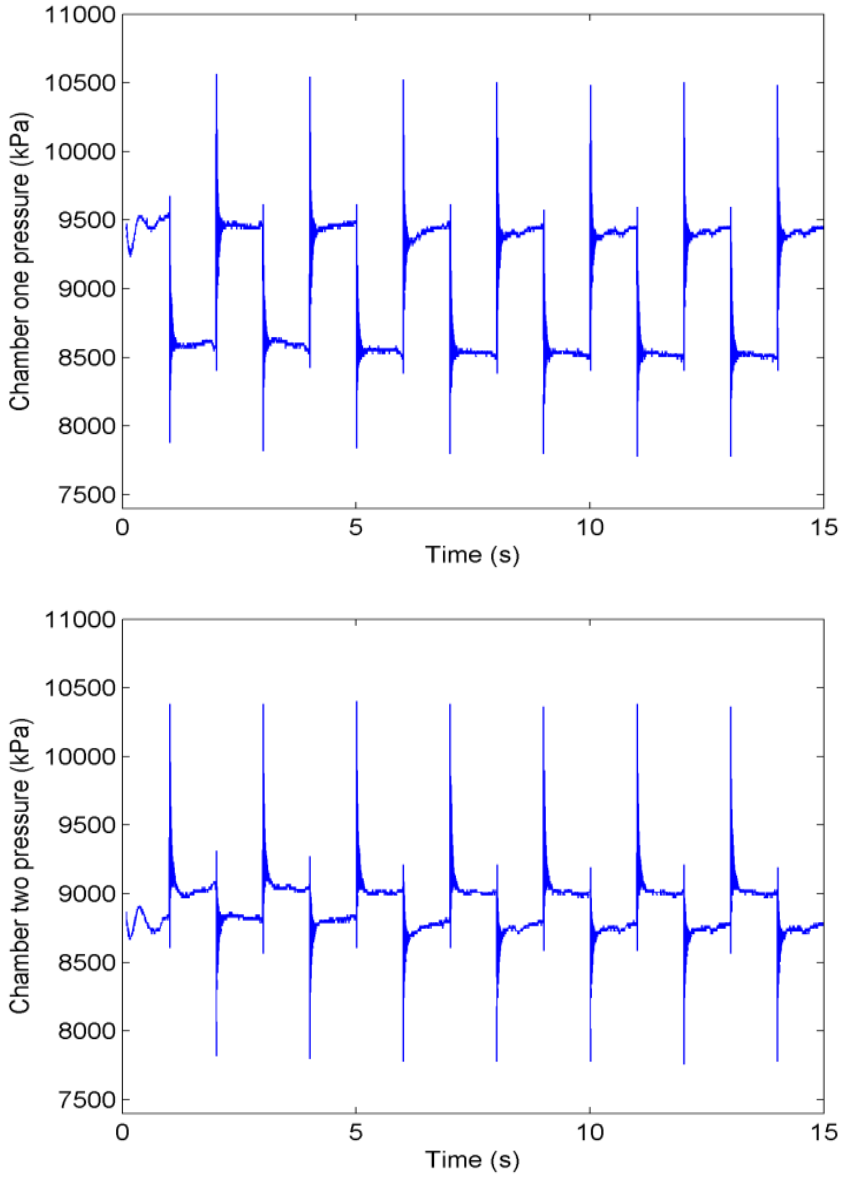

Figure 4.2: Pressure signals in chambers one and two under normal operating condition.

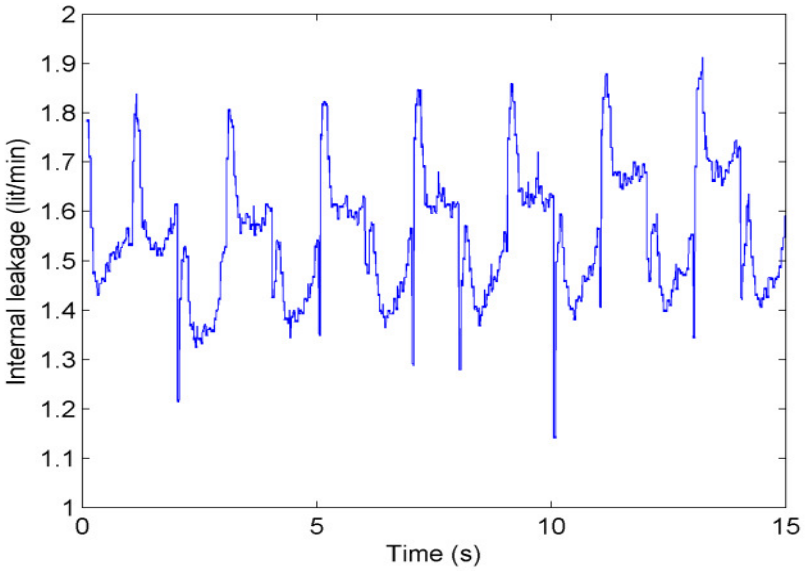

Figure 4.3: Plot of internal leakage flow (mean value of 1.54 lit/min) for actuator with faulty seal given the input signal shown in Fig. 4.1.

The results of applying FFT to chamber one pressure signal under normal and faulty operating conditions are shown in Figs. 4.5 and 4.6, respectively. From these plots, the feature frequency band is identified to be in the range of around 65 to 85 Hz. This is consistent with the frequency band determined by Bode plot in Fig. 2.5. As mentioned before, the internal leakage adds damping to the dynamics of the system resulting in a decrease in amplitude and energy of FFT spectrum of the pressure signal around the interesting frequency band.

To facilitate comparison, the root mean square (RMS) values of the processed pressure signal by FFT for frequency band of (65-85 HZ), are calculated. The results are shown in Table 4.1.

Table 4.1: RMS values of FFT from the measurement of chamber one pressure for normal actuator and actuator with internal leakage of 1.54 lit/min in average.

RMS index	Healthy Actuator	Faulty Actuator	Percentage of changes
FFT Method (65-85Hz)	7.01	5.08	**27.5**

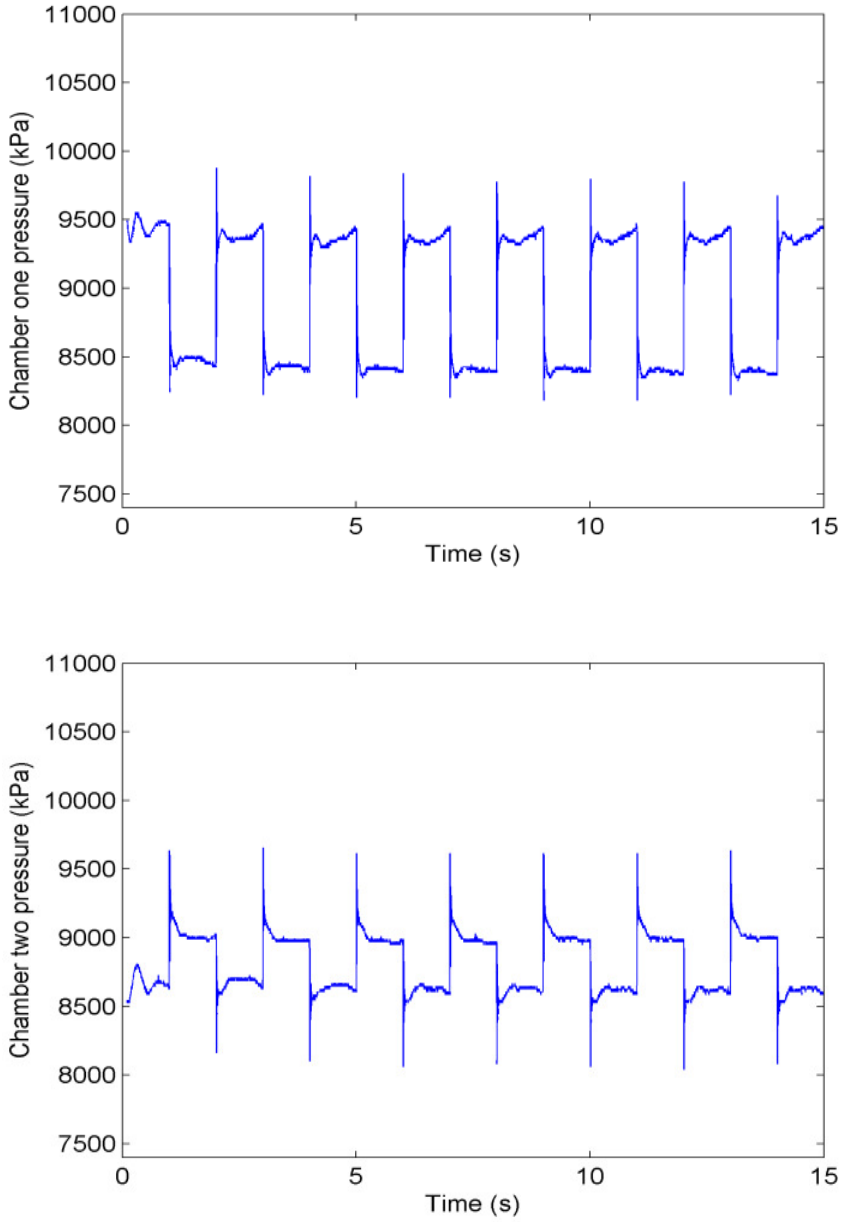

Figure 4.4: Pressures in chambers one and two of hydraulic actuator with internal leakage shown in Fig. 4.3.

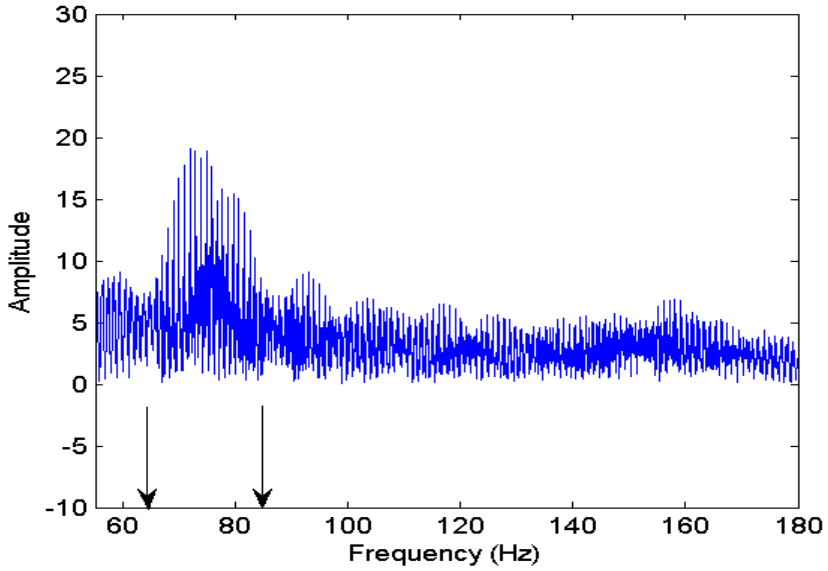

Figure 4.5: Fast Fourier transform of chamber one pressure signal for actuator under normal operating condition.

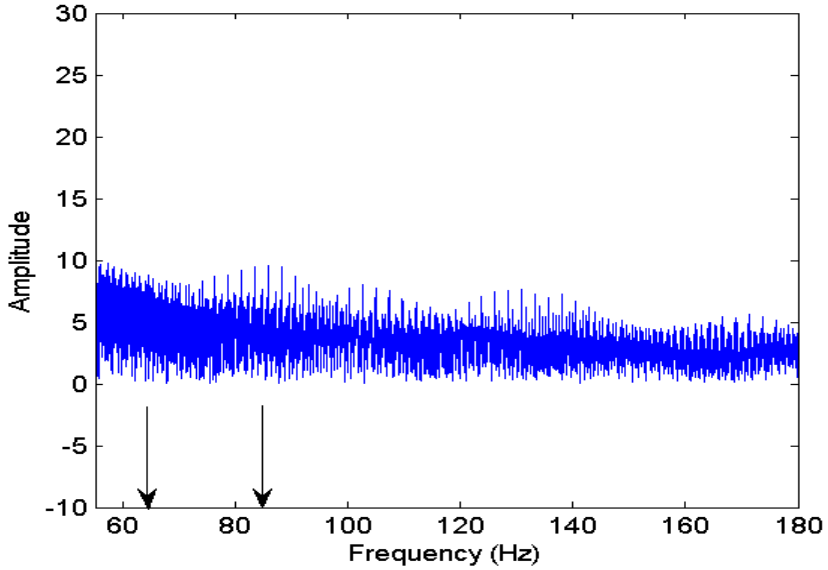

Figure 4.6: Fast Fourier transform of chamber one pressure signal for actuator with internal leakage shown in Fig. 4.3.

The final set of tests demonstrates the consistency of the results presented so far. In this set of experiments, the test rig was run 18 times under normal operating condition as well as small and medium leakage situations at various times. The small leakage (of average 0.124 lit/min) that was introduced in this test caused a reduction of ≈2.6% of

the available flow rate to the actuator. The medium leakage was of average 0.808 lit/min and caused an average reduction of ≈17% of the available flow rate. The average values, reported here, were taken over the entire 18 tests. The scaled RMS values using FFT spectrum in the frequency range of 65-85Hz are shown in Fig. 4.7. A baseline value is chosen as the minimum RMS value obtained under normal operating condition. Given this baseline value, small and medium internal leakages can be identified for 30% and 100% of the times, respectively.

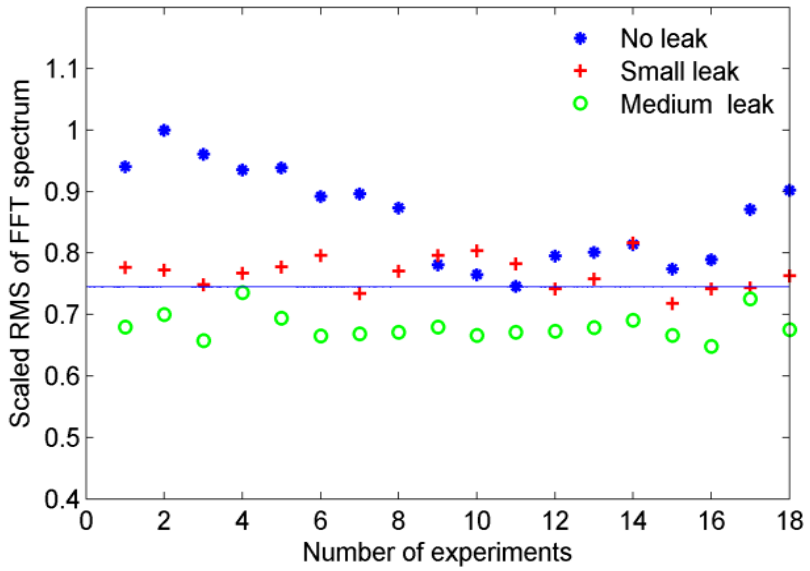

Figure 4.7: Scaled RMS values of FFT spectrum obtained from healthy actuator and actuator experiencing small and medium leakages with mean values of 0.124 lit/min and 0.808 lit/min, respectively.

Note that scaling is done by dividing the RMS values by the maximum one to facilitate the comparison. The mean RMS values (from all experiments) as well as standard deviations of the data for normal, small and medium leakages are depicted in Fig. 4.8. The results firstly show that the RMS values of the FFT spectrum of the pressure signal, in the frequency band of interest, reduce with the severity of internal leakage. Secondly, the variation of the RMS values over the entire tests is less, as the leakage level increases from no leak to medium leak. The change in the standard deviation of the RMS values is believed to be due to the fact that as the internal leakage increases, the

effect of damping becomes more dominant masking the effect of dry friction in the form of stick-slip friction that is considered to be somewhat random from experiment to experiment.

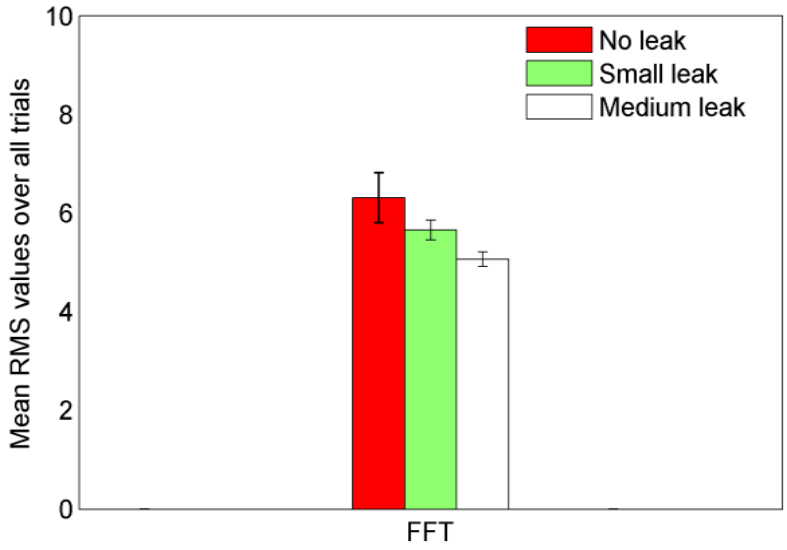

Figure 4.8: Mean RMS and standard deviations taken over all experiments using FFT.

Remark 1:

The issue of robustness to the changes of resonant peak frequency becomes important for optimal detection. One of the parameters that influences the peak frequency and can change is the effective bulk modulus Figure 4.9 (a) shows typical Fourier transform of chamber one pressure signal for the actuator under normal operating condition (similar to Fig. 4.5). Figure 4.9 (b) shows similar plot for the same normal actuator after many hours of operation. From this figure it is seen that, due to changes in the effective bulk modulus (as a result of temperature rise) the feature frequency band is shifted; however, the amplitude is not affected. Figure 4.9 (c) shows the Fourier transform of chamber one pressure with the introduction of leakage. As is seen, the amplitude of the feature frequency band is decreased, indicating that as long as the RMS values of the Fourier transform plots are calculated over the proper frequency band, the FFT method works. The interesting range of frequency must be shifted for optimal diagnosis.

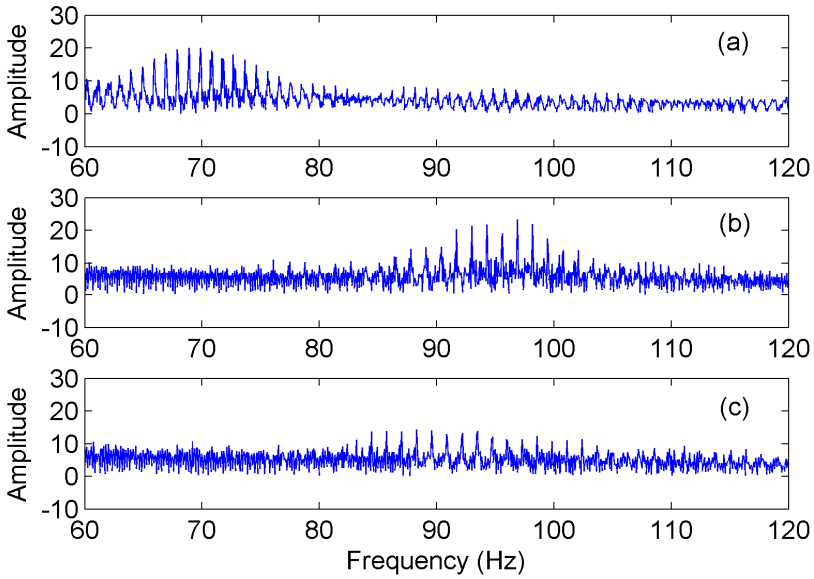

Figure 4.9: Typical frequency response of the actuator at different times: (a) and (b) healthy actuator; (c) faulty actuator (0.48 lit/min).

Remark 2:

Internal leakage is the result of seal wear which also influences the friction property of the actuator as mentioned before. To the best of the author's knowledge, there is no report on the influence of friction changes on internal leakage fault detection techniques. The effectiveness of FFT for internal leakage detection while the friction properties of the actuator are changed is studied. The sliding friction of the actuator can be increased from 258 N to 400 N when it is coupled with the slave cylinders. The test rig was run 10 times under normal (no leak) operating condition using the actuator coupled with slave cylinders (increased friction). All the RMS values are above the predetermined baseline which is shown in Fig. 4.10. This method is concluded to not be sensitive to the changes in the friction, which is desirable for the purpose of this study.

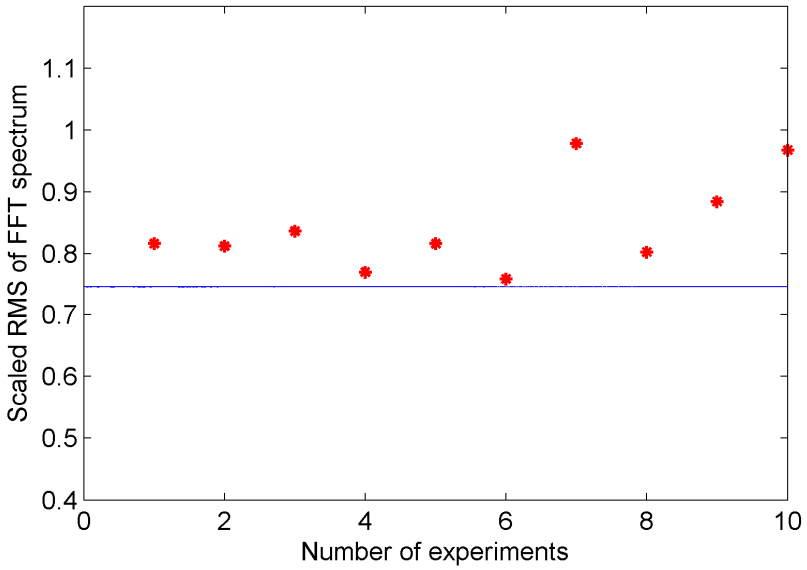

Figure 4.10: RMS values of FFT spectrum obtained from actuator with no leak.

4.3. Application of DWT using a structured input signal

The application of discrete wavelet transform (DWT) for internal leakage detection is described here. Figures 4.11 and 4.12 illustrate four detail coefficients of wavelet obtained from the pressure in chamber one, P_1, (see Fig. 2.3) under normal as well as faulty operating conditions due to internal leakage. Daubechies 8 wavelet (Daubechies, 1992) has been used as the mother wavelet among many other choices for mother wavelets (e.g., Coiflets, Meyer wavelet, Gaussian wavelet, Mexican hat wavelet, Morlet wavelet). Daubechies wavelets are compactly supported with external phase and the highest number of vanishing moments for a given support width (Daubechies, 1992; Ukil and Zivanovic, 2006); furthermore, the associated scaling filters are minimum-phase. From the view point of implementation, Daubechies wavelet is a good choice for this application. A high order mother wavelet is better to avoid overlapping between two adjacent frequency bands (Cusido et al., 2008); that is why the order eight has been chosen.

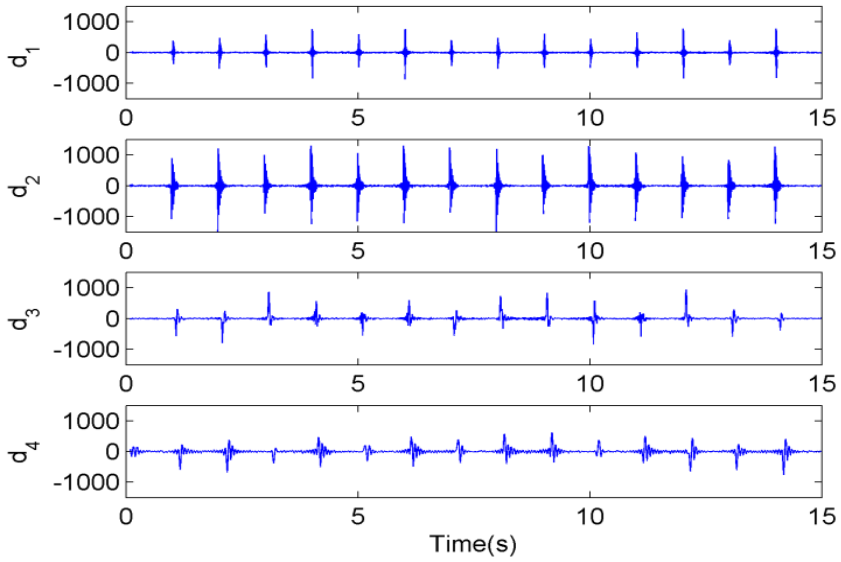

Figure 4.11: Four-level detail wavelet coefficients of chamber one pressure signal for actuator under normal operating condition.

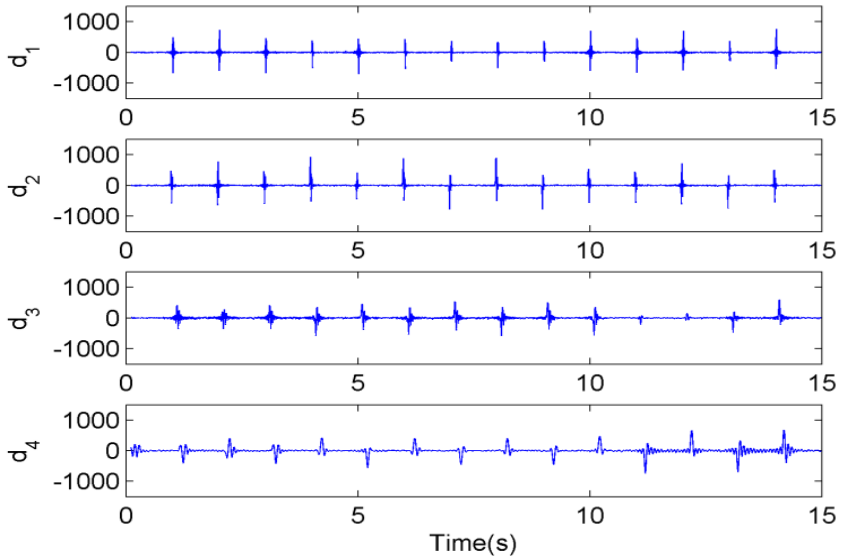

Figure 4.12: Four-level detail wavelet coefficients of chamber one pressure signal for actuator with internal leakage shown in Fig. 4.3.

To apply the wavelet decomposition method, it is necessary to determine how many levels of decomposition are required for a specific application. This is because the DWT splits the frequency spectrum into specific frequency bands. The frequency bands depend on the sampling frequency, f_s, as shown in Fig. 4.13. The highest band,

sweeping the frequency from $\frac{f_s}{2}$ to $\frac{f_s}{4}$, belongs to level one decomposition. For the next decomposition level, this frequency range is divided by two. Referring to Table 4.2, it is obvious that with four-level of wavelet decomposition, a wide range of frequency including the frequency range of interest (65-85 Hz), can be covered. Table 4.2 shows that the coefficient d_2 carries the most information about the effect of internal leakage. By comparing Figs. 4.11 and 4.12, the wavelet coefficient d_2 appears to change the most as compared to other coefficients.

The root mean square (RMS) values of the wavelet coefficients are calculated again. The results are shown in Table 4.3. From the results the wavelet coefficient, d_2, is seen to be more sensitive to the effect of internal leakage than the other wavelet coefficients or the index calculated by the FFT method.

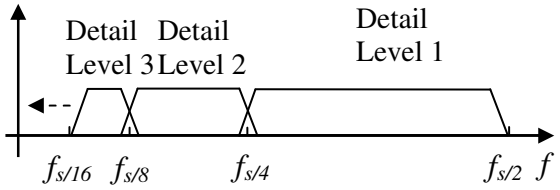

Figure 4.13: Frequency range covered by detail coefficients.

Table 4.2: Wavelet frequency bands for sampling rate of 500Hz.

Decomposition levels	Frequency bands (Hz)
d_1	250-125
d_2	125-62.5
d_3	62.5-31.25
d_4	31.25-15.625

Table 4.3: RMS values four-level wavelet detail coefficients from the measurement of chamber one pressure for normal actuator and actuator with internal leakage of 1.54 lit/min in average.

RMS indices	Healthy Actuator	Faulty Actuator	Percentage of changes
d_1	61	51.2	16
d_2	157.8	79.2	**49.8**
d_3	93.8	72.4	22.8
d_4	106.8	102.9	3.6

The final set of tests is to demonstrate the consistency of the results presented so far for WT. The same number of tests were run as Fig. 4.7 for normal operating condition as well as small and medium leakage situations at various times. The average values, reported here, were taken over the entire 18 tests. The scaled RMS values of detail coefficients, d_1, d_2, d_3 and d_4, obtained from the chamber one pressure signals, at various runs, are shown in Figs. 4.14 to 4.17, respectively.

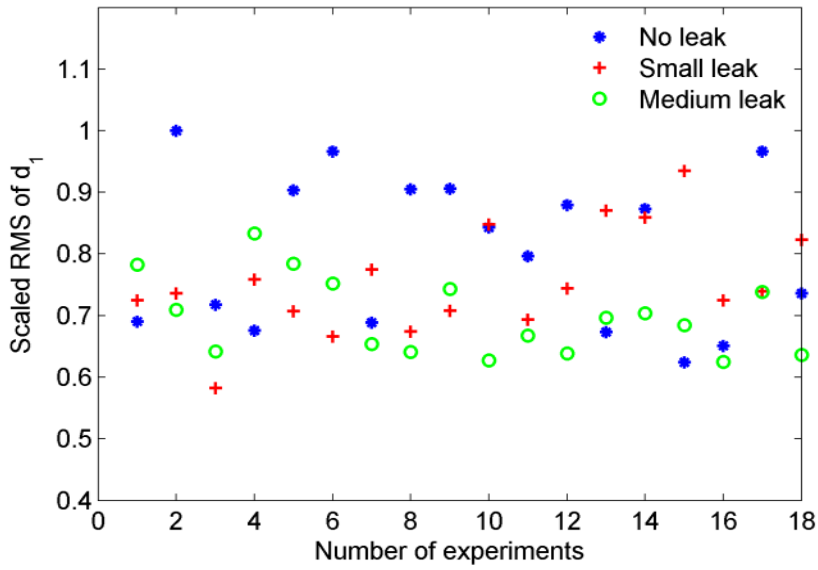

Figure 4.14: Scaled RMS values of detail coefficient, d_1, obtained from healthy actuator and actuator experiencing small and medium leakages with mean values of 0.124 lit/min and 0.808 lit/min, respectively.

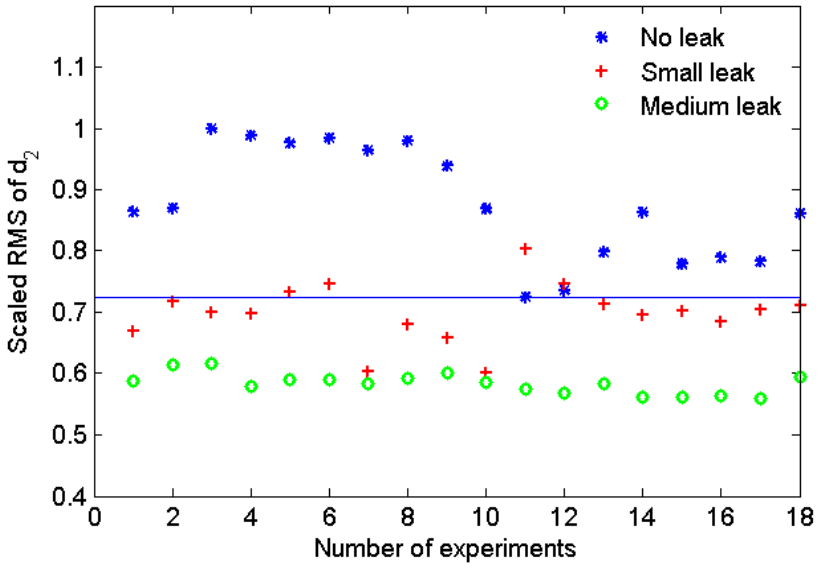

Figure 4.15: Scaled RMS values of detail coefficient, d_2, obtained from healthy actuator and actuator experiencing small and medium leakages with mean values of 0.124 lit/min and 0.808 lit/min, respectively.

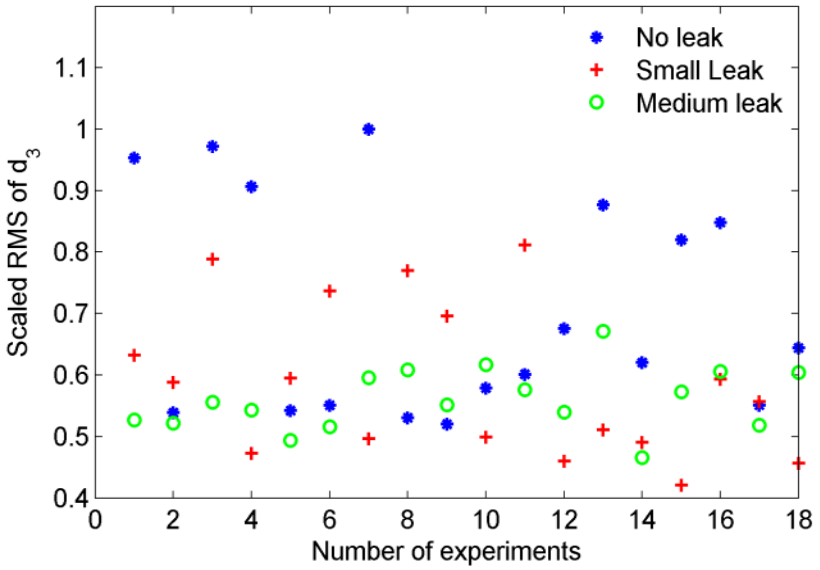

Figure 4.16: Scaled RMS values of detail coefficient, d_3, obtained from healthy actuator and actuator experiencing small and medium leakages with mean values of 0.124 lit/min and 0.808 lit/min, respectively.

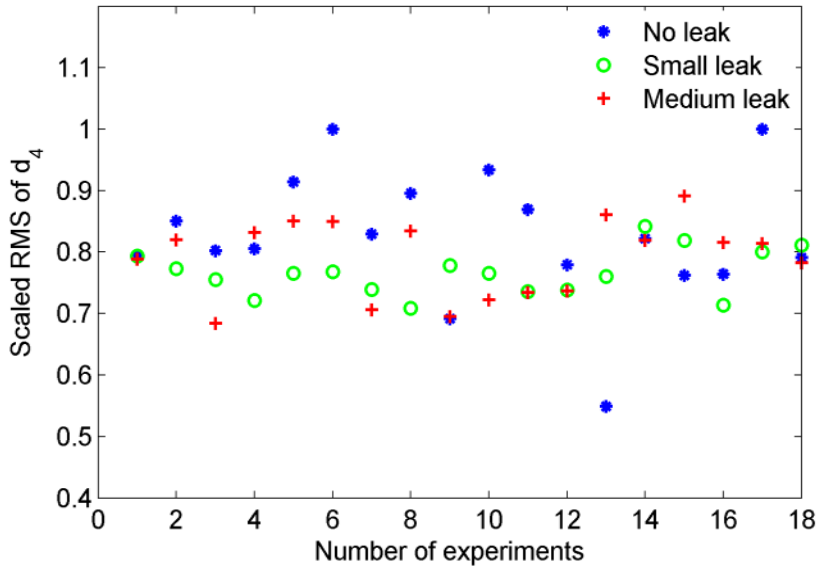

Figure 4.17: Scaled RMS values of detail coefficient, d_4, obtained from healthy actuator and actuator experiencing small and medium leakages with mean values of 0.124 lit/min and 0.808 lit/min, respectively.

From these plots, the difference between RMS values for no leak condition and RMS values associated with small and medium leakages is more distinguishable for detail coefficient d_2. The mean values as well as the standard deviations of the data for normal, small and medium leakages are shown in Fig. 4.18. The results show that the RMS values of the wavelet coefficients obtained from the pressure signal reduce with the severity of internal leakage and the variation of the RMS values over the entire tests is less, as the leakage level increases from no leak to medium leak. Referring to Fig. 4.15, a baseline value is chosen as the minimum RMS value under normal operating condition. Given this baseline value, small and medium internal leakages are identified for 80% and 100% of the times, respectively.

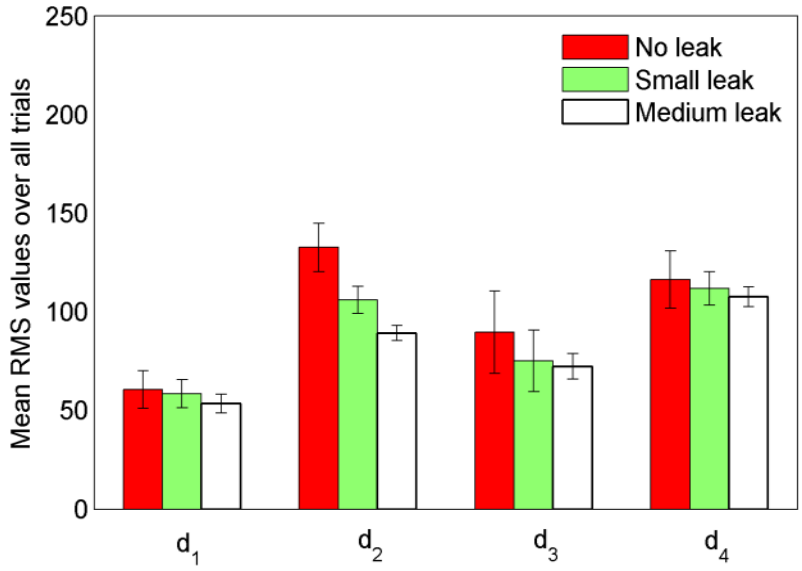

Figure 4.18: Mean RMS and standard deviation taken over all experiments for wavelet coefficients, obtained from healthy actuator and actuator experiencing small and medium leakages.

Remark 3:

Similar to the case in remark 2, the effect of increased friction on wavelet coefficient d_2 is studied. All the RMS values are above the predetermined baseline (see Fig. 4.15). It is concluded that d_2 is not sensitive to the changes in the friction, which is desirable for the purpose of this investigation.

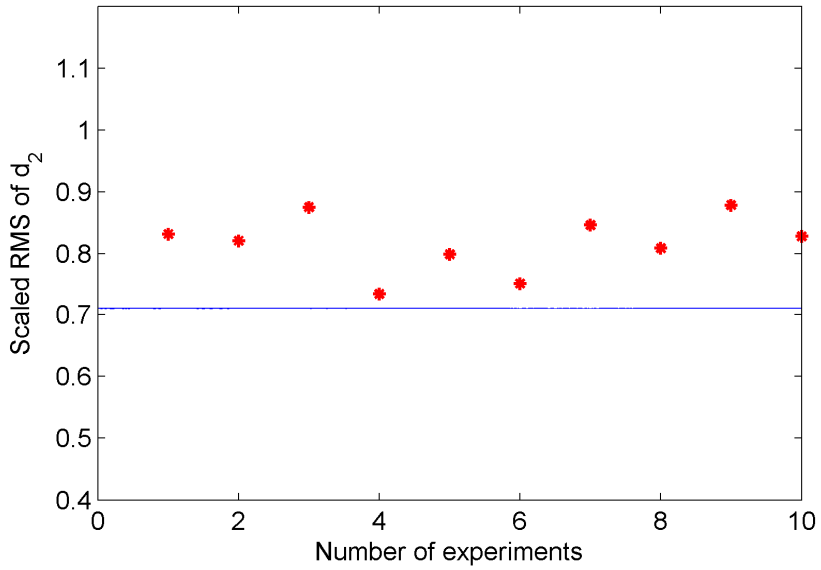

Figure 4.19: RMS values of detail coefficient, d_2, obtained from actuator with no leak.

4.4. Application of HHT using a structured input signal

The P_1 signal under normal and faulty conditions is decomposed into its IMFs ($C_1 - C_4$) shown in Figs. 4.20 and 4.21. The other IMFs are ignored in the figures because of their low amplitude. Mode C_1 contains the highest signal frequencies; mode C_2 contains the next frequency band and so on.

Internal leakage results in a decrease in the amplitude as well as the energy of some IMFs (compare Figs. 4.20 and 4.21), which is easier to detect and quantify than the original pressure signals. The mode C_1 changes the most while changes in other modes are smaller. This shows that C_1 is the most sensitive IMF to internal leakage. To show the significant decrease in amplitude of this mode under faulty operating condition compared with normal condition, its instantaneous amplitude obtained by Hilbert transform is depicted in Fig. 4.22.

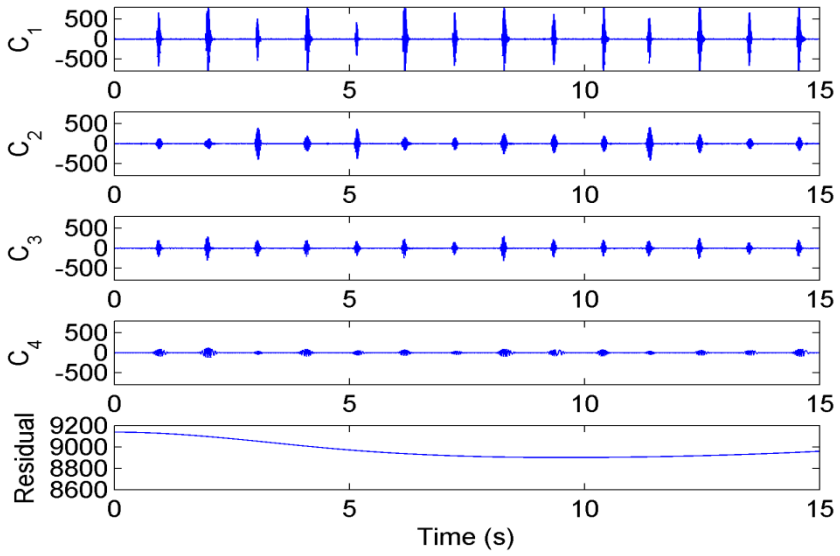

Figure 4.20: Decomposition of pressure signal at chamber one, P_1, under normal operating into intrinsic mode functions.

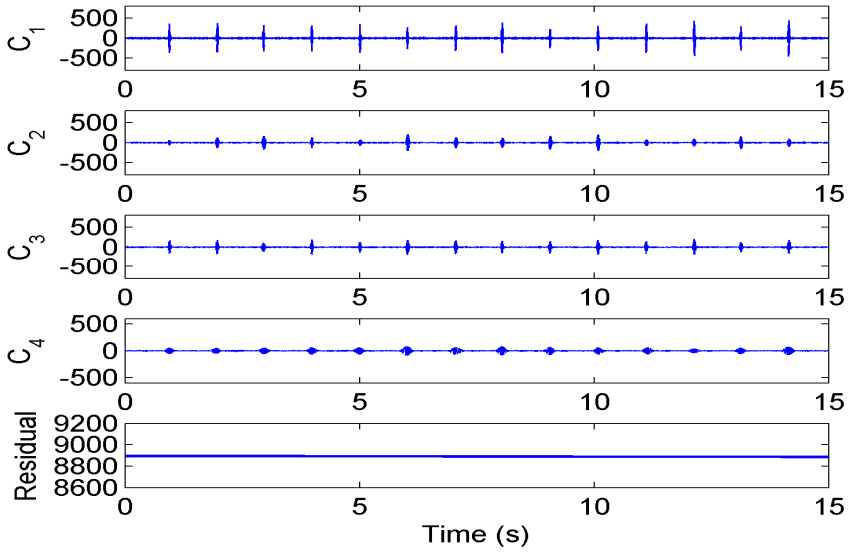

Figure 4.21: Decomposition of pressure signal at chamber one, P_1, with internal leakage shown in Fig. 4.4 into intrinsic mode functions.

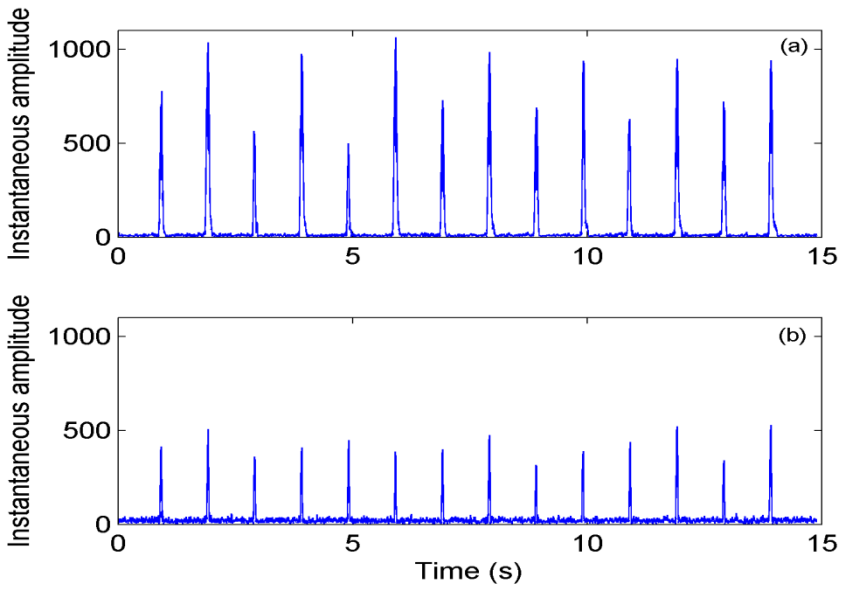

Figure 4.22: Instantaneous amplitude of the first IMF obtained by the decomposition of the pressure signal at chamber one, P_1. (a) Healthy actuator. (b) Actuator with internal leakage shown in Fig. 4.3.

To facilitate comparison, the root mean square (RMS) values of the instantaneous amplitude $a_i(t)$ of each IMF_i ($\sqrt{\frac{1}{T}\int_0^T a_i^2(t)dt}$, where T is the length of data) are calculated, over the entire test period. The RMS values are shown in Table 4.4. The RMS values have decreased as a result of introducing leakage.

Table 4.4: RMS values of instantaneous amplitude associated to different IMFs from the measurement of chamber one pressure for actuator under normal and faulty operating conditions for the leakage value of 1.54 lit/min.

Condition	RMS a_1	RMS a_2	RMS a_3	RMS a_4	RMS Residual
Normal	141.90	60.78	52.08	31.16	9.1e3
Faulty	56.07	29.15	31.61	22.44	8.89e3

Now, the repeatability of the results for HHT is investigated. In this set of experiments, the test rig was run 18 times under normal operating condition as well as small and medium leakage situations at various times. The small leakage (of average 0.124 lit/min) introduced in this test caused a reduction of ≈2.6% of the available flow rate to

the actuator. The medium leakage was of an average rate of 0.808 lit/min and caused an average reduction of ≈17% of the available flow rate. The average values were taken over the entire 18 tests. The scaled RMS values of instantaneous amplitude associated to modes C_1, C_2, C_3 and C_4 obtained from the chamber one pressure signals, are shown in Figs. 4.23 to 4.26. Note that scaling is done by dividing the RMS values by the maximum to facilitate the comparison. From these plots it is observed that the difference between RMS values for no leak condition and RMS values associated with small and medium leakages is more distinguishable for mode C_1 as compared to others. A baseline value is determined from the minimum RMS value obtained from a healthy actuator. Given this baseline value small and medium internal leakages are identified for 90% and 100% of the times.

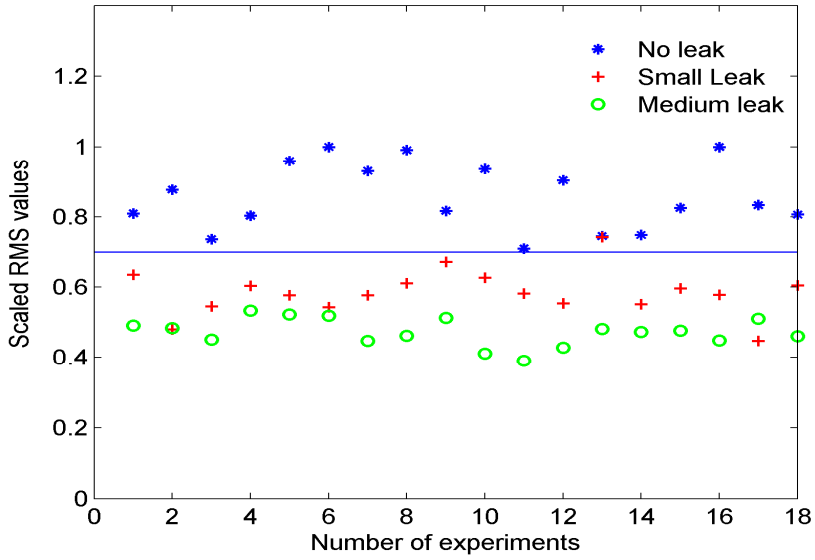

Figure 4.23: Scaled RMS values of instantaneous amplitude of mode, C_1, obtained from healthy actuator and actuator experiencing small and medium leakages with mean values of 0.124 lit/min and 0.808 lit/min, respectively.

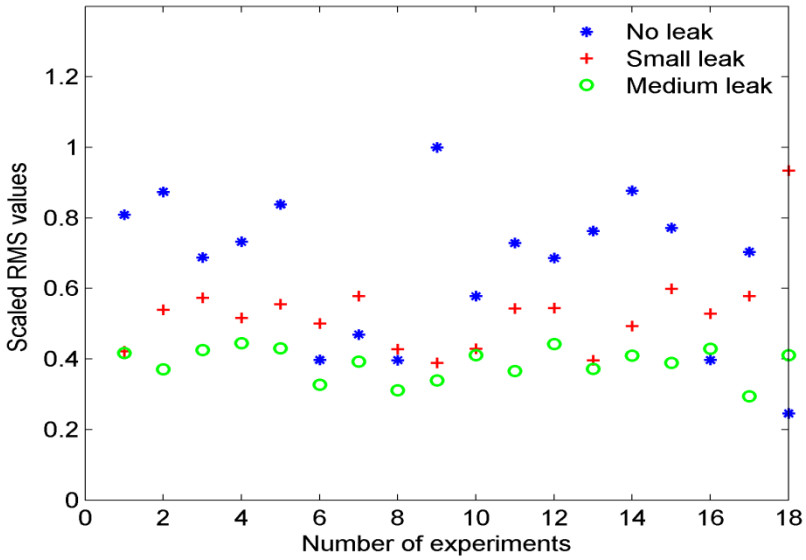

Figure 4.24: Scaled RMS values of instantaneous amplitude of mode, C_2, obtained from healthy actuator and actuator experiencing small and medium leakages with mean values of 0.124 lit/min and 0.808 lit/min, respectively.

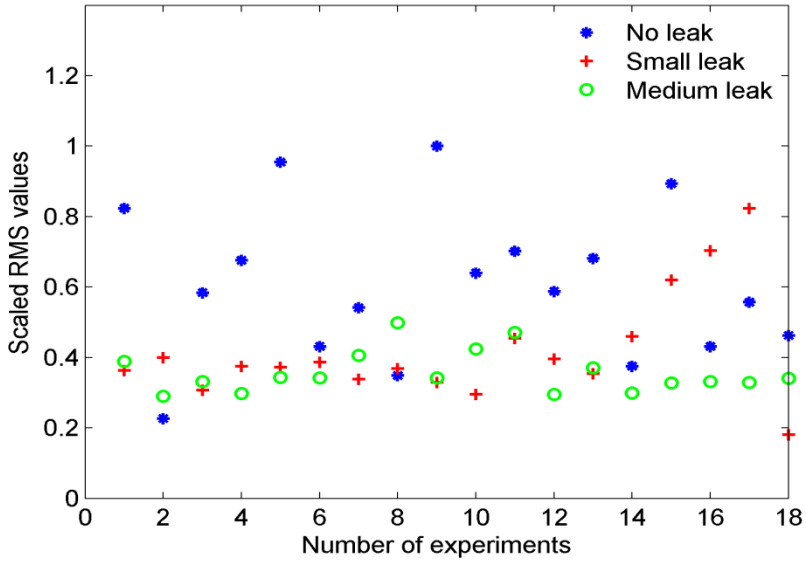

Figure 4.25: Scaled RMS values of instantaneous amplitude of mode, C_3, obtained from healthy actuator and actuator experiencing small and medium leakages with mean values of 0.124 lit/min and 0.808 lit/min, respectively.

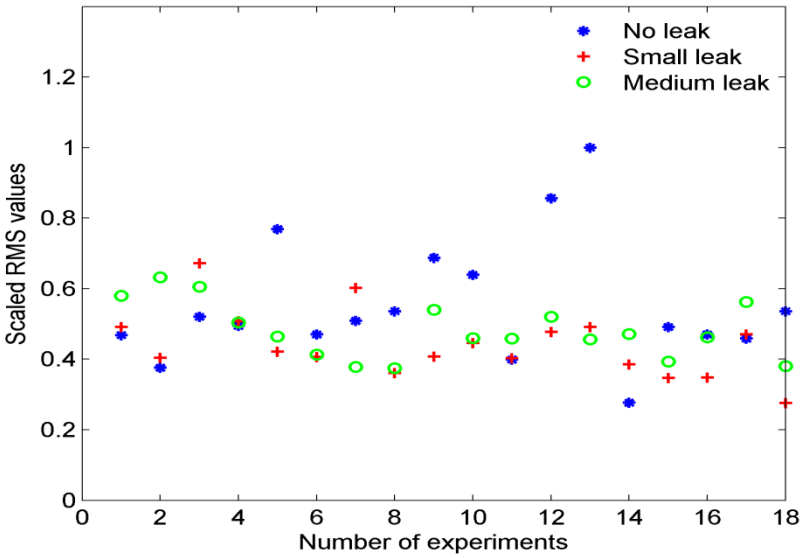

Figure 4.26: Scaled RMS values of instantaneous amplitude of mode, C_4, obtained from healthy actuator and actuator experiencing small and medium leakages with mean values of 0.124 lit/min and 0.808 lit/min, respectively.

The mean values as well as the standard deviations of the data for normal, small and medium leakages are shown in Fig. 4.27. The mode C_1 is more sensitive to the effect of internal leakage than other IMFs. The results show that the RMS values reduce with the severity of internal leakage and the variation of the RMS values over the entire tests is less, as the leakage level increases from no leak to medium leak. The change in the standard deviation of the RMS values is believed to be due to the fact that was explained for FFT and WT cases.

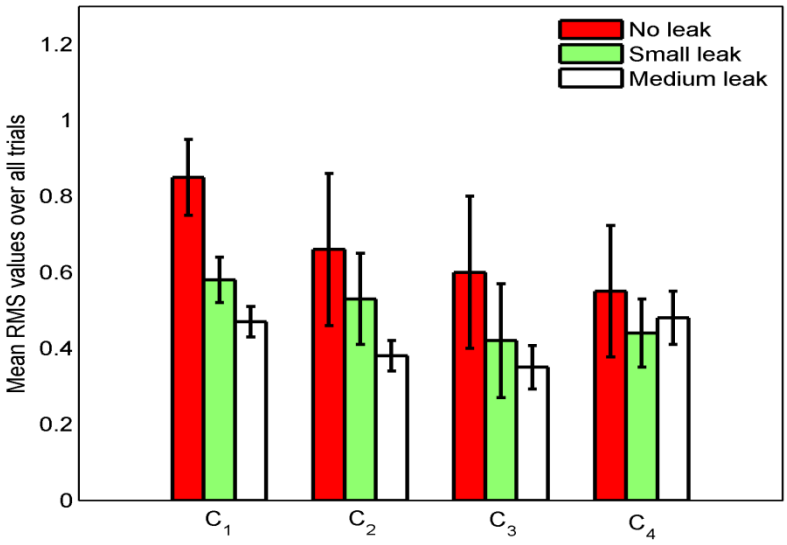

Figure 4.27: Mean RMS and standard deviation taken over all experiments for each IMF, obtained from healthy actuator and actuator experiencing small and medium leakages.

Remark 4:

The same as remark 2, here the effect of increased friction on mode C_1 is studied. Some of the RMS values associated with HHT fall below the predetermined baseline shown in Fig. 4.23.

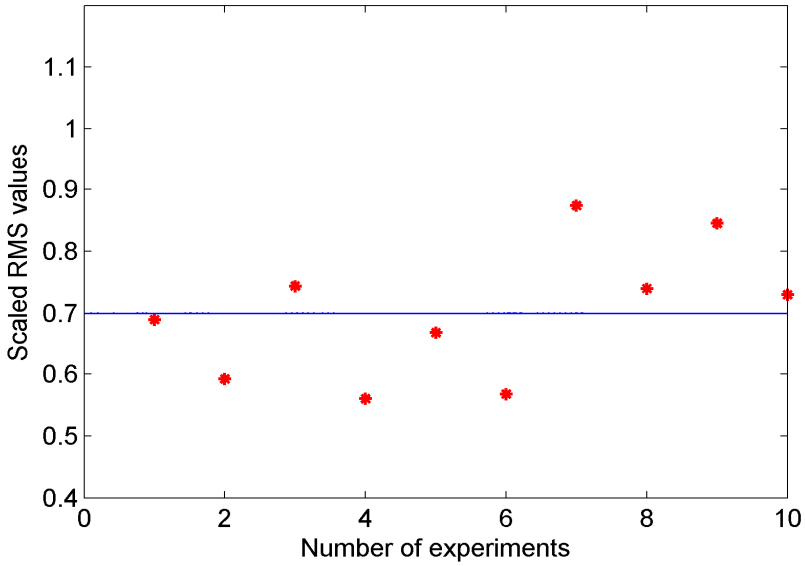

Figure 4.28: Scaled RMS values of instantaneous amplitude of mode, C_1, obtained from actuator with no leak.

4.5. Applications towards online leakage diagnosis

So far, the capability of the FFT, DWT and HHT using structured input (periodic steps) which is useful for offline internal leakage detection has been tested. The structured input was directly applied to the servovalve under a no load condition. The pseudorandom reference input is employed here to investigate the performance of these methods toward online application whereby the magnitude and duration of the input signal can change. The positioning of the actuator against the spring load is achieved according to the two-degree-of-freedom feedback system configuration shown in Fig. 4.29. The controller, $G(s)$, and the prefilter, $F(s)$, are designed to satisfy the desired closed-loop performance specifications. The pseudorandom signal is characterized with a series of desired step inputs having amplitudes between 0.025 m to 0.05 m and duration between 0.5 s to 4 s.

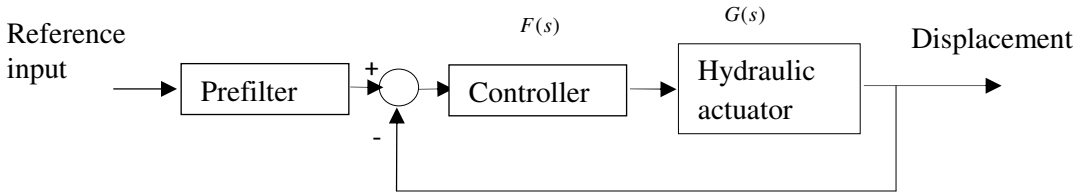

Figure 4.29: Block diagram showing controller and prefilter.

This type of signal resembles activities of flaps for typical in-flight maneuvers (Nguyen, 1979), and allows to investigate online fault detection ability of this method. The experiments are conducted with a QFT-based controller with an additional characteristic of holding a desirable performance even in the presence of an internal leakage fault up to 40% of the rated servovalve flow across the actuator piston. The structure of this controller is shown below:

$$G(s) = \frac{246.59s^3 + 7.18\times10^3 s^2 + 4.78\times10^7 s + 5.49\times10^8}{s^3 + 420s^2 + 9\times10^4 s} \tag{4.1}$$

$$F(s) = \frac{22.04s + 297.5}{s^2 + 43.5s + 297.5} \tag{4.2}$$

The detailed derivation of the QFT controllers has been reported elsewhere (Karpenko, 2008).

In this experiment a healthy actuator undergoes a set of positioning tasks against a spring having stiffness of 80 kN/m for 600 s. A small internal leakage is then manually introduced at t≈300s.

The close-up plots of displacement and the leakage fault are shown in Figs. 4.30 and 4.31. The controller works well even after the introduction of internal leakage after t≈300s, and there is no apparent steady-state error in the position response. This is due to the fact that the controller was designed to be robust to internal leakage. The FFT approach fails to diagnose a leakage in this kind of application. Since the FFT cannot reveal the time of changes, the processed pressure signals are shown in Fig. 4.32, for healthy and faulty zones separately.

The wavelet coefficient d_2, first IMF and its instantaneous amplitude are plotted in Figs. 4.33 and 4.34. By observing the pattern of changes in d_2, first IMF and its instantaneous amplitude one can recognize the occurrence of an internal leakage after t≈300s. These two methods are concluded to remain effective for online applications. In the case of having a pseudorandom reference input there is not a significant difference between using HHT and DWT for internal leakage detection.

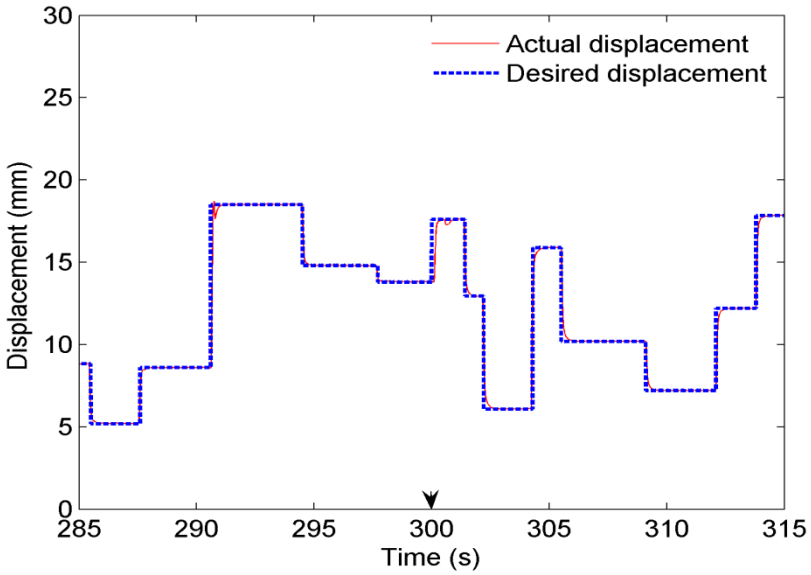

Figure 4.30: Close-up response of actuator with internal leakage introduced after t≈300s. The QFT-based controller is used and the total test time is 600s.

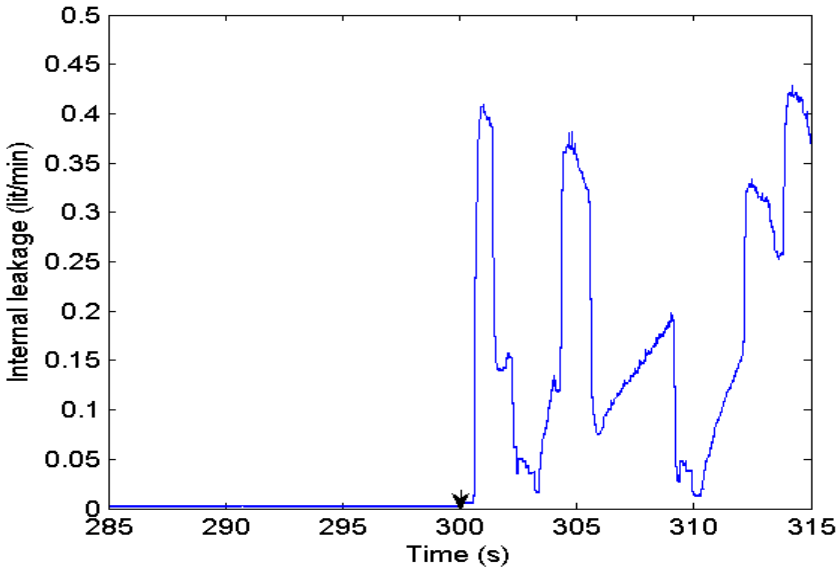

Figure 4.31: Close-up of internal leakage fault (mean value 0.23 lit/min).

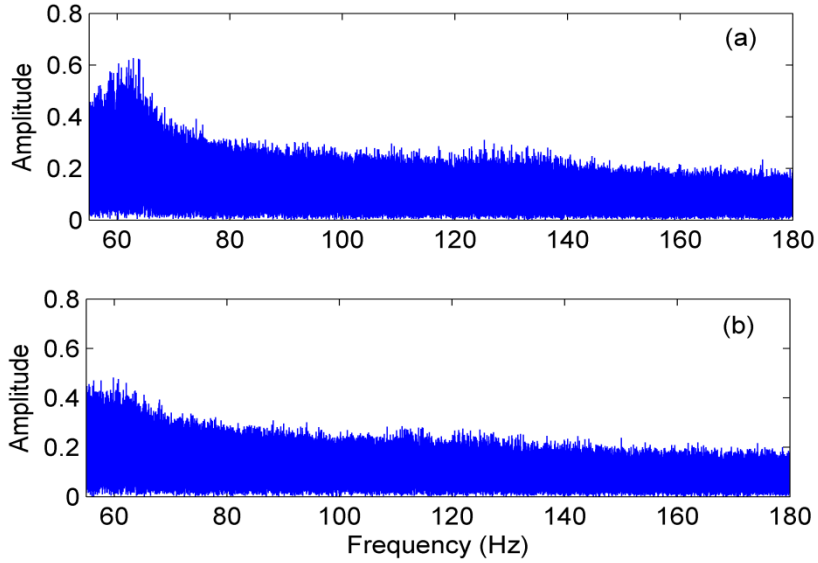

Figure 4.32: FFT spectrum pertaining experiments shown in Figs. 4.30 and 4.31: (a) Healthy zone; (b) Faulty zone.

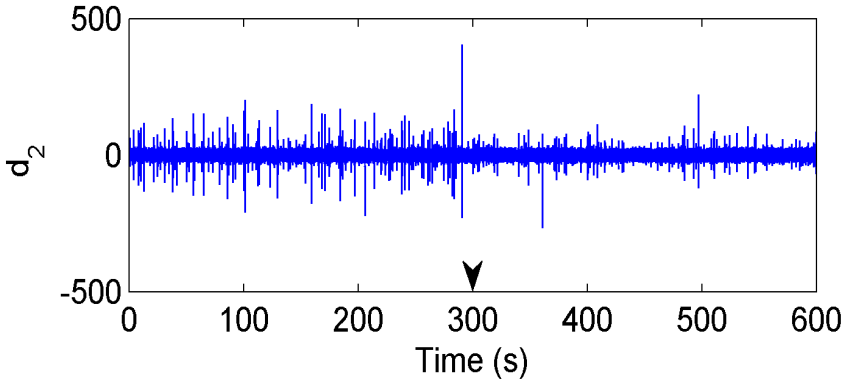

Figure 4.33: Wavelet coefficient d_2 pertaining experiments shown in Figs. 4.30 and 4.31.

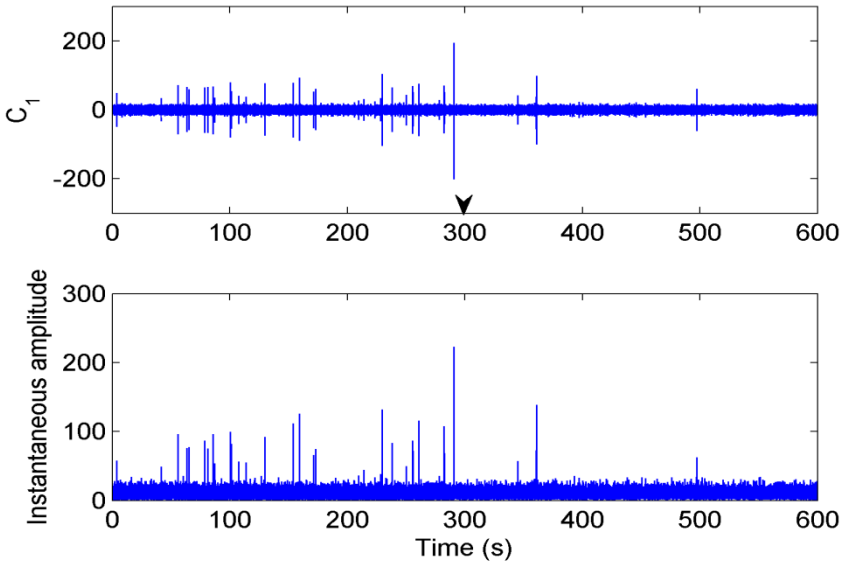

Figure 4. 34: First IMF and its instantaneous amplitude pertaining experiments shown in Figs. 4.30 and 4.31.

4.6. Summary

To see which of these methods is more suitable for the purpose of this work, a comprehensive comparison between FFT, HHT and DWT for internal leakage detection is made by using the same data obtained from the actuator running for 18 times under normal operating condition and 18 times including small and medium internal leakages presented before while a structured input is applied to servovalve. The results are summarized in Table 4.4. The mean values are taken from all the RMS values obtained from all 18 tests. The HHT shows more sensitivity to internal leakage detection while using a structured input signal. To further justify this, referring to baselines determined before for FFT, WT and HHT (see Figs 4.7, 4.15 and 4.23), small leakage type is identifiable 95% and 80% of the times with the HHT and WT respectively, and only 30% of the times with FFT.

Table 4.5: Comparison of FFT, HHT and DWT.

	Normal actuator	Leaky actuator	
	Mean value	Mean value	Percentage of changes
C_1	130.7	81.9	37.33
d_2	132.6	103.3	22
FFT	6.3	5.5	12.6

These methods are then investigated using an unstructured input signal. For a pseudorandom reference input, using simple method such as Fourier analysis is not very suitable. The wavelet transform is so far the most popular technique as it possesses good time and frequency localization properties. Despite the satisfactory results using the wavelet analysis in many applications, there are still some issues making this approach challenging. The analysis depends on the choice of the wavelet function. This leads to a subjective, a priori, assumption on the characteristics of the investigated phenomenon (Loutridis, 2004). As a consequence, only signal features that correlate well with the shape of the wavelet function have a chance to lead to coefficients of high value. All other features will be masked or completely ignored (Loutridis, 2004). Other issues lie in the overlap between frequency bands associated with the wavelet signals; however, a high order mother wavelet can reduces the overlapping. The frequency bands each wavelet coefficients covers is fixed and depends on the sampling frequency. This may lose the flexibility mainly when studying high frequency components introduced by faults. However, the application of DWT is simple and the patterns that arise from the application of this transform are clear and reliable, making it a robust tool for the diagnosis of the fault (Antonino-Davin et al., 2009). Moreover, the method is very easy to implement and the computational requirement are negligible (Antonino-Davin et al., 2009). For example, the computational time for calculating mode C_1 is 30 seconds; however, calculating d_2 takes only 2 seconds on the same personal computer (Pentium 4, CPU 2.8 GHz).

The strength of HHT lies in its use of a *posteriori*-defined basis. Unlike traditional signal decomposition techniques such as wavelets and FFT that decompose the original signal into a series of constituents of fixed predetermined frequencies, the generated IMFs do not necessarily have constant frequency or amplitude, and it is for this reason that it is often difficult to assign any physical meaning to them. This can create problems for selecting the most suitable numbers of IMFs to be considered for detection of the fault (Antonino-Davin et al., 2009). There is also no theoretical background for HHT. For this application, using FFT, the frequency range of interest sensitive to internal leakage can be determined. Utilizing DWT can be more readily as the exact range of frequency covered by each wavelet coefficient is known. For online application, DWT can provide a fast response as compared to HHT which takes a very long time. For these reasons the DWT is selected as a good candidate for the purpose of this thesis. DWT will be used for the rest of this thesis.

4.7. Internal leakage level detection

It is investigated whether leakage faults with different severities can be distinguished. Fig. 4.35 shows the results of introducing four levels of leakages given the same input signal as in Fig. 4.1. Table 4.5 summarizes the results of experiments and wavelet analysis. In Table 4.5, a leakage level causing a reduction of flow rate less than 10% is defined as small; a reduction between 10% to 25% is medium-small; a reduction between 25% to 40% is defined as medium-large, and finally any leakage level that causes a reduction of available flow rate over 40% is considered large. From Table 4.5 it is observed that as the severity of the fault increases, the RMS values of coefficient d_2 decrease.

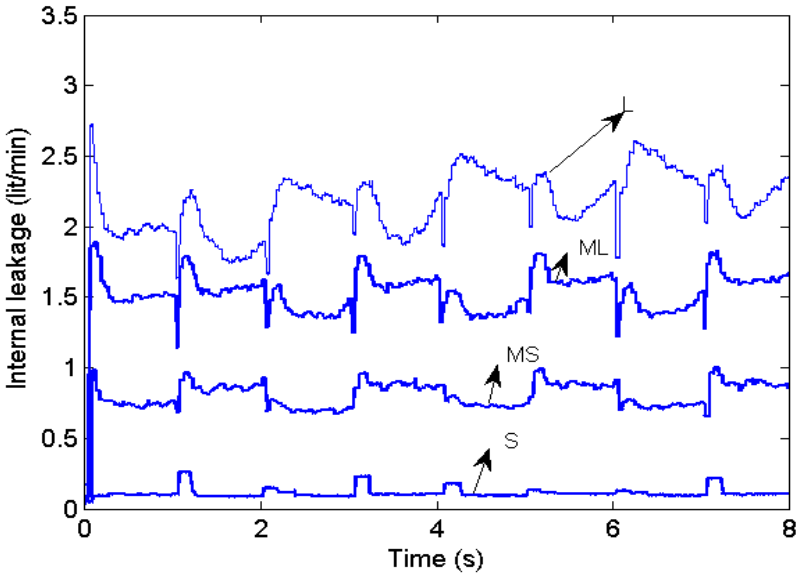

Figure 4.35: Internal leakage of various severity; S=small, MS=medium-small, ML= medium-large, L= large.

Table 4.6: RMS values of coefficient d_2 from the measurement of chamber one for actuator under normal and faulty operating conditions

Leakage level	Percentage reduction in the flow rate	Mean Leakage Value (lit/min)	RMS d_2	Percentage change
no leak-normal (N)	0	0	155.27	0
small (S)	2.0	0.09	108.29	30.2
medium-small (MS)	17.5	0.80	95.16	38.7
medium-large (ML)	33.2	1.52	81.05	47.8
large (L)	49.1	2.25	70.4	54.6

Chapter 5

5. Internal leakage detection using online measurements[1]

5.1. Introduction

Prompt diagnosis of faults associated with hydraulic actuators is important to maintain reliability and performance and to avoid complete loss of functionality. This Chapter presents a new development and evaluation of a wavelet-based method, intended for online detection of internal leakage in a valve-controlled hydraulic actuator. The positioning of the actuator against the spring load is achieved according to the two-degree-of-freedom feedback system configuration shown in Fig. 4.29. The controller, $G(s)$, and the prefilter, $F(s)$, are designed to satisfy the desired closed-loop performance specifications. Two controllers are used to examine the efficacy of the fault detection technique developed here. The first controller has been designed using quantitative feedback theory (QFT). It is a fixed gain controller that is robust against typical uncertainties inherent to hydraulic actuators. The elements of this controller, which is hereafter referred to as the 'basic controller,' are:

$$G(s) = \frac{2.76\times10^{6}(s+25)}{(s+16)(s^{2}+108s+120^{2})} \tag{5.1}$$

$$F(s) = \frac{100}{s+100} \tag{5.2}$$

The second controller is also a QFT-based controller with an additional characteristic of holding a desirable performance even in the presence of an internal leakage fault up to

[1] Some materials in this Chapter have been published in International Journal of Fluid Power, vol. 11, no.1, pp. 61-69, 2010.

40% of the rated servovalve flow across the actuator piston. The structure of this controller, hereafter called the 'fault tolerant controller,' is shown below:

$$G(s) = \frac{246.59s^3 + 7.18\times10^3 s^2 + 4.78\times10^7 s + 5.49\times10^8}{s^3 + 420s^2 + 9\times10^4 s} \tag{5.3}$$

$$F(s) = \frac{22.04s + 297.5}{s^2 + 43.5s + 297.5} \tag{5.4}$$

The detailed derivation of the QFT controllers has been reported by (Karpenko and Sepehri, 2005; Karpenko, 2008).

This chapter extends the Chapter 4 results to include the more realistic case of the actuator following a pseudorandom reference positioning signal and under a load emulated by a spring. The pseudorandom signal is characterized with a series of desired step inputs having amplitudes between 0.025 m to 0.05 m and duration between 0.5 s to 4 s. This type of signal resembles activities of flaps for typical in-flight maneuvers (Nguyen at al., 1979), and allows to investigate the online fault detection ability of the proposed method. All experiments are conducted with QFT-based controllers described by Eqs. (5.1) to (5.4) for very small leakages, since these type of leaks are most interesting for early detection of faults.

5.2. Experimental results

The first experiment relates to the case, where a healthy actuator undergoes a set of positioning tasks against a spring having stiffness of 80 *kN/m*. The basic controller described by Eqs. (5.1) and (5.2) is used for control purposes. After 15 seconds of operation, an internal leakage having a mean value of ≈0.21 lit/min is introduced. Assuming linear pressure dependence, this flow represents ≈0.12 lit/min/MPa. The actuator displacement response is plotted in Fig. 5.1. Fig. 5.2 shows the plot of internal leakage.

With reference to Fig. 5.1, it is clearly seen that there is an error in system response after the occurrence of internal leakage since the controller, although designed to be robust to uncertainty of the parameters of the system, was not robust to the internal leakage. The cylinder pressures are plotted in Fig. 5.3. As was mentioned earlier, the

approach for online internal leakage detection is based on studying level two detail coefficient, d_2, derived from the chamber one pressure signal, P_1 as shown in Fig. 5.4. Note that, the pressure signal in chamber two, P_2, may be equally chosen for the analysis.

With reference to Figs. 5.3 and 5.4, internal leakage adds damping to the system which suppresses the transient pressure response. This in turn decreases the amplitude as well as the energy of the detail wavelet coefficient d_2 (defined as $\sum_{k=1}^{N}\left|d_2(k)\right|^2$, where N is the number of data samples), which can be seen from Fig. 5.4. Note that the whole pressure signal is analyzed by using the WT. In online equipment health monitoring signals, are monitored and gathered during the operation. The next Section, the design of the online leakage detection method is described.

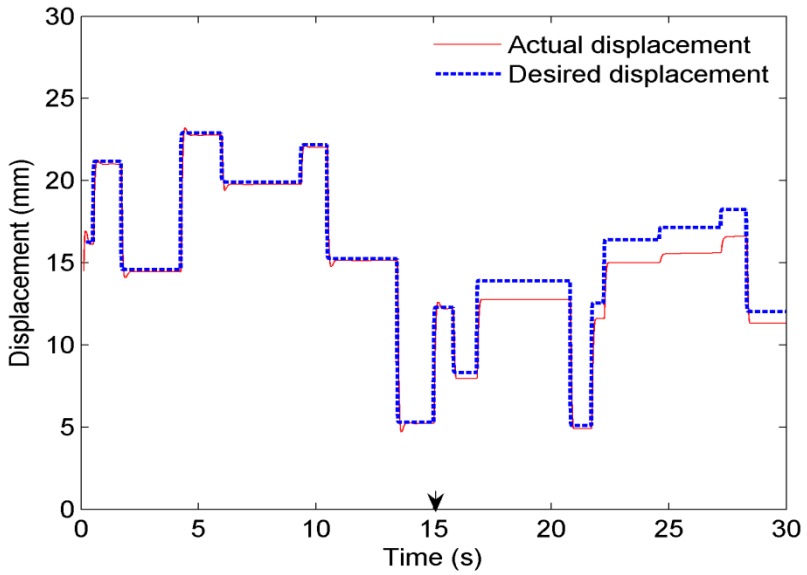

Figure 5.1: Desired and actual displacements of hydraulic actuator with internal leakage introduced at t≈15s.

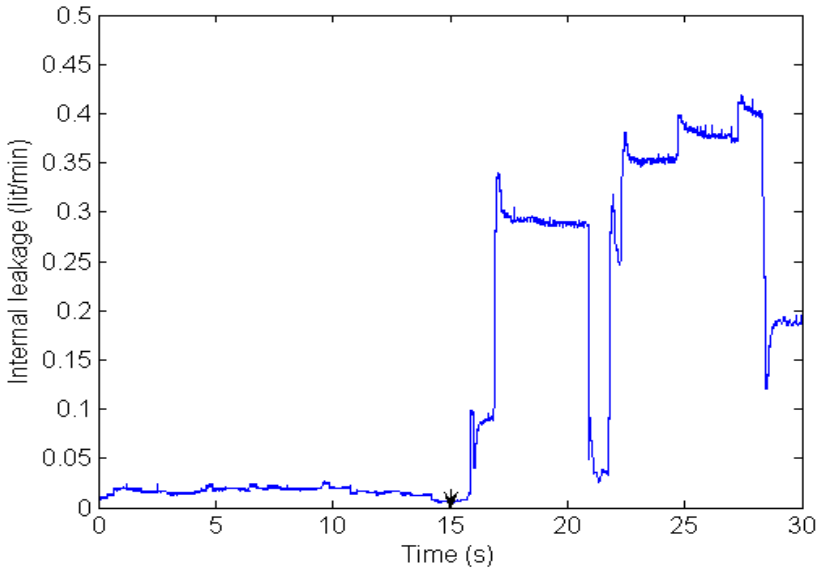

Figure 5.2: Internal leakage fault representing ≈0.12 lit/min/Mpa.

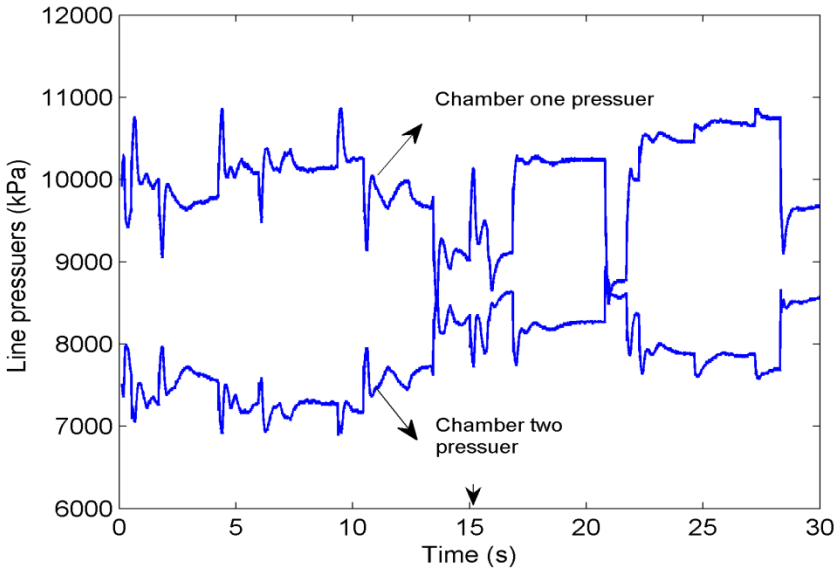

Figure 5.3: Pressures in chambers one and two with internal leakage introduced at t≈15s.

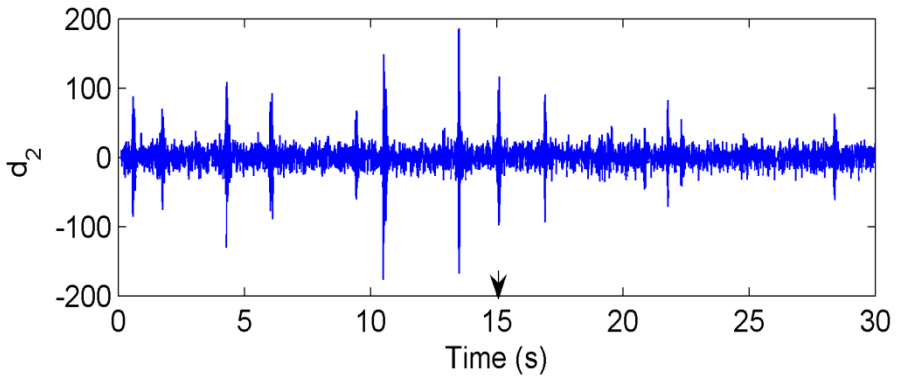

Figure 5.4: Level two wavelet coefficient of chamber one pressure with internal leakage introduced at t≈15s.

5.3. Design for online detection

For online processing, limited-duration pressure signal should be gathered. The wavelet analysis then breaks each limited-duration data sequence into packets containing only the signal components within certain frequency bands. Here, the sliding window by Zhao and Xu (2004) technique is adopted to form data segments.

With reference to Fig. 5.5, the data window has a length l_1. The past window contains data collected in the past and the current window which is the shift of the past window with a fixed step size l_2, contains data collected in the most recent time. Wavelet coefficients are repeatedly recalculated for intervals of l_2 samples, each based on the most recent l_1 samples of the signals. The root mean square (RMS) of the elements of vector of coefficients d_2 obtained from each window is then calculated as an index. Note that in order to extract reliable and complete information from the decomposed signals, each window should carry a sufficient length of data (Gao and Zhang, 2006). The length of the step size with respect to the window size should also be selected carefully. A small step size increases the computational cost and the nature of the windowed signal may not be sufficiently affected by the new data zone. A very large step size increases the detection delay as one needs to wait longer to update the relevant index. In this work, window size of l_1=400 samples and step size of l_2=20 samples were found to be appropriate. The measurement sampling rate was 500Hz.

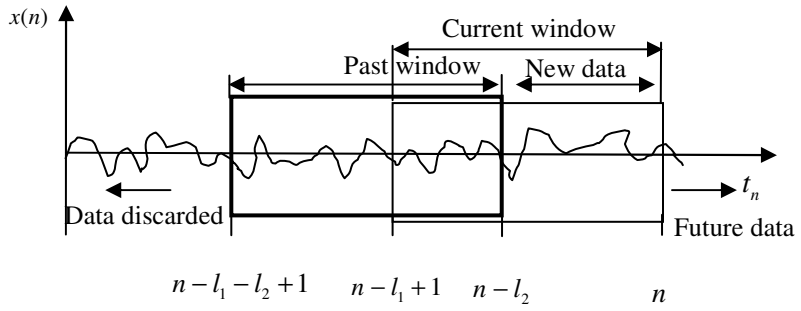

Figure 5.5: Sliding window technique.

The sliding window concept is now applied to the results of the case study reported earlier in this Chapter. The RMS values obtained from each updated window are plotted in Fig. 5.6. The RMS appears to decreases once the internal leakage is introduced to the system at t≈15s. Whereas d_2 in Fig. 5.4 was obtained using the entire data (gathered over 30 seconds), the plot shown in Fig. 5.6, is the result of information being processed online.

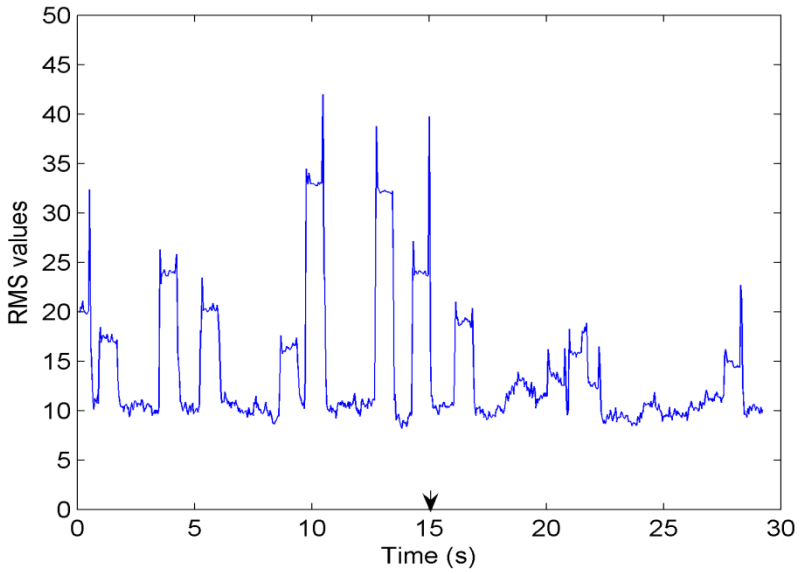

Figure 5.6: RMS of wavelet coefficient, d_2, obtained from chamber one pressure with internal leakage occurred at t≈15s.

In order to show the robustness of this method to the type of controller, two more tests are conducted with a small internal leakage. For each test, the reference position signal

is generated randomly, and the system runs for 600s. A small internal leakage is then manually introduced at t≈300 s. The test employs the basic control scheme described by Eqs. (5.1) and (5.2).

Figs 5.7 and 5.8 show the close-up plots of displacement response of the control system and the leakage, respectively. Fig. 5.9 shows the RMS values of level two detail coefficients of chamber one pressure signal obtained using the sliding window technique. The RMS values decrease after the introduction of internal leakage. To facilitate the comparison between healthy and faulty zones, a baseline value of 30 is chosen for the RMS values. It is seen that with the introduction of internal leakage the RMS values stay below the baseline close to 90% of the time.

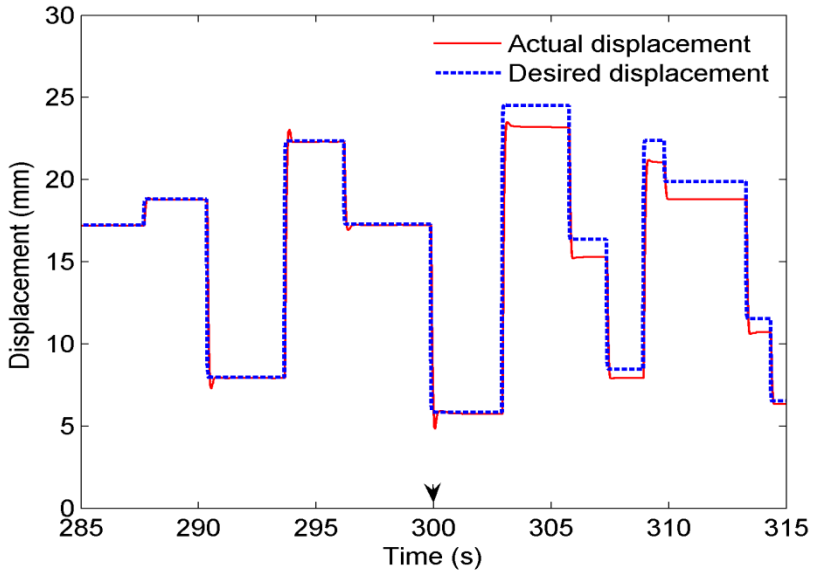

Figure 5.7: Close-up response of actuator with internal leakage introduced after t≈300s. The 'basic control scheme' is used and the total test time is 600 s.

The next test shows that this method is sensitive to small amounts of internal leakage even when the controller is capable to fulfill the commands. The 'fault tolerant controller' described by Eqs. (5.3) and (5.4) is implemented. The close-up plots of displacement and the leakage fault are shown in Figs. 5.10 and 5.11. The controller works well even after the introduction of internal leakage after t≈300s, and there is no

apparent steady-state error in the position response. This is due to the fact that the controller was designed to be robust to internal leakage.

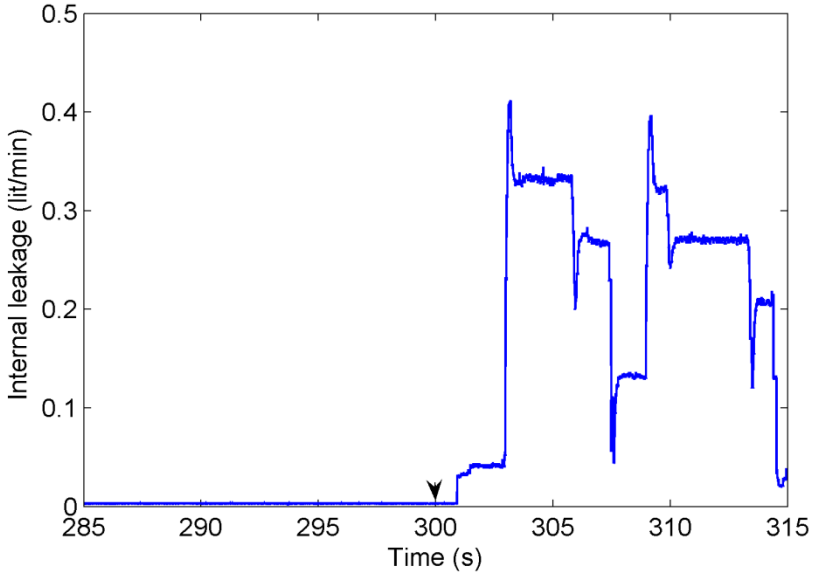

Figure 5.8: Close-up of internal leakage fault (mean value 0.25 lit/min representing ≈0.13 lit/min/Mpa).

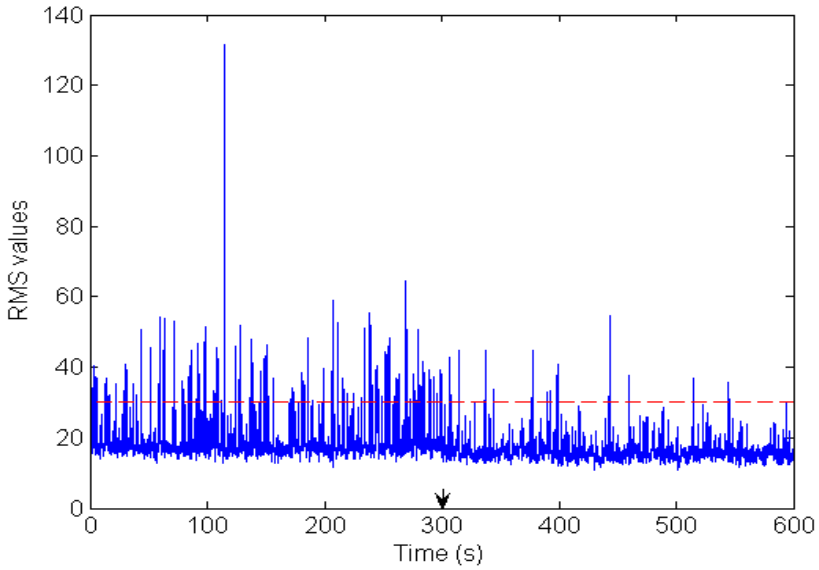

Figure 5.9: RMS values of wavelet coefficient, d_2, pertaining the experiment shown in Figs. 5.7 and 5.8.

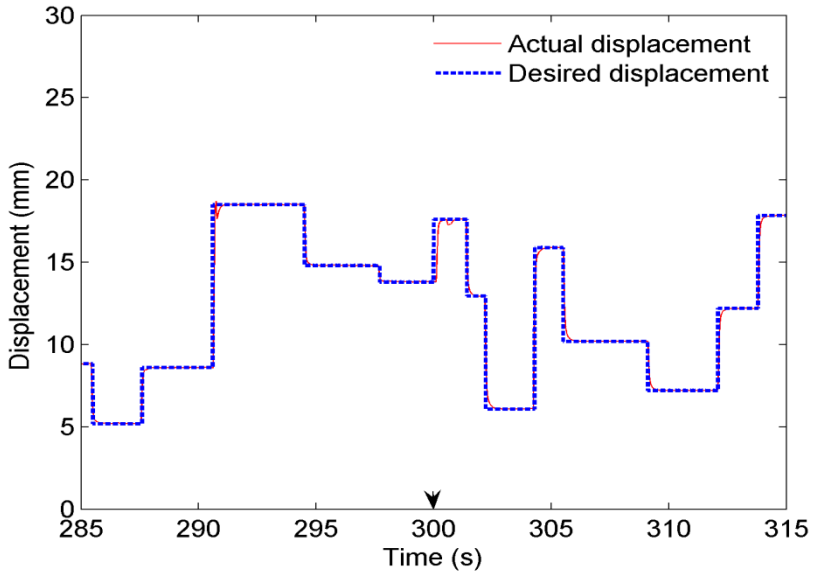

Figure 5.10: Close-up response of actuator with internal leakage introduced after t≈300s. The 'fault tolerant control scheme' is used and the total test time is 600s.

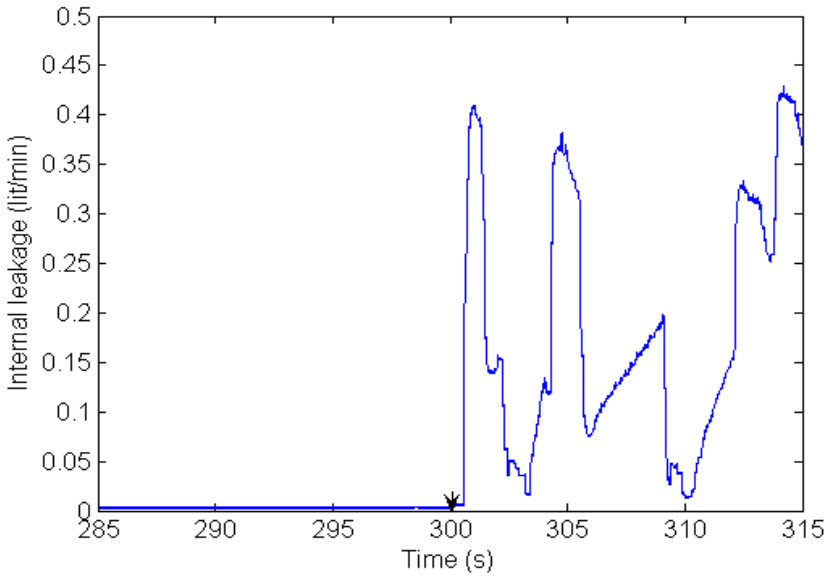

Figure 5.11: Close-up of internal leakage fault (mean value 0.23 lit/min, representing ≈0.149 lit/min/Mpa).

By studying the pattern of changes in the RMS of the detail coefficients, d_2 (see Fig. 5.12) one can recognize the occurrence of an internal leakage after t≈300s. Given the same baseline value as in Fig. 5.9, a substantial decrease in RMS values after the occurrence of internal leakage can be seen. It is then concluded that the method remains

effective even with a fault tolerant controller, which maintains the positioning of the leaky actuator.

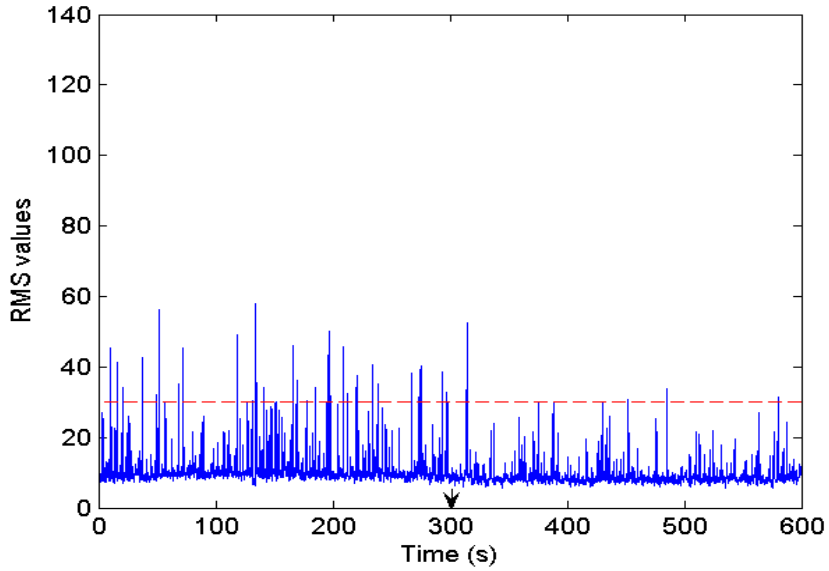

Figure 5.12: RMS values of wavelet coefficient, d_2, pertaining experiment shown in Figs. 5.10 and 5.11.

The final experiment is performed to illustrate that the method is robust to different loading conditions. A different spring with stiffness of 440 *kN/m* is used to accomplish this different loading. The 'fault tolerant controller' described by Eqs. (5.3) and (5.4) is implemented. The close-up plot leakage fault is shown in Figs. 5.13. Given the same baseline value as before, a substantial decrease in RMS values after the occurrence of internal leakage can be seen. It is concluded that the method remains effective even with a different loading condition.

In summary, an approach based on wavelet transform technique was developed for detecting internal leakage in hydraulic actuators. The proposed scheme is implementable for online diagnosis. The method allows information to be gathered while the actuator is controlled to perform arbitrary tracking, and under loading condition. Measurement of pressure signal at one side of the actuator is the only requirement in this method. Using a sliding window technique, limited-duration segments of measured pressure signal are collected. Each segment is then decomposed via a wavelet transform and RMS values of level two detail coefficients of the

decomposed signals, pertaining to each segment are analyzed to detect the occurrence of fault. When a leakage happens, the RMS values decrease both in magnitude and energy. Experimental results demonstrated the efficacy of the proposed technique. In the experimental setup, the actuator was set to track pseudorandom reference positions over a long period of time and against a load emulated by a spring. Using this technique, internal leakages, in the range of 0.2-0.25 lit/min, was detected regardless of the type of feedback controller used, reference input and loading condition.

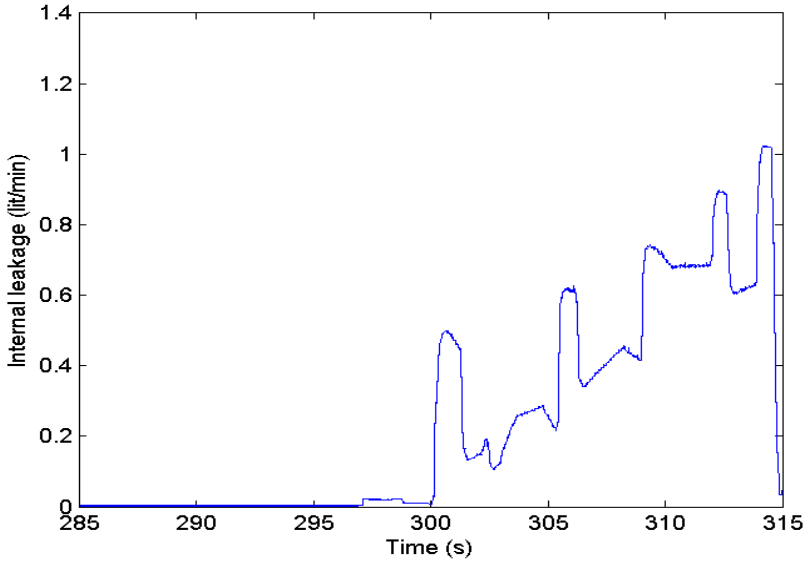

Figure 5.13: Close-up of internal leakage fault (mean value 0.59 lit/min, representing ≈0.38 lit/min/Mpa).

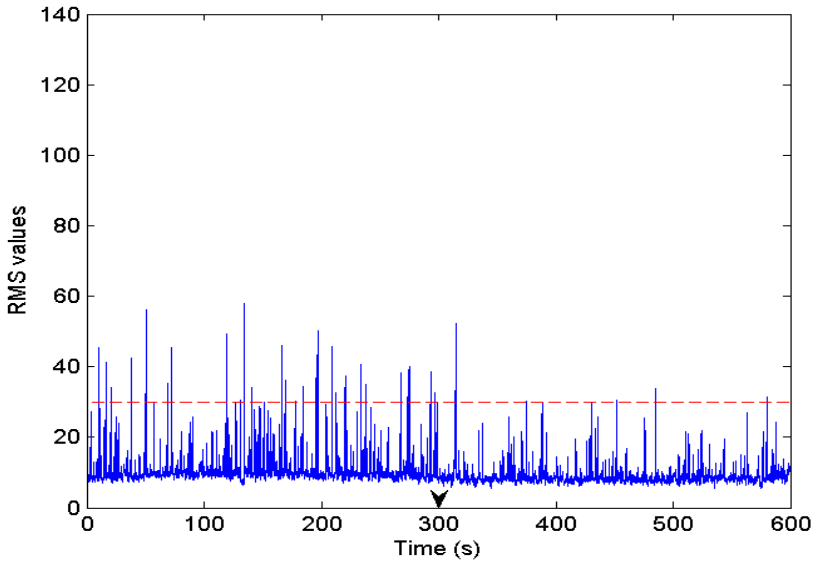

Figure 5.14: RMS values of wavelet coefficient, d_2, pertaining experiment shown in Fig 5.13.

Chapter 6

6. External leakage detection and isolation from internal leakage[1]

6.1. Introduction

As described in Chapter 2, external leakage alters the steady-state response, while internal leakage contributes to changing the transient response of pressure signal at either side of the hydraulic actuator. External leakage causes pressure to drop, and can be considered as a bias fault. When a bias or drift occurs in a signal, the event appears strongly in coarser scales represented by approximation coefficients of wavelet decomposition (Zhang and Yan, 2001). Thus, approximate wavelet coefficients of pressure signals can be used to detect the external leakage. The mother wavelet (db8) will be used throughout the rest of this Chapter. The db8 wavelet will also be shown that it is a good choice for external leakage detection as well as internal leakage fault.

6.2. External leakage detection using structured input signal

In this Section, external leakage detection is described using a structured input signal. This is useful when the offline detection of external leakage is desirable. The first experiment relates to the normal operating condition, which provides a baseline for comparison. The same signal as in Fig. 4.1 is applied to the servovalve which results in pressure signals as shown in Fig. 4.2. The rate at which the data are collected is 500Hz. In this thesis, the chamber one pressure, P_1, is used in the wavelet analysis to obtain the

[1] Some materials in this Chapter have been accepted for publication in IEEE Transaction on Industrial Electronics.

wavelet coefficients. The pressure signal in chamber two may be equally chosen for the analysis. Figure 6.1 shows the wavelet approximate coefficients $(a_1,...,a_5)$ obtained from the original signal, P_1, under normal operating condition. In the second experiment, an external leakage from chamber one is introduced having a mean value of 1.53 lit/min. The plot of the leakage is shown in Fig. 6.2 given the same structured input signal as in Fig. 4.1. The corresponding pressure signals are plotted in Fig.6.3. Figure 6.4 shows five-level approximate wavelet coefficients corresponding to the chamber one pressure signal. Comparing Figs. 6.1 and 6.4, all of the scales are seen to decrease as a result of external leakage. In this thesis, scale four, a_4, is used for external leakage detection having little computational burden as well as good sensitivity to this fault type.

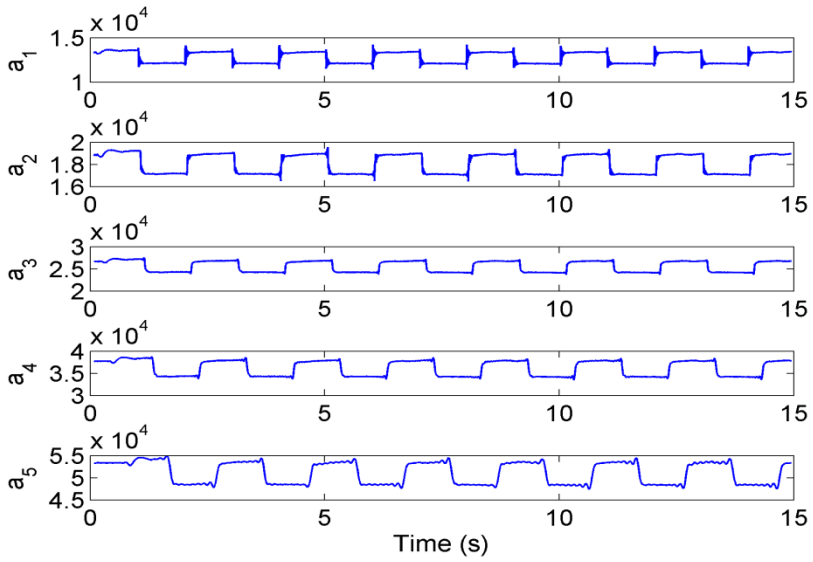

Figure 6.1: Five-level approximate wavelet coefficients of chamber one pressure signal for actuator under normal operating condition.

To facilitate the diagnosis, RMS value of approximate wavelet coefficient, a_4, ($\sqrt{\frac{\sum_{k=1}^{N} a_4^2(k)}{N}}$, where N is the number of data samples) is calculated over the entire test period. Table 6.1 shows the results when chamber one or two pressure signals are used to detect external leakage (having mean values of 1.53 lit/min) at either side of the

actuator. Note that scaling is done to set the RMS values between 0-1 for all the results in this Chapter to facilitate comparison. From Table 6.1, it is seen that either the pressure signal of chamber one, P_1, or chamber two, P_2, can be used for the analysis. However, the side from which, external leakage is originating cannot be detected.

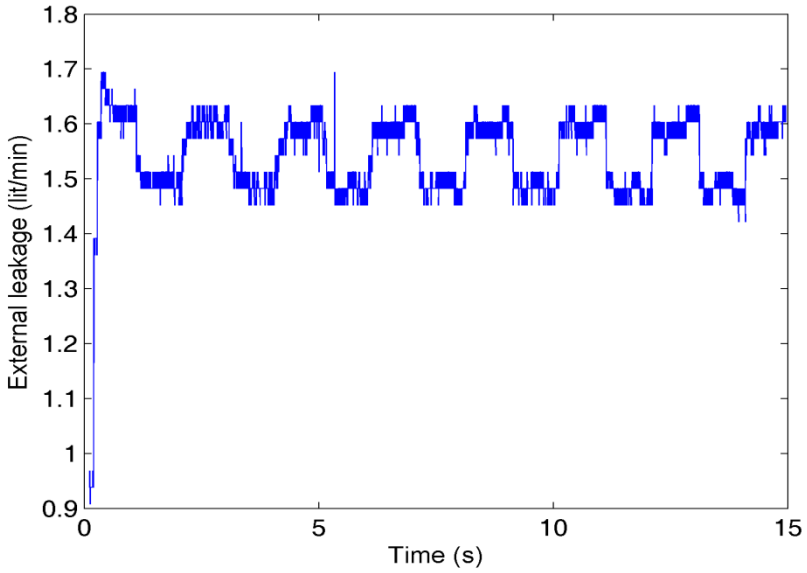

Figure 6.2: Plot of external leakage flow for actuator with faulty seal at chamber two given the input signal shown in Fig. 4.1.

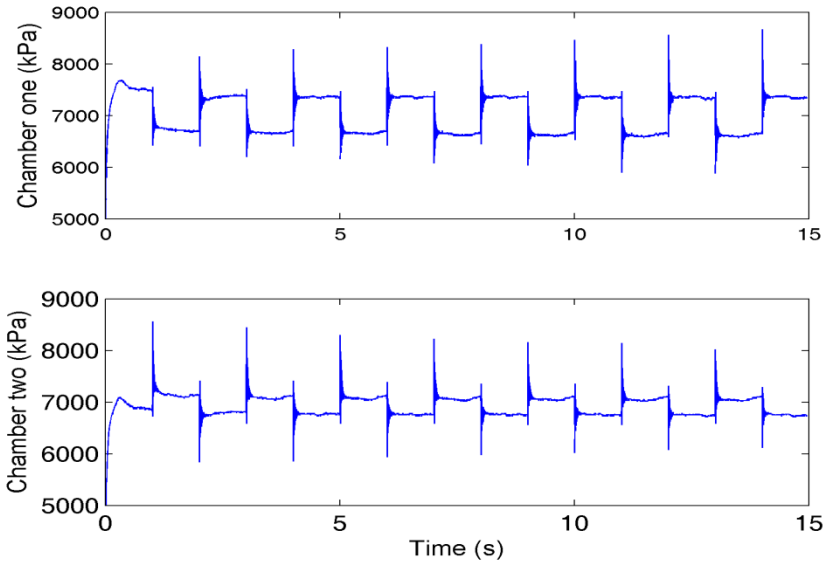

Figure 6.3: Pressures in chambers one and two of hydraulic actuator with external leakage shown in Fig. 6.2.

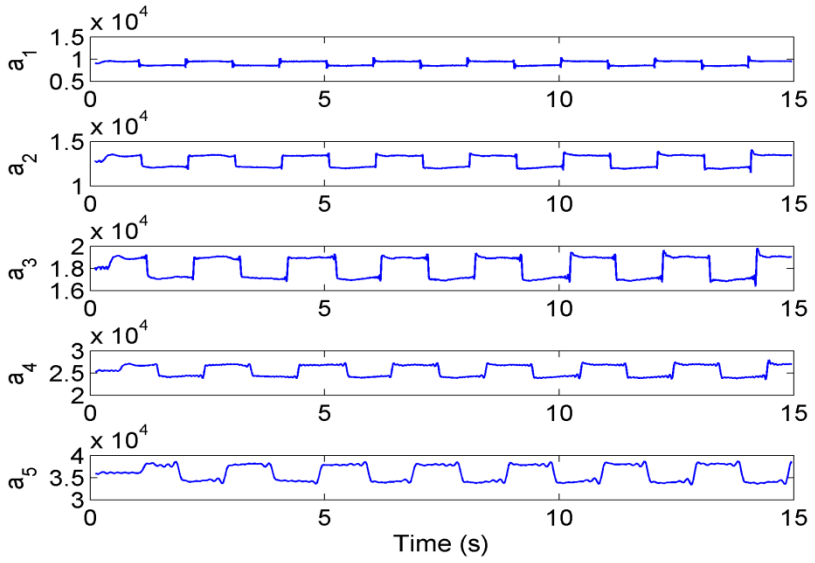

Figure 6.4: Five-level approximate wavelet coefficients of chamber one pressure signal for actuator under external leakage condition.

Table 6.1: Scaled RMS values for approximate wavelet coefficient, a_4, from measurement of chamber one and two pressure signals under normal and faulty operating conditions.

	Scaled RMS value of a_4 obtained from P_1	Scaled RMS value of a_4 obtained from P_2
Healthy	1	0.986
External leakage in chamber one	0.7	0.69
External Leakage in chamber two	0.7	0.69

In the third test, it is investigated whether leakage faults with different severities can be distinguished. Fig. 6.5 shows the results of introducing four levels of external leakages applied at the chamber one side, given the same input signal as in Fig. 4.1. Table 6.2 summarizes the results of experiments and wavelet analysis based on the pressure in chamber one, P_1. Table 6.2 illustrates that as the severity of the fault increases, the RMS value of coefficient a_4 decreases.

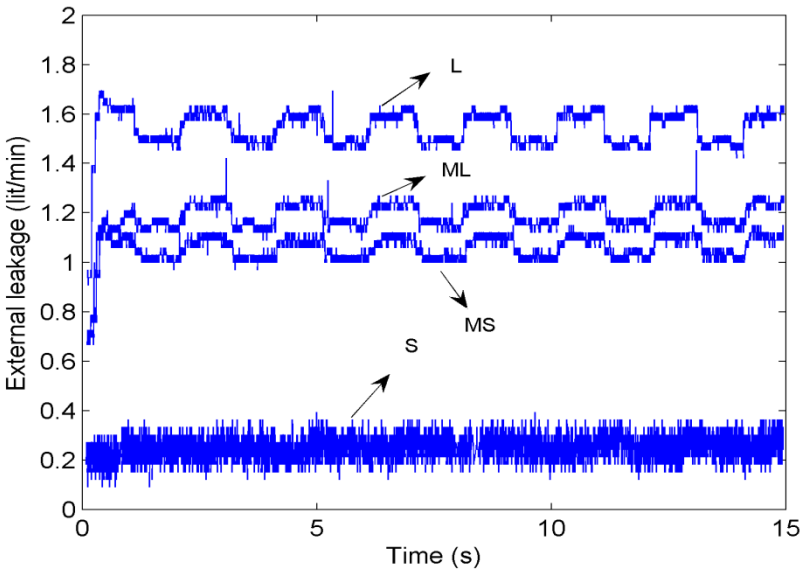

Figure 6.5: External leakage of various severity; S=small, MS=medium-small, ML= medium-large, L= large.

Table 6.2: RMS values of approximate wavelet coefficient, a_4, from measurement of chamber one pressure signal under normal and different external leakage conditions.

Leakage level	Mean Leakage Value (lit/min)	Percentage Reduction in the Flow Rate	Scaled RMS Value of a_4	Percentage change in RMS
no leak-normal (N)	0	0	1	0
small (S)	0.24	5	0.95	5
medium-small (MS)	1.05	22	0.78	22
medium-large (ML)	1.18	24.7	0.76	24
large (L)	1.53	32.3	0.69	31

The level four approximate coefficient, a_4, was shown to be useful for external leakage fault detection. The consistency of the results presented so far is shown by running the test rig, 18 times under normal operating condition and 18 times under small-type external leakage on either side of the actuator. Note that for the first nine experiments external leakage is applied to chamber one, and for the remaining nine tests, it is introduced to chamber two. Both chambers one and two pressure signals are used to

calculate a_4. This is to further confirm that either one of the pressure signals can be used to detect an external leakage in either side of the actuator. The focus is placed on small leakages, since these are most difficult to detect. The leakage value was, on average, 0.2935 lit/min, representing approximately 6.15% reduction of flow rate available to move the actuator.

The scaled RMS values of approximate coefficient, a_4, obtained from all tests, using random laboratory tests at various times, are shown in Fig. 6.6. The results show that the RMS value of level four approximate coefficient of the pressure signal is reduced significantly with the introduction of an external leakage. Choosing the baseline as the minimum RMS value of a_4 (0.97) observed for normal operating condition, the small leakages are identifiable all of the times. Using either pressure signal external leakage from either side cannot be distinguished.

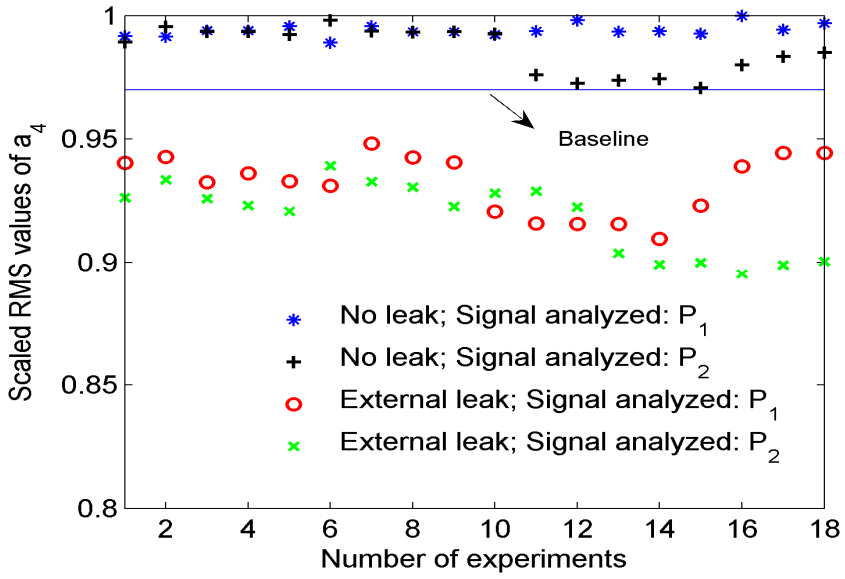

Figure 6.6: Scaled RMS values of approximate wavelet coefficient, a_4, obtained from healthy actuator and actuator experiencing small external leakage of 0.29 lit/min in average. In the first nine tests, external leakage is placed in chamber one; for the remaining tests, external leakage is placed in chamber two. Both pressure signals are used for analysis.

Please note that when there is an external leakage the actuator shifts towards the leaky chamber and this may affect the oscillations in pressures signals. It is better the actuator moves back and forth around the centre of it.

6.3. Isolation of external and internal leakages in a multiple fault environment using structured input signal

In this section, the isolation of external leakage from internal leakage is investigated. For all results presented in this section, the pressure at chamber one, P_1, is used for the analysis. From the previous Chapters internal leakage was shown to change the transient behavior of the pressure signals, and subsequently decrease the amplitude and energy of level two detail coefficient, d_2. In the first set of tests, the system was run for 18 times under normal operating conditions and 18 times under small internal leakage with average of 0.124 lit/min, representing approximately 2.6% reduction of flow rate available to the actuator. The scaled RMS values of the detail coefficient, d_2, fall below a baseline (chosen as the minimum RMS value obtained from normal operating conditions) 80% of the times (see Fig.6.7).

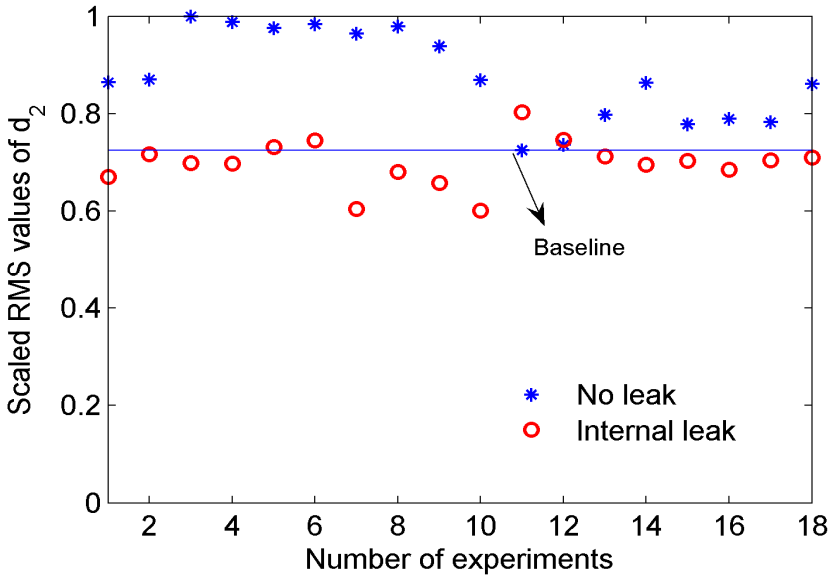

Figure 6.7: Scaled RMS values of detail wavelet coefficient, d_2, obtained from healthy actuator and actuator experiencing small internal leakage, (0.124 lit/min in average).

Now, it is shown that the coefficient, a_4, is insensitive to the internal leakage whereas it was shown to be sensitive to the external leakage. In this set of experiments, the system was run for 18 times under normal operating condition and 18 times with random internal leakages in the range of 0.1-1.6 lit/min. The results shown in Fig.6.8 illustrate that the internal leakage has no effect on the approximate coefficient, a_4.

The d_2 detail coefficient is investigated to determine its sensitivity to external leakage. For this test, random external leakages (0.24-1.6 lit/min in average) on either side of the actuator were created for 18 times. The results, presented in Fig. 6.9, reveal that the external leakage has a negligible effect on the detail coefficient, d_2, as the scaled RMS values of, d_2, are above the predetermined baseline for 90% of the times. The coefficients a_4 and d_2 are concluded to be independently sensitive to the effect of external and internal leakages. By inspecting the a_4 and d_2 coefficients not only can external and internal leakages be detected, but also, these faults can be isolated when they happen at the same time. The final tests relate to a multiple-fault environment that includes both internal and external leakages. To emulate the multi-fault environment the system was run for 9 times when there were both external and internal leakages with the average of 0.36 lit/min and average of 0.26 lit/min. The scaled RMS values of d_2 and a_4 are shown in Fig.6.10; as they fall below the predetermined baselines the occurrence of both faults can be reported 90% of the time.

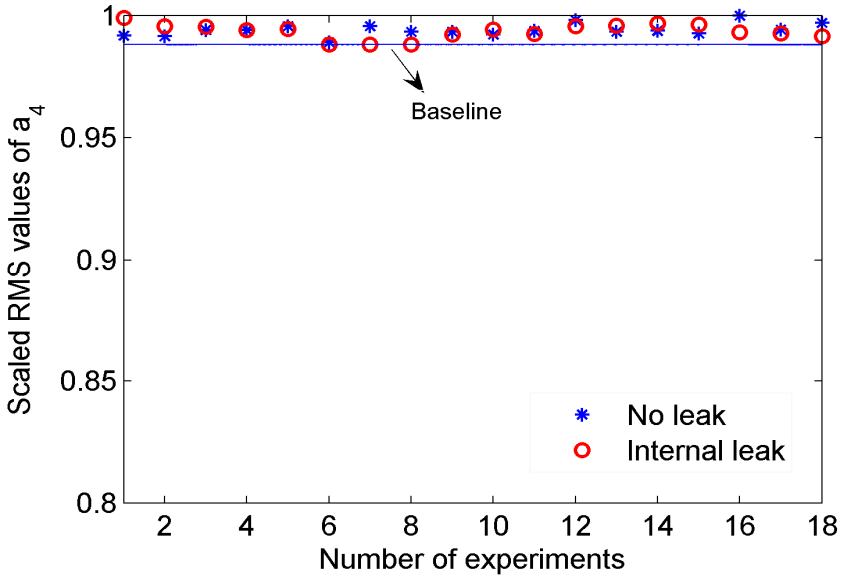

Figure 6.8: Scaled RMS values of approximate wavelet coefficient, a_4, obtained from healthy actuator and actuator experiencing internal leakages in the range of 0.1-1.6 lit/min.

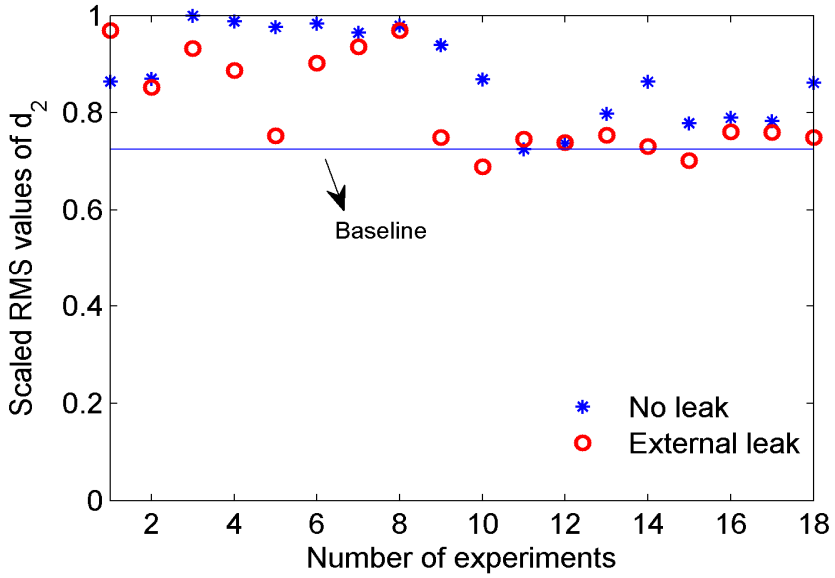

Figure 6.9: Scaled RMS values of detail wavelet coefficient, d_2, obtained from healthy actuator and actuator experiencing random small external leakages in the range of 0.24-1.6 lit/min, on either side on the actuator.

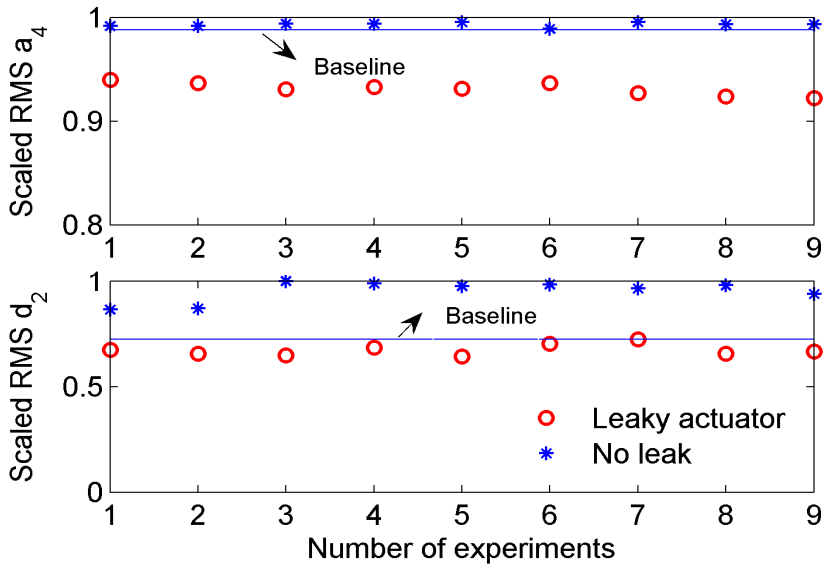

Figure 6.10: Scaled RMS values of approximate wavelet coefficient, a_4, and detail coefficient, d_2, obtained from actuator experiencing both small external leakages on either side of the actuator (0.36 lit/min in average), and internal leakages (0.26 lit/min in average).

6.4. Online external leakage detection via wavelet coefficients

6.4.1. External leakage detection using a pseudorandom reference input

This Section includes the more realistic case of the actuator following a pseudorandom reference positioning signal under a load emulated by a spring to investigate the effectiveness of this approach toward online diagnosis task. The pseudorandom signal is characterized with a series of desired step inputs having amplitudes between 0.025 m to 0.05 m and duration between 0.5 s to 4 s. The fact that it emulates in-flight maneuvers allows investigating online fault detection ability. All experiments are conducted with QFT-based controllers described by Eqs. (6.1) to (6.2) and for very small leakages, since they are most interesting for early detection of faults:

$$C(s) = \frac{3.18 \times 107(s+12)}{s(s^2 + 225s + 250^2)} \tag{6.1}$$

$$F(s) = \frac{25(s+13.5)}{(s+8.5)(s+35)} \tag{6.2}$$

The controller is used here to examine the efficacy of the fault detection technique developed here. The controller designed using the quantitative feedback theory (QFT) is tolerant to model uncertainty and certain leakage fault types associated to hydraulic actuators (Karpenko, and Sepehri, 2010). The structure of this controller is different from the two controllers used in Chapter 5. The effectiveness of the proposed wavelet based methods regardless of the controller type can be checked, using the controller in Eq. (6.2).

The first experiment relates to the case where a healthy actuator undergoes a set of positioning tasks against a spring of stiffness 80 *kN/m*. After 30 seconds of operation an external leakage having a mean value of ≈0.3 lit/min is introduced (see Fig. 6.11). Note that the external fault is created on the P_2 side and there is no deference in the results presented here if there is an external leakage on the other side. However, this method cannot distinguish between an external leakage from either side of the actuator. The resulting actuator displacements along with the desired displacements are shown in Fig. 6.12. The controller still can track the reference input without introducing any significant error even when there is an external leakage in the system after t≈30s. The changes in the pressures are plotted in Fig. 6.13.

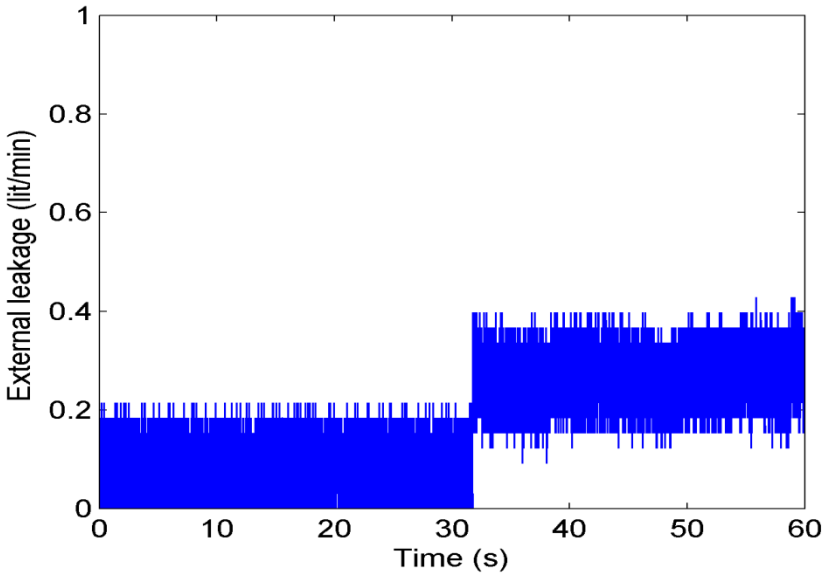

Figure 6.11: External leakage in chamber two of the hydraulic actuator (mean value of 0.3 lit/min).

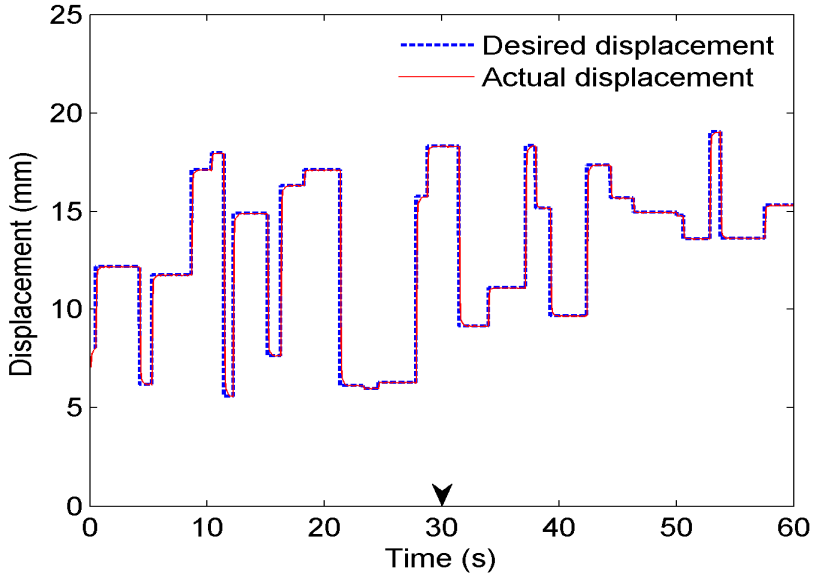

Figure 6.12: Desired and actual displacement of the hydraulic actuator with external leakage shown in Fig. 6.11.

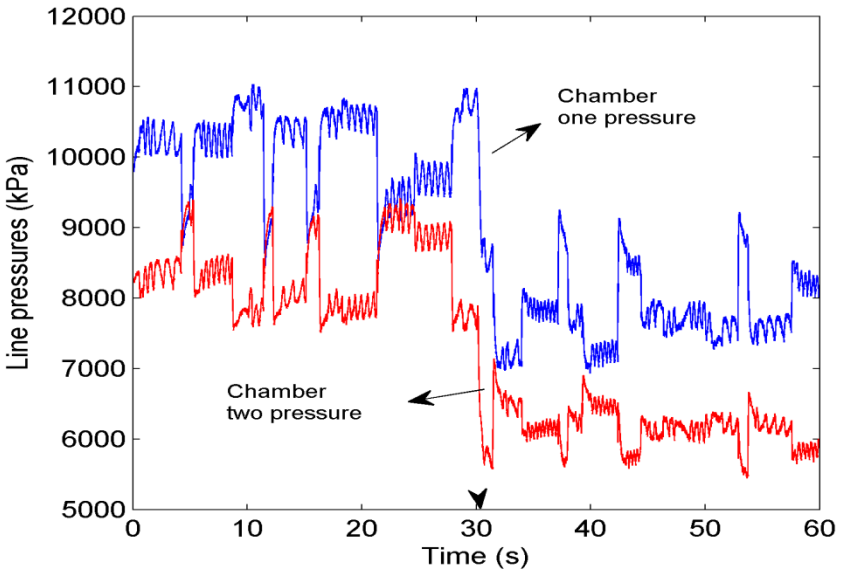

Figure 6.13: Line pressures with external leakage shown in Fig. 6.11.

This approach for online internal leakage detection is based on the multiresolution signal decomposition technique to decompose the pressure signal into smoothed and detailed version in the form of wavelet coefficients, namely as approximation and detail coefficients, respectively. The ability of the wavelets to focus on short intervals for high frequency components (detail coefficients) and long intervals for high frequency

components (approximation coefficients) improves the decomposition of the faulty pressure signal into finer and detailed scales, facilitating further effective signal processing and analysis. The decomposed approximate wavelet coefficients are shown to be more sensitive to effect of external leakage on the changes of the pressures than the original pressure signals. Therefore, these wavelet coefficients provide valuable information for the assessment of actuator health. In this analysis, the original chamber one pressure was decomposed into approximate (low frequency) components of a_4.

As mentioned earlier the external leakage causes a drift in the line pressures. This drift in the pressure decreases the amplitude as well as the energy of the approximate wavelet coefficient a_4 (see Fig. 6.14). Either pressure signal may be used equally for the analysis.

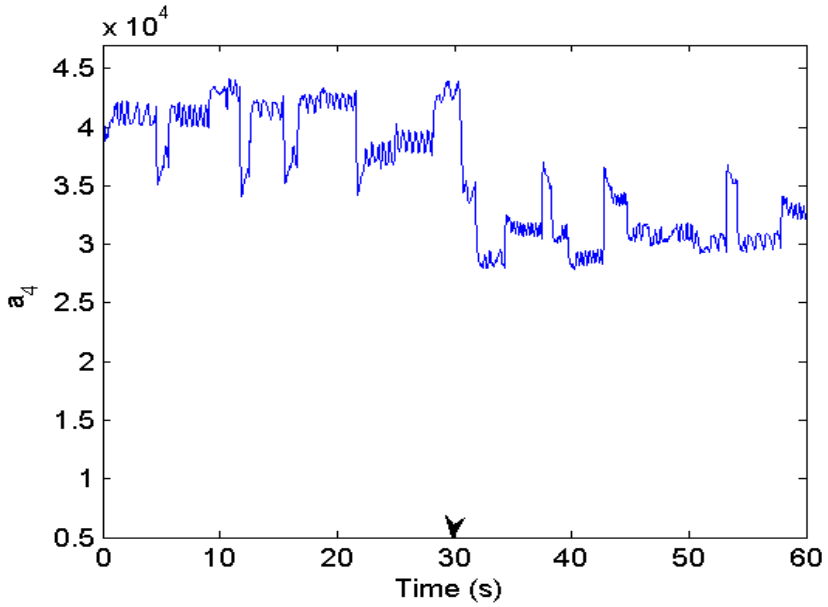

Figure 6.14: Level four approximate coefficient, a_4, obtained from the pressure signal at the chamber one with external leakage shown in Fig. 6.11.

6.4.2. External leakage detection using online measurements

In online equipment health monitoring, signals are monitored and gathered during operation. The same sliding window technique as in Fig. 5.5 is used for online measurements. In this thesis a window size of l_1=400 samples and step size of l_2=20 samples were found to be appropriate. The sliding window concept is now applied to

the results of the case study reported in Section 6.4.1. The RMS values obtained from each updated window are plotted in Fig. 6.15. The RMS decreases once the external leakage is introduced to the system at t≈30s (fig 6.15). Fig. 6.14 used the entire data set whereas Fig. 6.15 used the windowing approach. Another test was conducted with a more severe external leakage of the value 0.94 lit/min, introduced at t≈30s (see Fig. 6.16). The actuator displacement is also shown in Fig. 6.17. There is a different reference input for this case when comparing 6.12 and 6.17. The RMS values of a_4 by using online measurements are depicted in Fig. 6.18. As compared to Fig.6.15, the RMS values decreased more in this case. Therefore, with a more severe external leakage, the RMS values of a_4 drop more regardless the reference input.

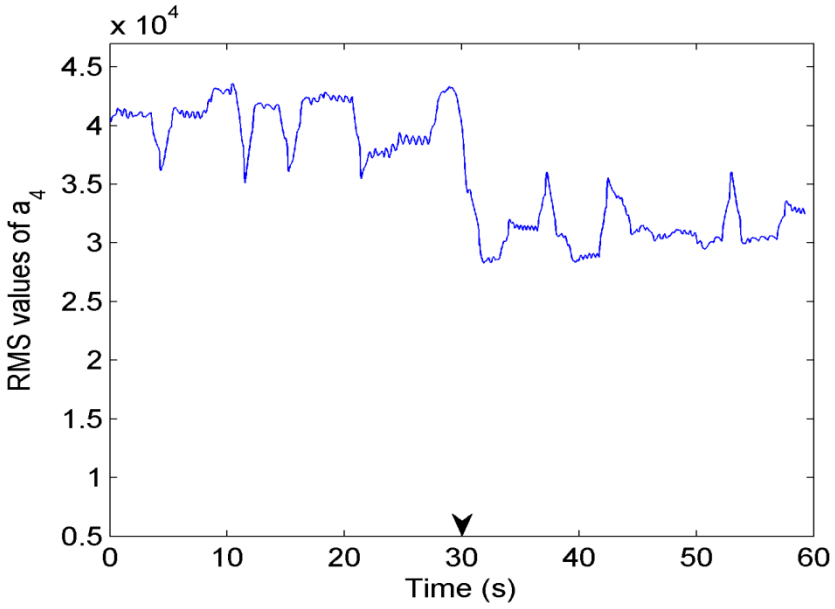

Figure 6.15: RMS values of level four approximate wavelet coefficient of chamber one pressure for actuator with external leakage shown in Fig. 6.11.

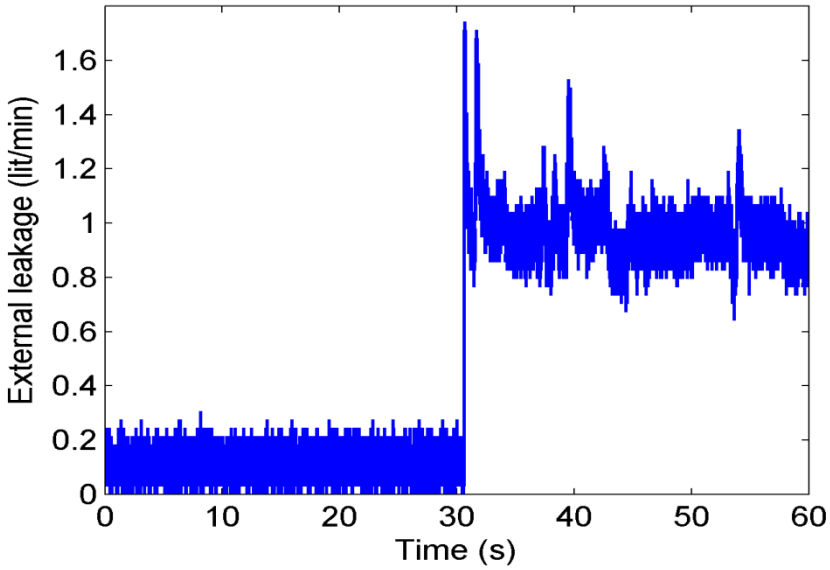

Figure 6.16: External leakage on chamber two of the hydraulic actuator with the mean value of 0.94 lit/min.

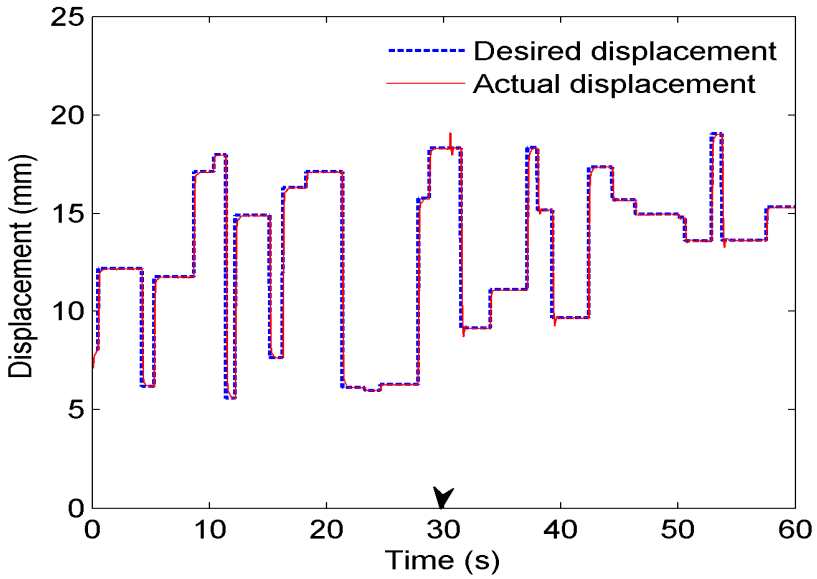

Figure 6.17: Desired and actual displacement of the hydraulic actuator with external leakage shown in Fig. 6.16.

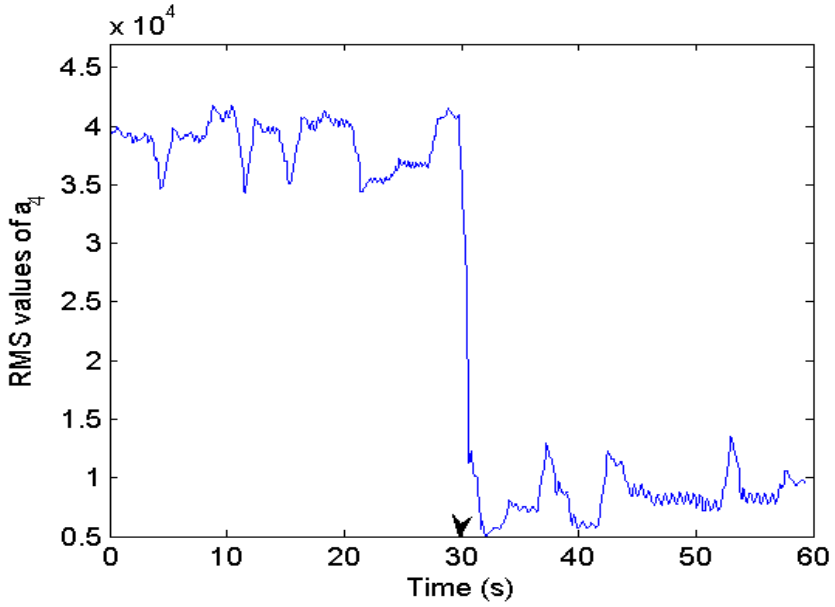

Figure 6.18: RMS values of wavelet coefficients of chamber one pressure for actuator with external leakage shown in Fig. 6.16.

6.5. Isolation of external leakage from internal leakage in a multiple-fault environment using online measurements

In this Section, the isolation of external leakage from internal leakage is investigated. These faults are assumed to happen singly but exist in a multiple-fault environment since in online applications the likelihood of external and internal leakages occurring at the same time is very low. For all results presented in this Section, the pressure at chamber one, P_1, is used for the analysis. From the previous Chapters, it is known that the internal leakage changes the transient behavior of the pressure signals, and subsequently decreases the amplitude and energy of level two detail coefficient, d_2. To further clarify this, another experiment in which the actuator experiences an internal leakage of the mean value of 0.48 lit/min after t≈30s is conducted. The plots of leakage flow and actuator displacement are shown in Figs.6.19 and 6.20. The controller still works well under present of internal leakage.

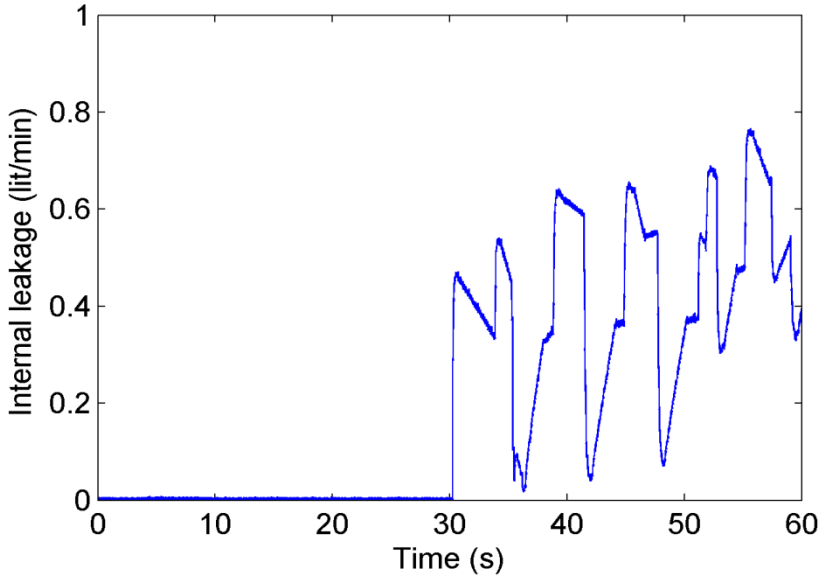

Figure 6.19: Internal leakage of 0.48 lit/min in average at t≈30s.

By applying the sliding window technique to the ongoing pressure data of chamber one, the RMS values of the wavelet coefficient, d_2, are calculated and plotted in Fig. 6.21. As can be seen these values decrease as the result of internal leakage after t≈30s. To facilitate the comparison between healthy and faulty zones, a baseline value of 30 is chosen for the RMS values. The RMS values of d_2 collapse under this baseline value after the occurrence of an internal leakage fault. The coefficient, a_4, is then shown to be insensitive to the internal leakage. The a_4 coefficient was shown to be sensitive to the external leakage. As compared to Fig. 6.15 and 6.18, Fig. 6.22 shows that the trend of, a_4, is not changed by the internal leakage after t≈30s. Therefore, the wavelet coefficient, a_4, is not sensitive to the internal leakage fault. As mentioned before the external leakage has no effect on the detail coefficient d_2. The RMS values of d_2 associated with the external leakage in Fig. 6.16 are depicted in Fig. 6.23. These values are still above the baseline value after the occurrence of external leakage after t≈30s; however, the RMS values of the low frequency wavelet coefficient a_4 decrease as a result of external leakage (see Fig 6.18). It is therefore, concluded that coefficients a_4 and d_2 are independently sensitive to the effect of external and internal

leakages. Thus, by inspecting them, one can not only detect external and internal leakages but also isolate them when they happen singly in a multiple-fault environment.

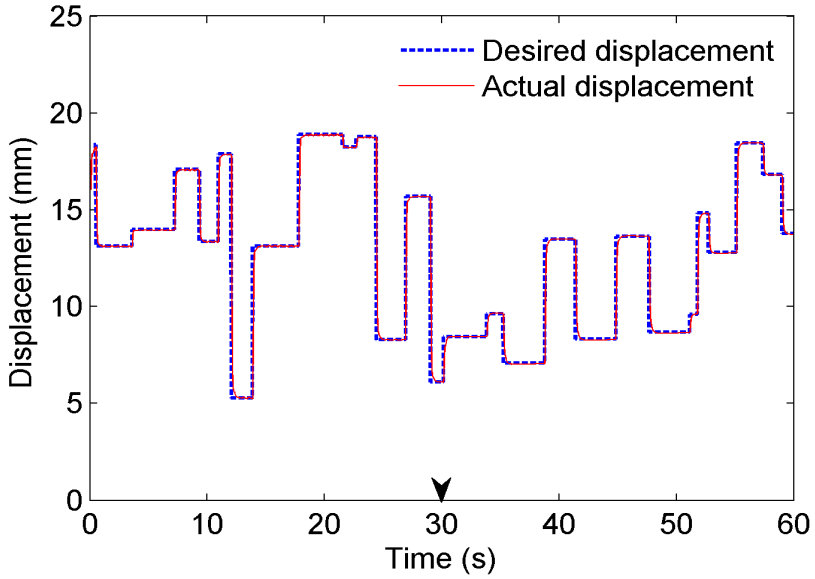

Figure 6.20: Desired and actual displacement of the hydraulic actuator with internal leakage shown in Fig. 6.19.

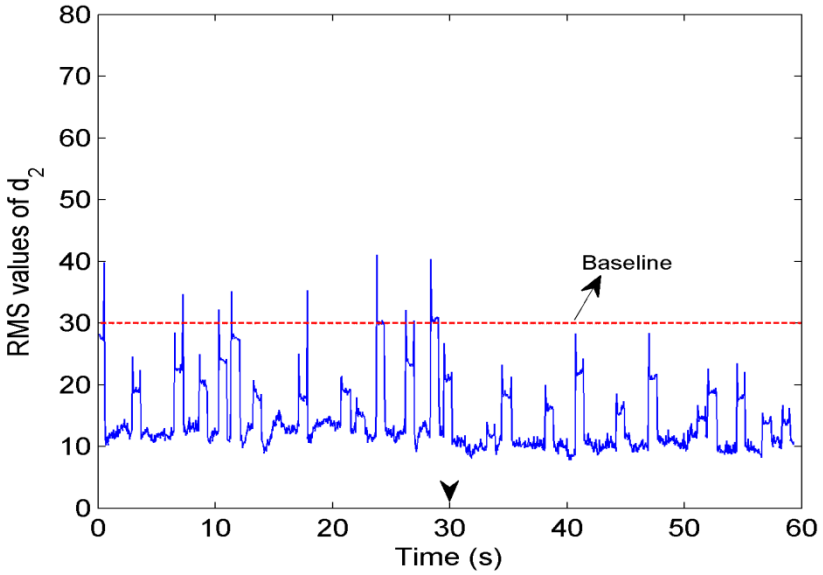

Figure 6.21: RMS values of wavelet coefficients of chamber one pressure for actuator with internal leakage shown in Fig. 6.19.

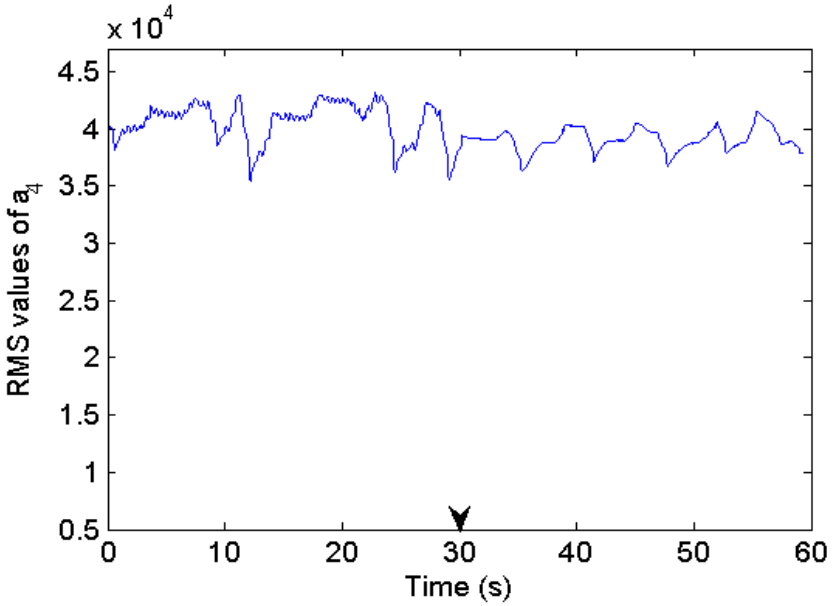

Figure 6.22: RMS values of wavelet coefficients of chamber one pressure for actuator with internal leakage shown in Fig. 6.19.

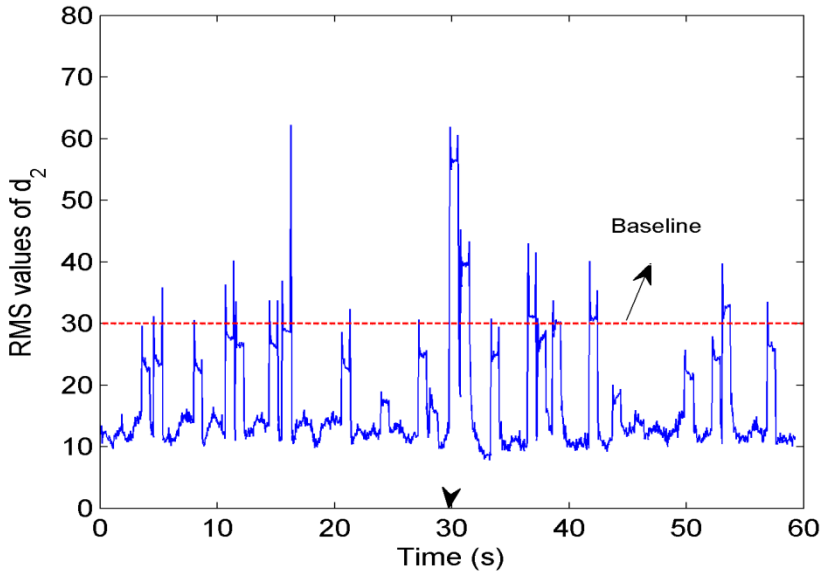

Figure 6.23: RMS values of wavelet coefficients of chamber one pressure for actuator with external leakage shown in Fig. 6.16.

Chapter 7

7. Concluding remarks

7.1. Contributions of this work

In this thesis, using the model of hydraulic functions, an internal leakage was shown to add damping to the hydraulic actuator dynamics and decreases the Bode magnitude of pressure signal over the valve spool displacement around the hydraulic natural frequency. The pressure transient response is changed as a result of internal leakage; however, an external leakage drops the pressure signals without having a significant effect on transient responses.

Three different signal processing methods were tested for internal leakage detection. The methods were fast Fourier transform (FFT), wavelet transform (WT) and Hilbert-Huang transform (HHT). The original pressure signal from one side of the actuator in response to a structured (periodic steps) input applied directly to servovalve was decomposed into more informative sub-band signals, sensitive to effect of internal leakage. The FFT spectrum within the feature frequency band (65-85 Hz) was shown to be an appropriate leakage fault indicator. Level two detail WT coefficient was shown to be used with confidence for internal leakage diagnosis. The instantaneous magnitude of first intrinsic mode function (IMF), using HHT, was demonstrated to be sensitive to internal leakage. Results from extensive experiments were used to show the capability of these methods to detect internal leakages as low as 0.124 lit/min without a need to include models of the actuator and/or the leakage fault. The results also revealed that HHT, WT and FFT based identification can perform the diagnosis task for 95%, 80%

and 30% of the time respectively; thus, HHT is more sensitive in diagnosis of internal leakage than the WT and FFT based approaches, while using a structured input signal. The effect of friction was also studied while the actuator was coupled with the slave cylinders which increased the sliding friction from 258 N to 400 N. It was observed that with an increase in friction, WT and FFT approaches still are able to identify small internal leakages; however, the performance of HHT was degraded by the changes in friction. Applicability of the proposed techniques towards an online diagnostic task with a pseudorandom reference input in a closed-loop scheme was tested. FFT failed to perform a satisfactory task with a pseudorandom reference input since it cannot reveal the time at which the fault happens; however, both WT and HHT illustrated the same results in this kind of application. Using WT is very straightforward and the computational burden is low compared to HHT. As opposed to HHT, there is an analytical background for WT and for this reason the exact level of decomposition can be determined according to the range of frequency required to be captured for a specific application. For these reasons, WT was found to be the most appropriate signal processing method for the purpose of this research.

A wavelet based method for online internal leakage was then developed. The proposed scheme was the extension of the offline method to make it implementable for online diagnosis. The present method allowed information to be gathered while the actuator was controlled to perform arbitrary tracking, and under loading condition. Using a sliding window technique, limited-duration segments of measured pressure signal were collected; each segment was then decomposed via a wavelet transform and RMS values of the level two detail coefficients were analyzed to detect the occurrence of fault. The RMS values of level two detail coefficients obtained in this manner, are sensitive to the internal leakage and can be used to distinguish between healthy and faulty conditions. When a leakage happens the RMS values decrease both in magnitude and energy. Experimental results demonstrated the efficacy of the proposed technique. In the experimental setup, the actuator was set to track pseudorandom reference positions over a long period of time against a load emulated by a spring. Internal leakages, in the range of 0.2-0.25 lit/min, were detected regardless of the type of the feedback controller, reference input and loading condition.

Similarly, a wavelet-based method was proposed for both offline and online external leakage fault detection. The RMS value of level four approximate coefficients can be used as an index for external leakage fault detection. This index value decreases with the level of external leakage. The consistency of this approach was verified by experimental tests. Although the approach can identify small external leakages, it cannot determine which side of the actuator the leak is coming from. Online diagnosis of external leakage could be achieved regardless of the type of feedback controller, reference input and loading condition.

The isolation of external leakage from internal leakage in a multiple-fault environment was studied as well. It was shown that level two detail coefficients and level four approximate coefficients are independently sensitive to the effect of internal and external leakages. By monitoring these indices from measurement of pressure signal, external leakage as low as 0.3 lit/min and internal leakage, as low as 0.2 lit/min, can be detected 90% of the times while using offline diagnosis task. Both leakages were assumed to occur at the same time. The isolation of these faults was also studied in online application; however, in an online application, internal and external leakages were assumed to happen separately. Thus, isolation of external leakage from internal leakage in a multiple-fault environment becomes possible with only one measurement and without a need to include the model of actuator or leakage.

7.2. Future work

Shifting interesting frequency range due to changes in effective bulk modules becomes a problem when using FFT for internal leakage detection. Future work will concentrate on weaving FFT method with some adaptive approaches to detect the optimal range of frequency.

Another issue which can be addressed in future work is to study the effect of noise on the proposed approaches. The issue of robustness is also crucial for any fault diagnostic scheme. Although the robustness of proposed approaches to effective bulk modulus and friction was addressed in this thesis, this issue can be extended to the changes in other parameters.

For online detection of internal leakage the trend of RMS values decrease after the occurrence of internal leakage. However, there is still a short come for predicting the exact time when the internal leakage happens. Future work will consider the development of a method for prediction of the time when internal leakage happens as well as a method that makes the diagnosis task more readily for the operator while observing the trend of changes in RMS values.

For online diagnosis, testing different windows other than the Rectangular window such as Hamming and Hanning windows can be considered for future work.

References

[1] Ayenu-Prah, A. Y. and Attoh-Okine N.O. 2009. Comparative study of Hilbert-Huang transform, Fourier transform and wavelet transform in pavement profile analysis. Vehicle Systems Dynamics, vol. 47, pp. 437-456.

[2] Antonino-Davin, J. A. Riera-Guasp, M. Pineda-Sanchez, M. and Perez, R. B. 2009. A critical comparison between DWT and Hilbert-Huang-Based methods for the diagnosis of rotor bar failures in induction machines. IEEE Trans. on Industry Applications, vol. 45, pp. 1794-1803.

[3] Anant, K. S. 1997. Wavelet transform analysis of transient signals: The Seismogram and the Electrocardiogram. Ph.D. Thesis, University of California.

[4] Al-Ammar, E. Karady, G. G. and Jin Sim, H. 2008. Novel technique to improve the fault detection sensitivity in transformer impulse test. IEEE Trans. on Power Delivery, vol. 23, pp.717-725.

[5] Alle Meije, W. 2004. Wavelet-based methods for the analysis of fMRI time series. Ph.D. Thesis, University of Groningen.

[6] An, L. and Sepehri, N. 2003. Hydraulic actuator circuit fault detection using extended Kalman filter. Proceeding of American Control Conference, pp. 4261-4266.

[7] An, L. and Sepehri, N. 2005. Hydraulic actuator leakage fault detection using extended Kalman filter. Int. Journal of Fluid Power, vol. 6, pp. 41-51.

[8] An, L. 2007. Actuator leakage fault detection and isolation based on extended Kalman filtering scheme. Ph.D. thesis, University of Manitoba.

[9] An, L. and Sepehri, N. 2008. Leakage fault detection in hydraulic actuators subjected to unknown external loading. Int. Journal of Fluid Power, vol. 9, pp.15-25.

[10] Adjallah, K. Maquin, D. and Ragot, J. 1994. Nonlinear observer-based fault detection. Proceeding of 3rd Conference on Control Applications, pp. 1115-1120.

[11] Burrus, C. S. Gopinath, R. A. and Guo, H. 1998. Introduction to wavelets and wavelet transforms. Prentice Hall.

[12] Balocchi, R. Menicucci, D. Santarcangelo, E. Sebastiani, L. Gemignani, A. Ghelarducci, B. and Varanini, M. 2004. Deriving the respiratory sinus

arrhythmia from the heartbeat time series using empirical mode decomposition. Chaos, Solitons and Fractals, vol. 20, pp.171–177.

[13] Crowther, W. J. Edge, K. A. Atkinson, R. M. and Woollons, D. J. 1998. Fault diagnosis of a hydraulic actuator circuit using neural networks-an output vector space classification. Proceedings of the Institution of Mechanical Engineers, vol. 212, pp. 57-68.

[14] Chinniah, Y. Burton, R. and Habibi, S. 2003. Viscous damping coefficient and effective bulk modulus estimation in a high performance hydrostatic system using extended Kalman filter. International Journal of Fluid Power, vol. 4, pp. 27-34.

[15] Cusido, J. Romeral, L. Ortega, J. A. Rosero, J. A. and Garcia, E. A. 2008. Fault detection in induction machines using power spectral density in wavelet decomposition. IEEE Trans. on Industrial Electronics, vol. 55, no. 2, pp. 633-643.

[16] Daubechies, I. 1992. Ten lectures on wavelets. Montpelier, Capital City Press.

[17] Daubechies, I. 1998. Orthonormal bases of compactly supported wavelets. Communications on Pure and Applied Mathematics, vol. 41, pp. 909 – 996.

[18] Davis, G. M. Nosratinia, A. 1998. Wavelet-based image coding: An overview. Applied and Computational Control, Signals, and Circuits, vol. 1, pp. 205- 269.

[19] Donoho, D. L. 1993. Unconditional bases are optimal bases for data compression and for statistical estimation. Applied and Computational Harmonic Analysis, vol. 1, pp. 100-115.

[20] Garimella, P. and Yao, B. 2005. Model based fault detection of an electro-hydraulic cylinder. American Control Conference, pp. 484-489.

[21] Gaddouna, B.O. and Ouladsine, M. 1997. Fault diagnosis in a hydraulic process using unknown input observers. Proceedings of the IEEE International Conference on Control Applications, pp. 490-495.

[22] Garcia, E. A. and Frank, P. M. 1997. Deterministic nonlinear observer-based approaches to fault diagnosis: A survey. Control Engineering Practice, vol. 5, pp. 663-670.

[23] Gao, Y. Zhang, Q. and Kong, X. 2003. Wavelet based pressure analysis for hydraulic pump health diagnosis. Trans. ASAE, vol. 46, pp. 969-976.

[24] Gao, Y. Zhang, Q. and Kong, X. 2005. Comparison of hydraulic pump fault diagnosis methods: wavelet vs. spectral analysis. Proceedings, ASME International Mechanical Engineering Congress and Exposition, pp. 73-78.

[25] Gao, Y. and Zhang, Q. 2006. A wavelet packet and residual analysis based method for hydraulic pump health diagnosis. Proc. IMechE, vol. 220, pp.735-745.

[26] Gao, Q. Duan, C. Fan, H. and Meng, Q. 2008. Rotating machine fault diagnosis using empirical mode decomposition. Mechanical Systems and Signal Processing, vol. 22, pp. 1072–1081.

[27] Hahn, J. Hur, J. Cho, Y. and Lee, K. 2001. Robust observer based monitoring of a hydraulic actuator in a vehicle power transmission control system. Proceeding of the IEEE International Conference on Control Applications, pp. 805-810.

[28] Huang, N. E. Shen, Z. Long, S. R. Wu, M. C. Shih, H. H. Zheng, Q. Yen, N. C. Tung, C. C. and Liu, H. H. 1998. The empirical mode decomposition and Hilbert spectrum for nonlinear and nonstationary time series analysis. Proc. R. Soc. Lond. A, Math. Phys. Sci., vol. 454, no. 1971, pp. 903-995.

[29] Isermann, R. 1992. Estimation of physical parameters for dynamic processes with application to an industrial robot. International Journal of Control, vol. 55, pp.1287-1298.

[30] Isermann, R. 1997. Fault-detection and fault-diagnosis methods - An introduction. Control Eng. Practice, vol. 5, pp. 639–652.

[31] Khan, M. A. S. K. Rahman, M. A. 2009. Development and implementation of a novel fault diagnostic and protection technique for IPM motor drives. IEEE Trans. on Industrial Electronics, vol. 56, no. 1, pp. 85-92.

[32] Khan, H. Abou, S. and Sepehri, N. 2002. Fault detection in electro-hydraulic servo-positioning systems using sequential test of Wald. Proceedings, Canadian conference on electrical & Computer Engineering, pp. 1628-1633.

[33] Karpenko, M. and Sepehri, N. 2005. Fault-tolerant control of a servohydraulic positioning system with crossport leakage. IEEE Trans. on Cont. Sys. Tech., vol. 13, no. 1, pp. 155-161, 2005.

[34] Karpenko, M., and Sepehri, N., "Quantitative fault tolerant control design for a hydraulic actuator with a leaking piston seal," ASME Journal of Dynamic Systems, Measurement, and Control, in press.

[35] Karpenko, M. 2008. Quantitative fault tolerant control design for a hydraulic actuator with a leaking piston seal. Ph.D. thesis, University of Manitoba, Winnipeg, Canada.

[36] Lischinsky, P. Canudas-de-Wit, C. and Morel, G. 1999. Friction compensation for an industrial hydraulic robot,' IEEE Control System Magazine, vol. 19, pp. 25-32.

[37] Le, T. T. Watton J. and Pham, D. T. 1998. Fault classification of fluid power system using a dynamic feature extraction technique and neural networks. J. of Sys. and Cont. Eng., vol. 211, pp.307-317.

[38] Loutridis, S. J. 2004. Damage detection in gear systems using empirical mode decomposition. Engineering Structures, vol. 26, pp. 1833-1841.

[39] Lim, H. S. Chong K. T. and Su, H. 2006. Motor fault detection method for vibration signal using FFT residuals. Int. J. of Applied Elec. and Mech., 24, pp.209-223.

[40] Merrit, H. E.1967. Hydraulic control systems, Wiley, New York.

[41] Mallat, S. 1989. A theory for multiresolution signal decomposition: The wavelet representation. IEEE Trans. Pattern Analysis and Machine Intelligence, vol. 11, pp. 674–693.

[42] Mallat, S. 1998. A wavelet tour of signal processing. Academic press, 1998.

[43] Niksefat, N. and Sepehri N. 2002. A QFT fault-tolerant control for electrohydraulic positioning systems. IEEE Transaction on control system technology, vol. 10, pp. 626-632.

[44] Nguyen, L. T. Ogburn, M. E. Gilbert, W. P. Kibler, K. S. Brown, P. W. and Deal, P. L. 1979. Simulation study of stall/post-stall characteristics of a fighter airplane with relaxed static stability. NASA Langley Research Center, Hampton, VA, Tech. Rep. NASA-TP-1538.

[45] Preston, G. L. Shields, D.N. Daley, S. 1996. Application of a robust nonlinear fault detection observer to a hydraulic system. UKACC International Conference on Control, vol. 2, pp. 1484-1489.

[46] Proakis, J. G. and Manolakis, D. G. 2007. Digital signal processing, 4th ed. Prentice Hall.

[47] Quek, S. Tua, P. Wang, Q. 2003. Detecting anomalies in beams and plate based on the Hilbert–Huang transform of real signals. Smart Materials and Structures, vol. 12, pp. 447-460.

[48] Roy, A. Wen, C. H. Doherty, J. F. and Mathews, J. D. 2008. Signal feature extraction from microbarograph observation using the Hilbert-Huang transform. IEEE Trans. on Geosci. and Remote Sensing, vol. 46, no. 5, pp. 1442-1447.

[49] Rao, N. 2001. Speech Compression Using Wavelets. The University of Queensland.

[50] Song, R. and Sepehri, N. 2002. Fault detection and isolation in fluid power systems using a parametric estimation method. Proceedings, IEEE CCECE Canadian Conference on Electrical and Computer Eng., vol. 1, pp. 144-149.

[51] Skormin, V. A. Apone, J. and Dunphy, J. J. 1994. Online diagnostics of a self-contained flight actuator. IEEE Trans. Aerospace and Electronic Systems, vol. 30, pp.186-196.

[52] Skormin, V. A. and Apone, J. 1995. Online diagnostics of a variable displacement pump of a flight actuation system. Proc. of the IEEE National Aerospace and Electronics Conference, vol. 1, pp. 503-510.

[53] Sridhar, B. Smith, P. Suorsa, R. E. and Hussien, B. 1993. Multirate and event-driven Kalman filters for helicopter flight. IEEE Control Systems Magazine, vol. 13, pp. 26-33.

[54] Shi, Z. Gu, F. Lennox, B. and Ball, A. D. 2005. The development of an adaptive threshold for model-based fault detection of a nonlinear electro-hydraulic system. Control Engineering Practice, vol. 13, pp. 1357–1367.

[55] Strang, G. and Nguyen, T.1996. Wavelet and filter banks. Wellesley-Cambridge Press, Wellesley.

[56] Tan, H. and Sepehri, N. 2002. Parametric fault diagnosis for electrohydraulic cylinder drive units. IEEE Trans. Industrial Electronics, vol. 49, pp. 96-106.

[57] The Mahworks. 2005. Wavelet toolbox user's guide. The Mathworks Inc., Natick, Massachusetts, USA.

[58] Thomas A. 2000. The Application of the wavelet transform to the processing of aeromagnetic data. Ph.D. Thesis, University of Western Australia.

[59] Werlefors, M. and Medvedev, A. 2008. Observer-based leakage detection in hydraulic systems with position and velocity feedback. 17th IEEE International Conference on Control Applications, pp. 948-953.

[60] Wang, X. and Syrmos, V. L. 2008. Fault detection, identification and estimation in electrohydraulic actuator system using EKF-based multiple-model estimation. 16th Mediterranean Conf. on Control and Automation, pp. 1693-1698.

[61] Yu, D. 1997. Fault diagnosis for a hydraulic drive system using a parameter-estimation method. Control Engineering Practice, vol. 5, pp. 1283-1291.

[62] Yu, D. Shields, D. N. and Mahtani, J. L.1994. Fault detection for bilinear systems with application to a hydraulic system. Proceedings of 3rd IEEE Conference on Control Applications, vol. 2, pp. 1379-1384.

[63] Yu, X. Liao, R.Yao, C. 2001. Fault diagnosis in hydraulic turbine governor based on BP neural network. Proceeding of 5th International Conference on Electrical Machines and Systems, vol. 1, pp. 335-338.

[64] Zafarifar, B. 2002. Micro-codable discrete wavelet transform. Master thesis, Delft University of Technology, Netherland.

[65] Zhou, R. Lin, T. Han, J. and Yan, D. 2002. Fault diagnosis of airplane hydraulic pump. Proceeding of the 4th World Congress on Intelligent Control and Automation, vol. 4, pp. 3150-3152.

[66] Zavarehi, M. K. Lawrence, P. D. and Sassani F. 1999. Nonlinear modeling and validation of solenoid controlled pilot-operated servovalves. IEEE/ASME Tran. Mechatronics, vol. 4, pp. 324-334.

[67] Zhang, Y. M. and Jiang, J. 2002. Active fault-tolerant control system against partial actuator failures," IEEE Proc. of Control Theory Application, vol. 149, pp. 95-104.

[68] Zhang, J. Q. and Yan, Y. 2001. A wavelet-based approach to abrupt fault detection and diagnosis of Sensors. IEEE Trans. Instrumentation and Measurement, vol. 50, pp. 1389-1396.

[69] Zhao, Q. and Xu, Z. 2004. Design of a novel knowledge-based fault detection and isolation scheme. IEEE Tran. on Systems, Man, and Cybernetics, vol. 34. pp.1089-1095.

[70] Ukil, A. and Zivanovic, R. 2006. Abrupt change detection in power system fault Analysis using adaptive whitening filter and wavelet transform. Elec. power Sys. Research, vol. 76, pp. 815-823.